

REVIEW ARTICLE**Secondary anisotropies of the CMB****Nabila Aghanim¹, Subhabrata Majumdar² and Joseph Silk³**¹ Institut d’Astrophysique Spatiale (IAS), CNRS, Bât. 121, Université Paris-Sud, F-91405, Orsay, France² Department of Astronomy & Astrophysics, Tata Institute of Fundamental Research (TIFR), Homi Bhabha Road, Mumbai, India³ Denys Wilkinson Building, University of Oxford, Keble Road, Oxford, OX1 3RH, UKE-mail: nabila.aghanim@ias.u-psud.fr, subha@tiffr.res.in**Abstract.**

The Cosmic Microwave Background fluctuations provide a powerful probe of the dark ages of the universe through the imprint of the secondary anisotropies associated with the reionisation of the universe and the growth of structure. We review the relation between the secondary anisotropies and the primary anisotropies that are directly generated by quantum fluctuations in the very early universe. The physics of secondary fluctuations is described, with emphasis on the ionisation history and the evolution of structure. We discuss the different signatures arising from the secondary effects in terms of their induced temperature fluctuations, polarisation and statistics. The secondary anisotropies are being actively pursued at present, and we review the future and current observational status.

1. Introduction

In the post WMAP era for Cosmic Microwave Background (CMB) measurements and in preparation of Planck and the post-Planck era, attention is now shifting towards small angular scales of the order of a few arc-minutes or even smaller. At these scales, CMB temperature and polarisation fluctuations are no longer dominated by primary effects at the surface of last scattering but rather by the so-called secondary effects induced by the interaction of CMB photons with the matter in the line of sight.

Current and future CMB experiments have two main goals: i) measuring small angular scale temperature fluctuations (below a few arc minutes), and ii) measuring the CMB polarisation power spectrum. These goals are fundamental for our understanding of the universe. The small-scale anisotropies are directly related to the presence of structures in the universe whereas the two types of polarisation (*E* and *B*-modes, which we discuss later) probe both the reionisation of the universe, i.e. the formation of the first emitting objects, and the inflationary potential. In this review, we focus on the end of the dark ages and the astrophysical probes of reionisation.

There have been rapid and important advances in the recent past. We already have on the one hand measurements, by ACBAR, CBI, BIMA, VSA, of the temperature power spectrum for $2000 < \ell < 4000$ with CBI and BIMA data showing an excess of power as compared with the predicted damping tail of the CMB (Figure 1). On the other hand, DASI, Archeops, Boomerang, Maxipol, CBI, QUaD and WMAP have direct measurements of the *E*-mode polarisation. The situation will change even more in the near future with anticipated results from experiments currently taking data or in preparation (QUaD, BICEP, EBEX, CLOVER, QUIET, SPIDER, Planck).

All of this experimental activity is motivated by what now amounts to the standard model of cosmology. The CMB temperature fluctuations which are generated prior to decoupling are measured on scales from 90 degrees to several arc minutes. This has led to a model of precision cosmology. The basic infrastructure is the Friedmann-Lemaitre model with zero curvature, a cosmological constant (or dark energy), a baryonic content and non-baryonic dominant cold dark matter component (with fractions given by the recent WMAP data (Spergel et al. 2007)). Superimposed on the cosmological background are the primordial adiabatic density fluctuations, described by a nearly scale-invariant power spectrum $|\delta_k|^2 \propto k^{n-1}$, at horizon crossing (in the comoving gauge), that generated the large-scale structure via gravitational instability of the cold matter component. However it has become increasingly apparent that to further refine these parameters, and to face the more intriguing challenge of establishing possible deviations from the concordance model one has to address the degeneracies between cosmological parameters with those from the secondary anisotropies as well as the extragalactic astrophysical foregrounds.

The primary CMB anisotropies are due to the gravitational redshift at large angular scales (Sachs & Wolfe 1967) and to the evolution of the primordial photon-baryon fluid evolution under gravity and Compton scattering at lower scales (Silk 1967, Peebles & Yu

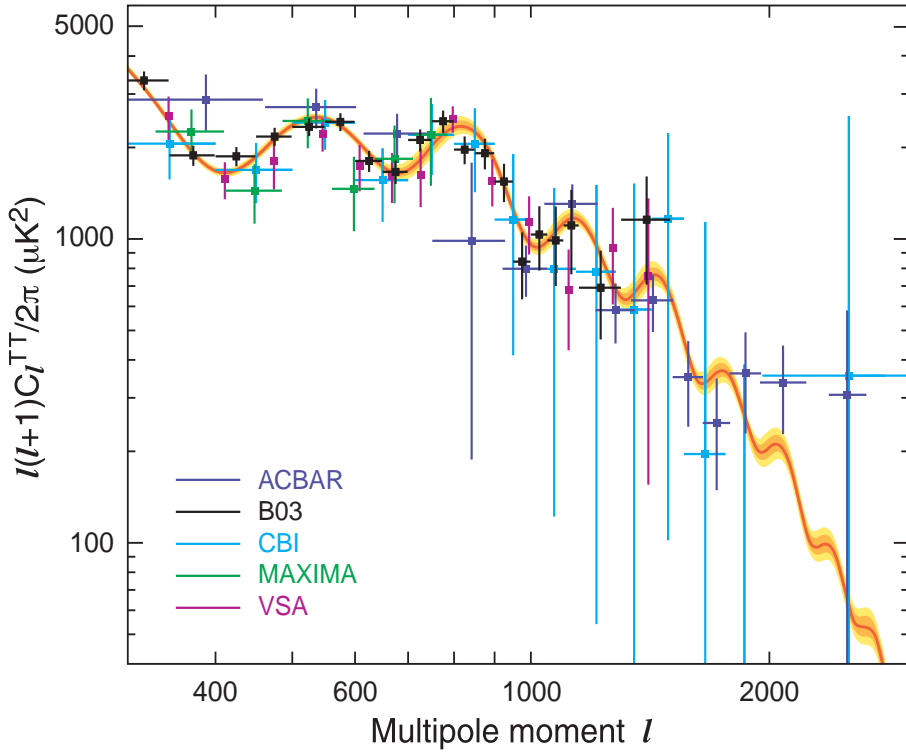


Figure 1. From Spergel et al. (2006): The compilation of the small scale CMB measurements from ground-based and balloon experiments (Ruhl et al. 2003, Abroe et al. 2004, Kuo et al. 2004, Readhead et al. 2004, Dickinson et al. 2004). The red, dark orange and light orange lines represent the predictions from the Λ CDM model fit to the WMAP data for the best fit, the 68% and 95% confidence levels respectively. Excess of power is seen at the largest l values.

1970, Sunyaev & Zel'dovich 1970) to which one adds photon diffusion damping at small scales (Silk 1967). Primary fluctuations have provided us with an unparalleled probe of the primordial density fluctuations that seeded large-scale structure formation. Indeed on large angular scales, greater than the angular scale subtended by the sound horizon at recombination, one can directly view the approximately scale-invariant spectrum of primordial quantum fluctuations.

On their way towards us, the photons interact with cosmic structures and their frequency, energy or direction of propagation are affected. These are the secondary effects that involve the density and velocity fields and incorporate Compton scattering off electrons. This review is devoted to a study of these secondary anisotropies.

The CMB photons we observe today have traversed the universe from the last scattering surface to us and have thus interacted with matter along their path through the universe. These interactions generate the secondary anisotropies that arise from two major families of interactions. The first family includes the gravitational effects (Figure 2 panel a), including gravitational lensing, the Rees-Sciama effect (RS), moving lenses and decaying potentials usually referred to as the integrated Sachs-Wolfe effect (ISW). These anisotropies arise from the interactions of the photons with gravitational potential

wells. The second family incorporates the effects of scattering between CMB photons and free electrons (Figure 2 panel b) such as inverse Compton interaction (the Sunyaev-Zel'dovich (SZ) effect) and velocity-induced scatterings such as the Ostriker-Vishniac (OV) effect and inhomogeneous reionisation.

We define secondary anisotropies in the CMB to include all temperature fluctuations generated since the epoch of matter-radiation decoupling at $z \sim 1100$. The following contributions may be distinguished.

- (i) The integrated Sachs-Wolfe (ISW) effect is due to CMB photons traversing a time-varying linear gravitational potential. The relevant scale is the curvature scale freeze-out in concordance cosmology: the horizon at $1 + z \sim (\Omega_\Lambda/\Omega_m)^{1/3}$. This corresponds to an angular scale of about 10° .
- (ii) The Rees-Sciama (RS) effect is due to CMB photons traversing a non-linear gravitational potential, usually associated with gravitational collapse. The relevant scales are those of galaxy clusters and superclusters, corresponding to angular scales of 5-10 arc minutes.
- (iii) Gravitational lensing of the CMB by intervening large-scale structure does not change the total power in fluctuations, but power is redistributed preferentially towards smaller scales. The effects are significant only below a few arc minutes. Its effects may be significant on large scales when the observable of interest is the B -mode power spectrum.
- (iv) The Sunyaev-Zel'dovich (SZ) effect from hot gas in clusters is due to the first order correction for energy transfer in Thomson scattering. It is on the scale of galaxy clusters and superclusters, although it may be produced on very small scales by the first stars in the universe. There is a spectral distortion, energy being transferred from photons in the Rayleigh-Jeans tail of the cosmic blackbody radiation to the Wien tail.
- (v) The kinetic Sunyaev-Zel'dovich effect is the Doppler effect due to the motion of hot gas in clusters that scatters the CMB. It causes no spectral distortion.
- (vi) The Ostriker-Vishniac (OV linear) effect is also due to Doppler boosting. It is the linear version of the kinetic Sunyaev-Zel'dovich effect. It is proportional to the product of Δn_e and Δv_{\perp} . This is effective on the scale of order 1 arc minute.
- (vii) Discrete sources provide an appreciable foreground, especially at lower frequencies for radio sources and high frequencies for infra-red and submillimetre sources.
- (viii) Polarisation is primarily a secondary phenomenon. The primary effect from last scattering is induced by out-of-phase velocity perturbations and provides evidence for the acausal nature of the fluctuations. The secondary polarisation is associated with the reionisation of the universe and is on large scales corresponding to the horizon at reionisation. Inhomogeneous reionisation and scattering at the galaxy cluster scale leads to smaller scale polarisation. The reionisation signal is weak, amounting to no more than 10 percent of the primary signal.

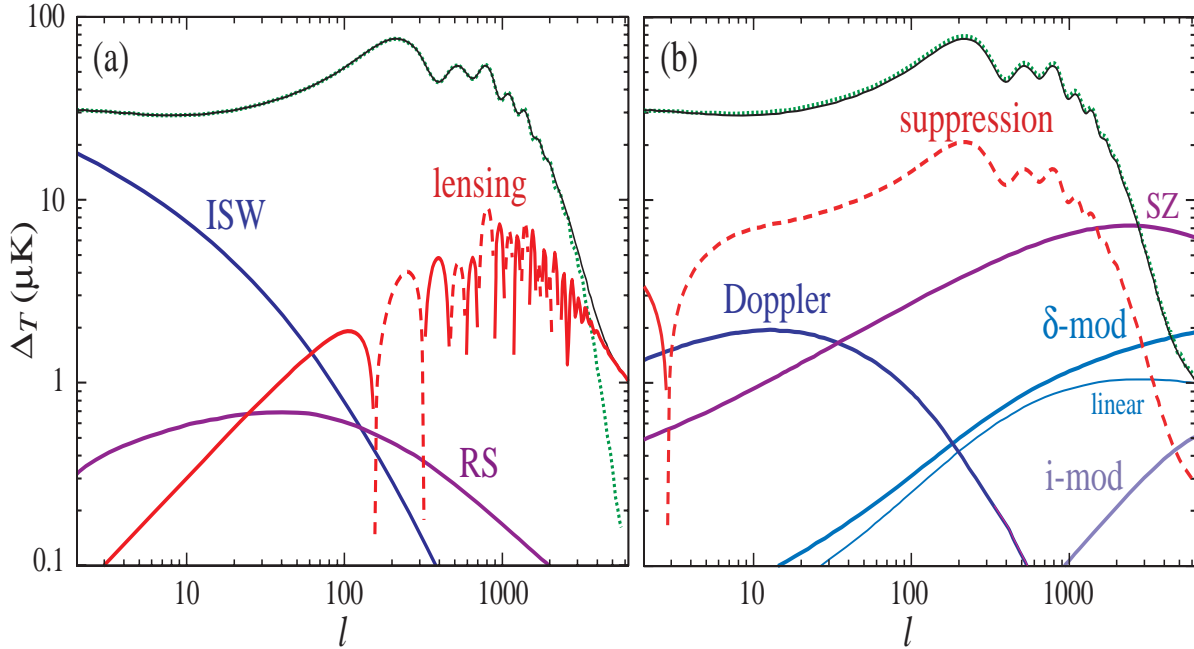


Figure 2. From Hu & Dodelson (2002): The power spectrum of the secondary temperature anisotropies arising from gravitational effects (panel a) and scattering effects (panel b). The power spectrum of primary anisotropies is shown for comparison. The calculations use a flat universe with $\Omega_\Lambda = 0.67, \Omega_b h^2 = 0.02, \Omega_m h^2 = 0.16, n = 1$. Acronyms are defined in the text. δ - and i-mod refer to density and ionisation fraction modulation respectively (Sect. 2). “Suppression” and “Doppler” refer to the damping and anisotropy generation at reionisation (Sect. 2).

- (ix) *B*-mode polarisation can be induced by shear perturbations. One source is gravitational lensing of primary CMB fluctuations. A second is relic gravity waves from inflation. These are pure *B*-modes, and fall off rapidly on scales smaller than the horizon at recombination, corresponding to about half a degree. Mixing by Faraday rotation in the intracluster medium also contributes to *B*-mode generation on small angular scales. The *B*-mode polarisation amplitude only amounts to about a percent of the primary signal, and its discovery will pose the major challenge for future experiments.

2. Reionisation

2.1. Basics of Physics

In dealing with secondary CMB anisotropies at reionisation or arising from ionised structure like the hot gas in galaxy clusters, we are concerned with the scattering of the CMB photons by the plasma. A specific example of this is the Sunyaev-Zel'dovich effect, which is discussed in detail in section 5, where the intra-cluster gas up-scatters the cold microwave photons.

Since the secondary anisotropies are distortions of the CMB, which is the radiation field, we start by looking at the properties of an isotropic and thermal radiation background. The distribution function, $f_\alpha(\mathbf{r}, \mathbf{p}_\nu, t)$, of any radiation field is defined such that $f_\alpha d^3r d^3p_\nu$ is the number of photons in the real space volume d^3r about \mathbf{r} and the momentum space volume d^3p_ν about \mathbf{p}_ν (ν being the frequency) at time t with polarisation $\alpha = 1, 2$. This distribution can be related to the photon occupation number, $n_\alpha(\mathbf{r}, \mathbf{p}_\nu, t)$, by

$$n_\alpha(\mathbf{r}, \mathbf{p}_\nu, t) = h^3 f_\alpha(\mathbf{r}, \mathbf{p}_\nu, t). \quad (1)$$

For polarisation a description in terms of the pure polarisation states pre-supposes fully polarised radiation. For CMB radiation, the occupation number has a Planckian distribution given by

$$n_\alpha = \left(e^{h_{\text{pl}}\nu/k_B T_{\text{cmb}}} - 1 \right)^{-1} \quad \text{for } \alpha = 1, 2 , \quad (2)$$

where T_{cmb} is the temperature of the CMB photons. The specific intensity of radiation is related to the distribution function by

$$I_\nu(\hat{\mathbf{k}}, \mathbf{r}, t) = \sum_{\alpha=1}^2 \left(\frac{h_{\text{pl}}^4 \nu^3}{c^2} \right) f_\alpha(\mathbf{r}, \mathbf{p}_\nu, t) . \quad (3)$$

Commonly, the specific intensity is described in units of brightness temperature, $T_{\text{R-J}}$, which is defined as the temperature of the thermal radiation field which in the Rayleigh-Jeans (R-J) limit (*i.e.*, low frequency) would have the same brightness as the radiation that is being described. In the R-J limit, the specific intensity reduces to $I_\nu = 2k_B T_{\text{cmb}} \nu^2 / c^2$, so that

$$T_{\text{R-J}}(\nu) = \frac{c^2 I_\nu}{2k_B \nu^2} . \quad (4)$$

Now let us consider the scattering between two species (namely photons and electrons). For an ensemble of particles, if the motion of one particle is completely independent of all other particles, then to describe the state of the particles, one can specify the single particle distribution function given by $f(\mathbf{r}, \mathbf{p}, t) d^3r d^3p$, which is the probability of finding a single particle in the phase space volume $d^3r d^3p$ around the point (\mathbf{r}, \mathbf{p}) at time t . If there are no interactions between the particles and if they are non-relativistic, then the distribution obeys the Liouville equation

$$df \partial dt = \partial f \partial t + \mathbf{p} \partial m \cdot \partial f \partial \mathbf{r} + \mathbf{F}(\mathbf{r}, \mathbf{p}, t) \cdot \partial f \partial \mathbf{p} , \quad (5)$$

where \mathbf{F} is any force that may be present, and m is the mass of a particle, assumed to be the same for all particles.

In the case of inter-particle interactions being random and statistical in nature, one cannot describe the system by a mean force \mathbf{F} , but one has to consider instantaneous collisions between the particles (this is the case for photon - electron interactions). These collisions will remove particles from (or add particles to) a cell in phase-space. If one

carefully balances these changes of particles in each cell, then for non-relativistic elastic collisions, one ends up with the Boltzmann equation

$$df\phi dt = \partial f\phi \partial t + \mathbf{p}\phi m \cdot \partial f\phi \partial \mathbf{r} + F(\mathbf{r}, \mathbf{p}, t) \cdot \partial f\phi \partial \mathbf{p} = \\ \int d^3\mathbf{p}_1 |\mathbf{p} - \mathbf{p}_1| \phi m d\sigma \phi d\Omega d\Omega [f(\mathbf{p}'_1) f(\mathbf{p}') - f(\mathbf{p}_1) f(\mathbf{p})], \quad (6)$$

where the scattering solid angle $d\Omega$ is determined by the conservation of momentum and energy and $d\sigma$ is the scattering cross section. Moreover, the collisions take place between particles with momenta \mathbf{p} and \mathbf{p}_1 and produced particles with momenta \mathbf{p}' and \mathbf{p}'_1 . The Boltzmann equation, being integro-differential, is difficult to solve analytically. However, it can be tackled under some approximations which can be made when \mathbf{p} is close to \mathbf{p}' and \mathbf{p}_1 is close to \mathbf{p}'_1 . It is then possible to expand the right hand side of Equation (6) in powers of $\Delta \mathbf{p} = \mathbf{p}' - \mathbf{p}$ and carry out the integral. The result can be expressed in terms of a Taylor series to give the Fokker-Planck equation. A simplification of the Fokker-Planck equation yields the Kompaneets equation, whose solution for the case of photon-electron collisions in astrophysical situations gives the Sunyaev-Zel'dovich distortion (Section 5).

At matter-radiation decoupling, the free electrons are non-relativistic and the scattering between them and the photons is simply Thomson scattering. The incident electromagnetic radiation with linear polarisation ϵ_i is scattered by an electron at rest in a radiation field of polarisation ϵ_e into a solid angle $d\Omega$ with a probability:

$$d\sigma = \frac{3\sigma_T}{8\pi} |\epsilon_i \cdot \epsilon_e|^2 d\Omega.$$

In the plane perpendicular to the scattering direction there is no variation of the polarisation. In the scattering plane, however, there is a net polarisation. As a consequence, if the incident radiation propagating along the z axis comes from two orthogonal directions there will be no polarisation transmitted along the z axis. Isotropic non-polarised incident radiation will induce the same identical polarisation along x and y axis. If the incident radiation is anisotropic and quadrupolar the scattered radiation shows an excess of energy and thus a non-zero polarisation oriented according to the quadrupole orientation. As a result, the Thomson scattering induces a linear polarisation under the condition that the incident radiation has at least a quadrupolar geometry. In the cosmological context, anisotropies are induced by density perturbations and the velocity gradients are responsible for the quadrupole moment. We therefore expect a Thomson scattering-induced polarisation for the primary anisotropies.

The polarisation intensity is governed by the Boltzmann equation (Peebles & Yu 1970, Sunyaev & Zel'dovich 1972, Bond & Efstathiou 1984, Ma & Bertschinger 1995, Hu & White 1997). This yields:

$$\dot{\Delta}_{Q\pm iU} + \hat{\mathbf{n}}_i \partial_i \Delta_{Q\pm iU} = n_e \sigma_T a(\eta) \left(-\Delta_{Q\pm iU} + \sqrt{\frac{6\pi}{5}} \sum_{m=-2}^{m=2} {}_{\pm 2}Y_2^m(\hat{\mathbf{n}}) \Pi^{(m)} \right), \quad (7)$$

where Q and U are the two Stokes parameters, $\eta \equiv \int dt/a$ is the conformal time, a is the expansion factor, and $\hat{\mathbf{n}}$ the direction of photon propagation. ${}_s Y_\ell^m$ are the spherical harmonics with spin-weight s , and $\Pi^{(m)}$ is defined in terms of the quadrupole components of the temperature ($\Delta_{T2}^{(m)}(\mathbf{r}, \eta)$) and polarisation perturbations

$$\Pi^{(m)}(\mathbf{r}, \eta) \equiv \Delta_{T2}^{(m)}(\mathbf{r}, \eta) + 12\sqrt{6}\Delta_{+,2}^{(m)}(\mathbf{r}, \eta) + 12\sqrt{6}\Delta_{-,2}^{(m)}(\mathbf{r}, \eta), \quad (8)$$

\mathbf{r} is the comoving coordinate. In equation 7, the dot stands for the time derivative, σ_T is the Thomson cross section, and n_e is the free electron number density which can be written as $n_e(\mathbf{r}, \eta) = \bar{n}_e(\eta)[1 + \delta_e(\mathbf{r}, \eta)]$, with δ_e and \bar{n}_e the fluctuation and the background of the electron number density, respectively. The electron density fluctuations can be due to matter density perturbations or to spatial variations of the ionisation fraction. Replacing $n_e(\mathbf{r}, \eta)$ in equation 7 by its full expression allows us to separate first order effects (proportional to \bar{n}_e) from second order effects (proportional to δ_e). Finally, the polarisation perturbations at present can be obtained by integrating the Boltzmann equation (Equation (7)) along the line of sight.

Assuming that primary temperature fluctuations dominate over polarisation perturbations, the polarisation at reionisation is due to coupling between the electron density and the quadrupole moment. The solution for a single Fourier mode, $\Delta_{Q \pm iU}$, of the Boltzmann equation Eq. (7) is then given (e.g. Ng & Ng 1996) by:

$$\Delta_{Q \pm iU}(\mathbf{k}, \hat{\mathbf{n}}, \eta_0) = \sqrt{\frac{6\pi}{5}} \int_0^{\eta_0} d\eta e^{ik(\eta_0 - \eta)\mu} g(\eta) \sum_m {}_{\pm 2}Y_2^m(\hat{\mathbf{n}}) X^{(m)}(\mathbf{k}, \eta), \quad (9)$$

where $X^{(m)}(\mathbf{k}, \eta)$ equals $\Pi^{(0)}(\mathbf{k}, \eta)$ for the first order contribution and $S^{(m)}(\mathbf{k}, \eta) = \delta_e(\mathbf{k}, \tau)Q(\eta)$ for the second order contribution, with $Q(\eta)$ being the radiation quadrupole. The visibility function $g(\eta)$:

$$g(\eta) \equiv -\frac{d\tau}{d\eta} e^{-\tau(\eta)}, \quad (10)$$

provides us with the probability that a photon had its last scattering at η and reached the observer at the present time, η_0 . In equation (10), $\tau(\eta) \equiv \int_\eta^{\eta_0} d\eta' a(\eta') n_e \sigma_T$ is the optical depth and $\mu = \mathbf{k} \cdot \hat{\mathbf{n}}$.

2.2. Constraints on reionisation

As the CMB radiation possesses an rms primary quadrupole moment Q_{rms} , Thomson scattering between the CMB photons and free electrons generates linear polarisation. This is the case at recombination but in particular it is true at reionisation. Re-scattering of the CMB photons at reionisation generates a new polarisation anisotropy at large angular scale because the horizon has grown to a much larger size by that epoch (Ng & Ng 1996). The location of the anisotropy (a bump), ℓ_{peak} , relates to the horizon size at the new “last scattering” and thus depends on the ionisation redshift z_{ion} . A fitting formula was given by Liu et al (2001):

$$\ell_{\text{peak}} = 0.74(1 + z_{\text{ion}})^{0.73}\Omega_0^{0.11}. \quad (11)$$

The height of the bump relates to the optical depth or in other words to the duration of the last scattering. Such a signature (bump at large scales) has first been observed by WMAP (Kogut et al. 2003, Spergel et al. 2003) by correlating the temperature and the polarisation power spectra. The first year WMAP observations constrained the optical depth at reionisation to a high value $\tau \sim 0.17$ and provided a simple model for the reionisation, the ionisation redshift was found to be $z_{\text{ion}} \sim 17$. The optical depth is degenerate with the tilt of the primordial power spectrum.

The WMAP first year result came as a surprise, in the context of earlier studies of the Gunn-Peterson effect inferred to be present in the most distant quasars at $z \sim 6$ (*e.g.* Fan et al. 2003) and of the high temperature of the intergalactic medium at $z \sim 3$ (Theuns et al. 2002). The situation was soon rectified with the WMAP 3 year data release (Spergel et al. 2007). The improved data included an *E*-mode polarisation map. The power spectrum is proportional to τ^2 and the new constraints on polarisation yielded an optical depth $\tau = 0.09 \pm 0.03$. Together with a better understanding of polarisation foregrounds, the improved measurements enabled the degeneracy with the tilt to be reduced. The new tilt value of $n = 0.95 \pm 0.02$ lowers the small-scale power. Despite the reduced WMAP 3 year normalisation, $\sigma_8 = 0.74 \pm 0.06$, the lower optical depth implies that the constraints on the possible sources of reionisation remain essentially unchanged (Alvarez et al. 2006). Precise measurements (cosmic variance-limited) of the *E*-mode polarisation power spectrum will eventually allow us to phenomenologically reconstruct the reionisation history (*e.g.* Hu & Okamoto 2004). This will help constrain the reionisation models and enable us to explore the transition between partial and total reionisation (*e.g.* Holder et al. 2003).

Reionisation must have occurred before $z \sim 6$ and the universe is now generally considered to have become reionised at a redshift between 7 and 20. The major question now is to identify the sources responsible for the reionisation of the universe. The ionising sources cannot be a population of normal galaxies or known quasars. Optical studies of the bright quasar luminosity function (Haiman, Abel & Madau 2001, Wyithe & Loeb 2003), as well the associated X-ray background (Dijkstra, Haiman & Loeb 2004) rule out the known quasar population as a reionisation source. However miniquasars with correspondingly softer spectra could evade this constraint. Recourse must therefore be had to Population III stars or to miniquasars, both of which represent hypothetical but plausible populations of the first objects in the universe that are significant sources of ionising photons.

We discuss theoretical issues in Section 2.3.2. Here we ask whether one can observationally distinguish between the alternative hypotheses of stellar versus miniquasar ionisation sources. The most promising techniques for probing reionisation include 21 cm emission and absorption, Lyman-alpha absorption against high redshift quasars, and the statistics of Lyman-alpha emitters. One distinguishing feature is the intrinsic source spectrum, which is thermal for stars but with a cut-off at a few times the Lyman limit frequency, whereas it is a power-law for miniquasars with a spectrum that extends to higher energies with nearly equal logarithmic increments in

energy per decade of frequency. One can also explore the evolution of the intergalactic medium during reionisation through the study of the redshifted 21 cm hyperfine triplet-singlet level transition of the ground state of neutral hydrogen (HI). This line allows the detection of the HI gas in the early universe. It thus represents a unique way to map the spatial distribution of intergalactic hydrogen (e.g. Madau, Meiksin & Reese 1997, Ciardi & Madau 2003). Therefore it permits, in principle, a reconstruction of the reionisation history as governed by the first luminous sources. The size of the ionised structures that could be detected depends on the design of future radio telescopes. The forthcoming radio telescope, in the frequency range 80-180 MHz, LOw Frequency ARray (LOFAR)‡ should have the sensitivity and resolution (~ 3 arc minutes) needed. Using cosmological radiative transfer numerical computations with an idealised LOFAR array, Valdes et al. (2006) have simulated observations of the reionisation signal for both early and late reionisation scenarios. They show that if reionisation occurs late, LOFAR will be able to detect individual HI structures on arc minute scales, emitting at a brightness temperature of ≈ 35 mK as a 3σ signal in about 1000 hours of observing time. Zaroubi & Silk (2005) showed that we could even distinguish between stars and miniquasars as sources of reionisation since there is a dramatic difference between these two cases in the widths of the ionisation fronts. Only the miniquasar model translates to scale-dependent 21 cm brightness temperature fluctuations that should be measurable by forthcoming LOFAR studies of the 21 cm angular correlation function (Zaroubi et al. 2007). A hitherto undetected population of Lyman alpha-emitting galaxies is a possible reionisation source and may be visible during the pre-reionisation era. One can hope to detect such objects to $z \sim 10$ relative to the damping wing of the Gunn-Peterson absorption from the neutral intergalactic medium outside their HII regions (Gnedin & Prada 2004).

2.3. Secondary anisotropies from reionisation

When reionisation is completed, the scattering between CMB photons and electrons moving along the line of sight generates secondary anisotropies through the Doppler effect. The amplitude of the fluctuations is given by:

$$\frac{\Delta T}{T}(\theta) = \int d\eta a(\eta) g(\eta) v_r(\theta, \eta) = - \int dt \sigma_{Te} e^{-\tau(\theta, t)} n_e(\theta, t) v_r(\theta, t) \quad (12)$$

with $v_r(\theta, t)$ the velocity along the line of sight (i.e. radial velocity). The electron density can be written as $n_e(\theta, t) = n(\theta, t) \times \chi_e(\theta, t)$ the product of the matter density $n(\theta, t)$ and the ionisation fraction $\chi_e(\theta, t)$. Both quantities vary around their average values. We can finally write the electron density as $n_e(\theta, t) = \bar{n}_e(\theta, t)[1 + \delta + \delta_{\chi_e}]$, with $\bar{n}_e(\theta, t)$ the average number of electrons and δ and δ_{χ_e} the fluctuations of density field and ionisation fraction respectively.

By replacing the electron density expression in equation 12, we can see that there is a first order effect which suffers from cancellations, and two second order effects

‡ www.lofar.org

which affect the probability of scattering of the CMB photons (e.g. Dodelson & Jubas 1995). They both generate secondary anisotropies. They are sometimes referred to as modulations of the Doppler effect (i.e. the velocity field) by density and ionisation spatial variations.

2.3.1. Density-induced anisotropies These are produced when the ionisation fraction is homogeneous, i.e. reionisation is completed, and when the Doppler effect is modulated by spatial variations of the density field. The computation in the linear regime first appeared in Sunyaev & Zel'dovich (1970), was revisited by Vishniac and Ostriker (Ostriker & Vishniac 1986, Vishniac 1987), and is known as the Ostriker-Vishniac (OV) effect (see also Dodelson & Jubas (1995), Hu & White (1996), Jaffe & Kamionkowski (1998), Scannapieco (2000), Castro (2003)). The OV effect is a second order effect which weights as density squared ($\propto \delta^2$) and peaks at small angular scales (arc minutes) with an *rms* amplitude of the order of μK . The computation of the density-induced anisotropies can be generalised to mildly non-linear and non-linear regimes. Because these regimes are difficult to describe analytically, a more appropriate tool is numerical simulations (e.g. Gnedin & Jaffe 2001, Zhang, Pen & Trac 2004), see also Figure 4. However, one can also use the halo model (see review by Cooray & Sheth 2002) to model analytically the mildly non-linear regime as done for example by Santos et al. (2003) or Ma & Fry (2000, 2002). These studies showed that reionisation-induced anisotropies are dominated by the OV effect at large angular scales. The contribution from non-linear effects only intervenes at smaller scales with amplitudes of \sim a few μK at $\ell > 1000$ (Figure 3). The non-linear contributions from collapsed and fully virialised structures such as galaxy clusters is historically known as the kinetic Sunyaev-Zel'dovich effect and will be discussed separately in section 5.

2.3.2. Sources of patchy reionisation Before reionisation is completed, ionised and neutral regions of the universe co-exist. This is called the inhomogeneous reionisation (IHR) regime. In that case, the Doppler effect is modulated by variations of the ionisation fraction χ_e . Aghanim et al. (1996) computed the first estimate of the power spectrum of secondary anisotropies induced by early QSOs ionising the universe from $z = 12$ to complete reionisation at $z \sim 6$. They predicted a large contribution from such fluctuations whose amplitude and distribution depended on the number density of sources, their luminosities and their lifetimes. The model was revisited by Gruzinov & Hu (1998) and Knox, Scoccimarro & Dodelson (1998) who added the effect of spatial correlations between sources. The effect of an IHR on the CMB has been recently revisited in the context of a reionisation scenario compatible with WMAP data. In this work, Santos et al. (2003) found that secondary fluctuations from IHR dominates over density-modulated (OV) anisotropies. IHR is intimately linked to the nature of the ionising sources, to their formation and evolution history and to their spatial distribution. As a result, predictions of the IHR effect span a large range of amplitudes and angular scales. A precise forecast of the effects of IHR on the CMB anisotropies

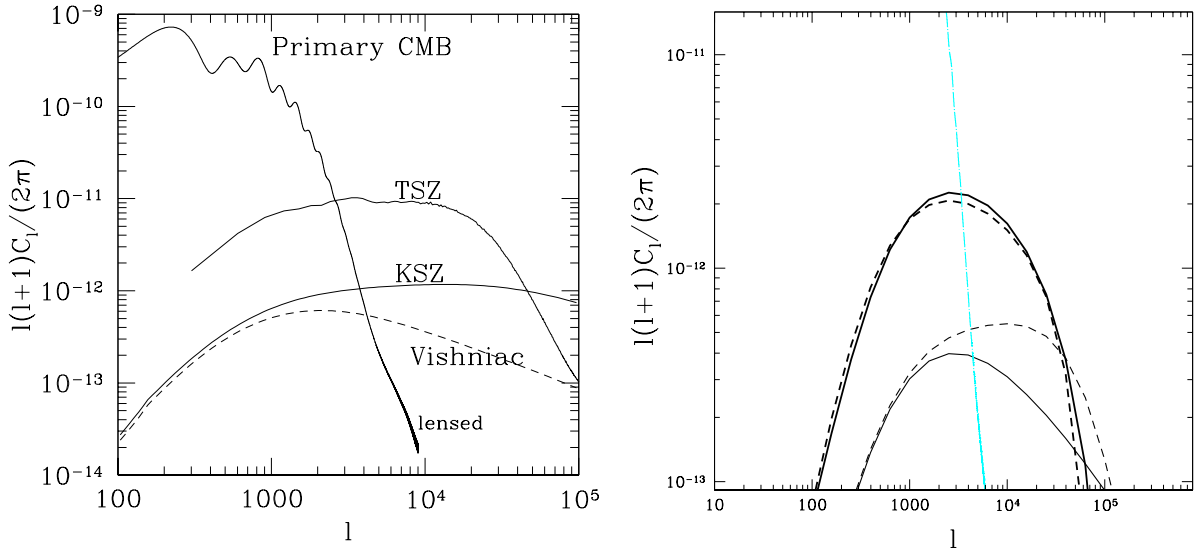


Figure 3. Left panel, from Zhang, Pen & Trac (2004): The Doppler effect induced temperature anisotropies (kinetic SZ) from numerical simulations. The results include non-linear regime and are obtained by assuming universe was reionised at $z = 16.5$ and remained ionised after that. The contribution from the linear regime, OV effect, (dashed line) is plotted for comparison, together with primary power spectrum and thermal SZ spectrum in the R-J region (see Sect. 5). Right panel, from Santos et al. (2003): Analytic computation of the secondary anisotropies produced by reionisation. Top thick lines are for the inhomogeneous reionisation-induced fluctuations. Bottom lines are for density-induced fluctuations where the solid thin line is for the linear OV effect and the dashed for the non-linear contribution to OV.

requires a precise treatment of the reionisation history of the universe together with the formation of the first ionising sources including radiative transfer (e.g. Iliev et al. 2007a).

Stellar ionising sources have been studied by many authors (e.g. Cen 2003, Ciardi, Ferrara & White 2003, Haiman & Holder 2003, Wyithe & Loeb 2003, Sokasian et al. 2003, Somerville & Livio 2003). The first cosmological 3D simulations incorporating radiative transfer of inhomogeneous reionisation by protogalaxies were performed by Gnedin (2000). He found that reionisation by protogalaxies spans the redshift range from $z \sim 15$ until $z \sim 5$. HII regions gradually expand into the low-density intergalactic medium, leaving behind neutral high-density protrusions, and within the next 10% of the Hubble time, the HII regions merge as the ionising background rises by a large factor. The remaining dense neutral regions are gradually ionised. Sources as luminous as protogalaxies are too rare at these redshifts and recourse must be had to a population of galactic building blocks that are plausibly associated with dwarf galaxies or miniquasars.

Recent studies find in general that in order to provide enough ionising flux at, or before, $z = 15$, for the usual scale-invariant primordial density perturbation power spectrum, one needs Population III stars, which provide about 20 times more ionising

photons per baryon than Population II (Schaefer 2002, Bromm, Kudritzki & Loeb 2001), or an IMF that is initially dominated by high mass stars (Daigne et al. 2004). This is in agreement with recent numerical simulations of the formation of the first stars from primordial molecular clouds suggesting that the first metal-free stars were predominantly very massive, $m_{\text{star}} \geq 100M_{\odot}$ (Abel, Bryan & Norman 2000, 2002, Bromm, Coppi & Larson 2002). In general, possibly unrealistically high ionising photon escape fractions are required for a stellar reionisation source (Sokasian et al. 2004).

Miniquasars have also been considered as a significant ionising source (e.g. Ricotti & Ostriker 2004, Ricotti, Ostriker & Gnedin 2005, Madau et al. 2004, Oh 2001, Dijkstra, Haiman & Loeb 2004). In view of the correlation between central black hole mass and spheroid velocity dispersion (Ferrarese & Merritt 2000, Gebhardt et al. 2000), miniquasars are as plausible ionisation sources as are Population III stars, whose nucleosynthetic traces have not yet been seen even in the most metal-poor halo stars nor in the high z Lyman alpha forest. The observed correlation suggests that seed black holes must have been present before spheroid formation. Recent observations of a quasar host galaxy at $z = 6.42$ (Walter et al. 2004) (and other AGN) suggest that supermassive black holes were in place and predated the formation of the spheroid. Theory suggests that the seeds from which the Super Massive Black-Holes formed amounted to at least $1000M_{\odot}$ and were in place before $z \sim 10$ (Islam, Taylor & Silk 2003, Madau & Reese 2001, Volonteri, Haardt & Madau 2003).

Decaying particles remain an option for reionisation that is difficult to exclude. One recent example is provided by a decaying sterile neutrino whose decay products, relativistic electrons, result in partial ionisation of the smooth gas (Hansen & Haiman 2004). A neutrino with a mass of ~ 200 MeV and a decay time of $\sim 10^8$ yrs can account for an electron scattering optical depth as high as 0.16 without violating existing astrophysical limits on the cosmic microwave and gamma-ray backgrounds. In this scenario, reionisation is completed by subsequent star formation at lower redshifts. Dark matter annihilation during hydrogen recombination (at $z \sim 1000$) can modify the recombination history of the Universe (Padmanabhan & Finkbeiner 2005). The residual ionization after recombination is enhanced. The surface of last scattering is broadened, partially suppressing the small-scale primary temperature fluctuations and enhancing the polarization fluctuations. In addition, the extended recombination phase weakens some of the cosmological parameter constraints, most notably on the scalar spectral index (Bean, Melchiorri & Silk 2007).

2.4. Second order Polarisation at reionisation

In this section, we focus on the polarisation signal at small scales induced at reionisation by the coupling between primary quadrupole and fluctuations in the electron density at the new last scattering surface. These electron density fluctuations can again have two origins: They are either due to density fluctuations in a homogeneously ionised universe (Seshadri & Subrahmanian 1998, Hu 2000), or they can be associated with fluctuations

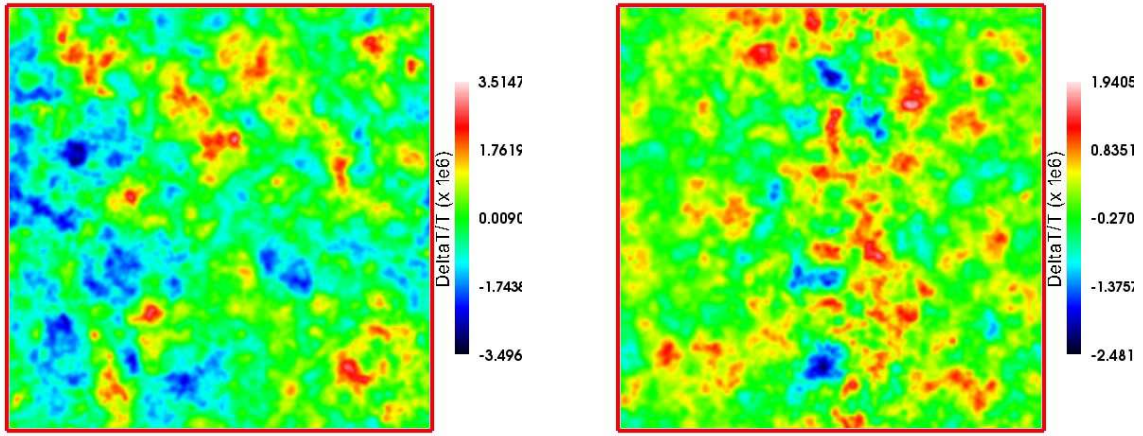


Figure 4. From Iliev et al. (2007b): Doppler effect induced temperature fluctuation maps from numerical simulations including radiative transfer (right panel). The left panel shows the result after correcting for the missing large-scale velocities.

of the ionising fraction in an inhomogeneously ionised universe (Hu 2000, Mortonson & Hu 2007). Additional polarisation fluctuations from collapsed and virialised structures, such as galaxy clusters, will be treated separately in Sect. 9.

The dominant second order polarisation fluctuations are due to coupling between primary quadrupole anisotropy Q_{rms} and electron density fluctuations δ_e and are given by:

$$\Delta_{Q \pm iU} \propto \int d\tau g(\tau) Q_{\text{rms}} \delta_e \propto \kappa Q_{\text{rms}} \delta_e. \quad (13)$$

The quadrupole considered for generating polarisation through Thomson scattering is in general the primary quadrupole. However in the rest frame of the scattering electrons, a quadrupole moment is also generated from quadratic Doppler effect (Sunyaev & Zel'dovich 1980). The amplitude of the polarisation induced by coupling with electron density fluctuations in this case is smaller than those produced by the primary quadrupole as discussed by (Hu 2000).

In all cases, the polarisation signal from secondary anisotropies takes place at small angular scales, and has quite a small amplitude (Figure 5). Liu et al. (2001) found a typical amplitude of $\sim 10^{-2} \mu\text{K}$ in a pre-WMAP reionisation model using numerical simulations to describe reionisation (Figure 5 left panel). More recently, this result was confirmed by Doré et al. (2007) who also used numerical simulation compatible with current cosmological constraints. In a model reproducing the high optical depth suggested by 1st year WMAP observations, Santos et al. (2003) generalised the computations to the non-linear regime using the halo model. They conclude that the modulation by ionising fraction inhomogeneities, i.e. patchy reionisation, dominates over the modulation by density fluctuations but the amplitudes remain small (Figure 5, right panel).

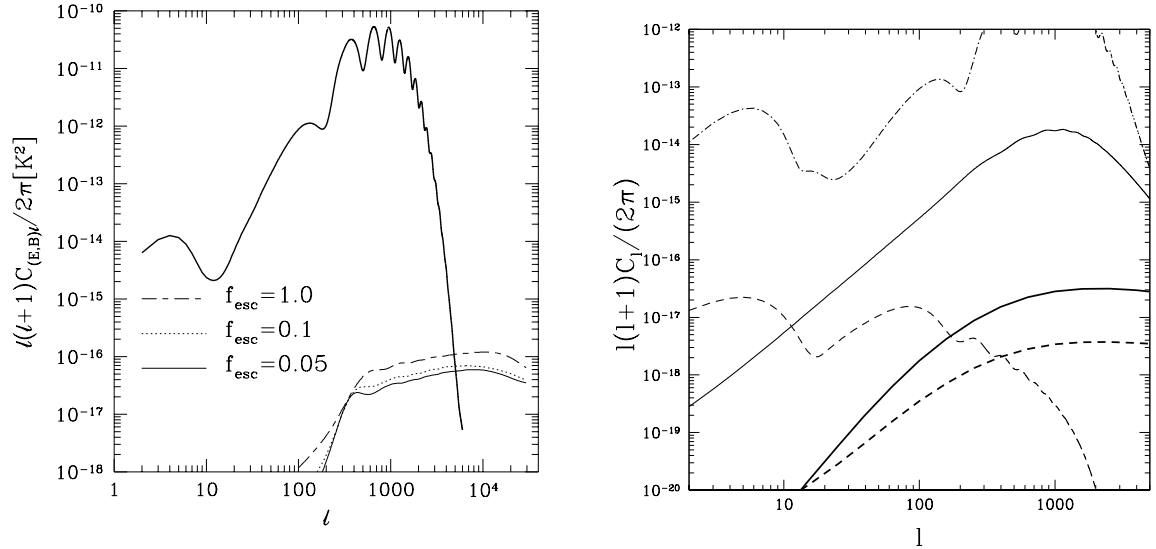


Figure 5. Left panel, from Liu et al. (2001): Reionisation-induced polarisation (dashed, dotted and thin solid lines) with the first-order E -mode power spectrum (thick solid line). The second order reionisation-induced polarisation is computed from numerical simulations with different escape fractions of ionising photons f_{esc} . Right panel, from Santos et al. (2003): B -mode polarisation with contributions from lensing (thin solid line) and tensor modes (thin-dashed). The contribution, at reionisation, from density (thick dashed) and ionisation (thick solid) modulated scattering is also shown. The density modulated contribution uses the halo model for non-linear corrections. Also shown for comparison is the first-order E -mode power spectrum (dot-dashed line).

3. Secondary effects from large-scale structure

3.1. The ISW effect

After decoupling, as the universe continues to expand, seeds of cosmic structures that scattered the CMB at the last scattering surface grow due to gravitational instability giving rise to large scale structure. The gravitational potential evolves with evolution of the structure and the CMB photons are influenced once again by the change in the gravitational potential which they traverse. One can subdivide the gravitational secondaries broadly into two classes, one arising from the time-variable metric perturbations and the other due to gravitational lensing. The former is generally known as the integrated Sachs-Wolfe effect (Sachs & Wolfe 1967) in the linear region and goes by the names of Rees-Sciama effect and moving-halo effect (sometimes called the proper-motion effect) in the non-linear regime. The integrated Sachs-Wolfe (ISW) effect is further divided in the literature into an early ISW effect and a late ISW effect. The early ISW effect is only important around recombination when anisotropies can start growing and the radiation energy density is still dynamically important. The final anisotropy for these gravitational secondaries depends on the parameters of the

background cosmology and is also tightly coupled to the clustering and the spatial and temporal evolution of the intervening structure.

In general, the temperature anisotropies, along any direction \mathbf{n} , associated with the gravitational potential and proper motions can be written in the form (Sachs & Wolfe 1967, Hu, Scott & Silk 1994, see Martinez-González, Sanz & Silk 1990, for a simple derivation)

$$\frac{\Delta T(\mathbf{n})}{T} = (\phi_{\text{rec}} - \phi_0) + \int_{\eta_{\text{rec}}}^{\eta_0} 2\dot{\phi}d\eta, \quad (14)$$

where η_{rec} is the recombination time, η_0 the present time and ϕ is the gravitational potential. The first term represents the Sachs-Wolfe effect due to different gravitational potentials at recombination and present. The second term is the integrated ISW effect and depends on the time derivative of ϕ with respect to the conformal time. The numerical factors multiplying each term in the equation depends on the choice of gauge and hence differ among various authors. A point to note is that the temperature change due to the gravitational redshifting of photons is frequency independent (in contrast to the SZ effect) and cannot be separated from the primary anisotropies using spectral information only.

The origin of the late ISW effect lies in the decay of the gravitational potential (Kofman & Starobinsky 1985, Mukhanov, Feldman & Brandenberger 1992, Kamionkowski & Spergel 1994). When the CMB photons pass through structures they are blue and red-shifted when they respectively enter and exit the gravitational potential wells of the cosmic structures. The net effect is zero except in the case of a non-static universe. This can happen naturally in a low matter density universe and at the onset of dark energy (or spatial curvature) domination typically occurring at late times. The increased rate of expansion of the universe reduces the amplitude of gravitational potential. The differential redshift of the photons climbing in and out of the potential gives rise to a net temperature anisotropy. There is one qualitative difference between the early ISW and the late ISW effects. For the late ISW effect, the potential decays over a much longer time (of the order of the present day Hubble time). Thus the photons have to travel through multiple peaks and troughs of the perturbations and the chances of cancellation of the coherence in gravitational redshifts becomes greater leaving, little net perturbation to the photon temperature (Tuluie, Laguna & Anninos 1996).

To study the amplitude of the late ISW effect, we start by constructing its power spectrum. We expand the potential time derivative, $\dot{\phi}$, in spherical basis to get the expression for the power spectrum in a flat universe as

$$C_\ell = (4\pi)^2 \int k^2 P_\phi(k) dk \left[\int_0^{\eta_0} 2\dot{F}(\eta) j_\ell(kr) d\eta \right]^2, \quad (15)$$

where $j_\ell(x)$ is the spherical Bessel function and r is the comoving distance between the photon at a conformal time η and the observer. $F(k, \eta) = D/a$ is the growth rate of potential, where a is the expansion factor normalised to have $a_0 = 1$ and D is the linear

growth factor. $D(z)$ governs the growth of amplitude of density perturbation with time. It is simply equal to unity for $\Omega_m = 1$ flat universe. For universe with both matter and vacuum energy (i.e Ω_Λ), one has accurate fitting formulae for the growth function (Carroll, Press & Turner 1992). The power spectrum of the potential, P_ϕ , is given by

$$\langle \phi(\vec{k})\phi(\vec{k}') \rangle = (2\pi)^3 \delta_D(\vec{k} + \vec{k}') P_\phi(k). \quad (16)$$

The main assumption in writing equation (15) is that in the linear regime the mode does not change in phase and so the change in its amplitude with time is simply described through the growth factor. The equation also ignores gravitational lensing to be discussed later.

In the small angular scale limit and under the assumptions that the correlations at a distance k^{-1} are slowly changing on a timescale $(ck)^{-1}$, the radial integral in equation (15) can be broken into a product of the spherical Bessel function $j_\ell(kr)$ and a slowly changing function of time. Taking out the slowly varying part outside the radial integral and using the large ℓ approximation for the Bessel function, we can use the Limber approximation to get

$$C_\ell = 32\pi^3 \int_0^{\eta_0} \frac{\dot{F}^2(k = \ell/r, \eta) P_\phi(k = \ell/r) d\eta}{r^2}, \quad (17)$$

From the above equation, we can define the power spectrum of the potential time derivative as $P_{\dot{\phi}}(k, \eta) = \dot{F}^2(k, \eta) P_\phi(k)$. Note that in the non-linear regime, the growth factor depends on the wavenumber k . However, equation (17) is still valid due to the slow time dependence of $P_{\dot{\phi}}$.

To calculate $\dot{\phi}$ as a function of time and scale, we relate the potential to the matter density via the Poisson equation. In k -space, this can be written as

$$\phi + \frac{3}{2} \frac{\Omega_m}{a} \left(\frac{H_0}{k} \right)^2 \delta = 0, \quad (18)$$

where Ω_m is the present day matter density parameter and δ is the matter density perturbation.

At this point it is straightforward to calculate the late ISW effect once we put in an appropriate expression for $F(\eta)$. After we do this, the first thing to notice is that for a flat matter-dominated $\Omega_m = 1$ universe, $D(\eta) \propto a(\eta)$, and so in the linear regime there is no ISW effect. Until non-linear effects are considered, the late ISW effect occurs only in open and lambda dominated universes. The linear ISW effect, the non-linear ISW effect and gravitational lensing effect are shown in figure 6.

The ISW effect is seen mainly in the lowest ℓ -values in the power spectrum (Tuluie, Laguna & Anninos 1996). Its importance comes from the fact that it is very sensitive to the amount, equation of state and clustering properties of the dark energy. Detection of such a signal is, however, limited by cosmic variance. The time evolution of the potential that gives rise to the ISW effect may also be probed by observations of large scale structure. One can thus expect the ISW to be correlated with tracers of large scale

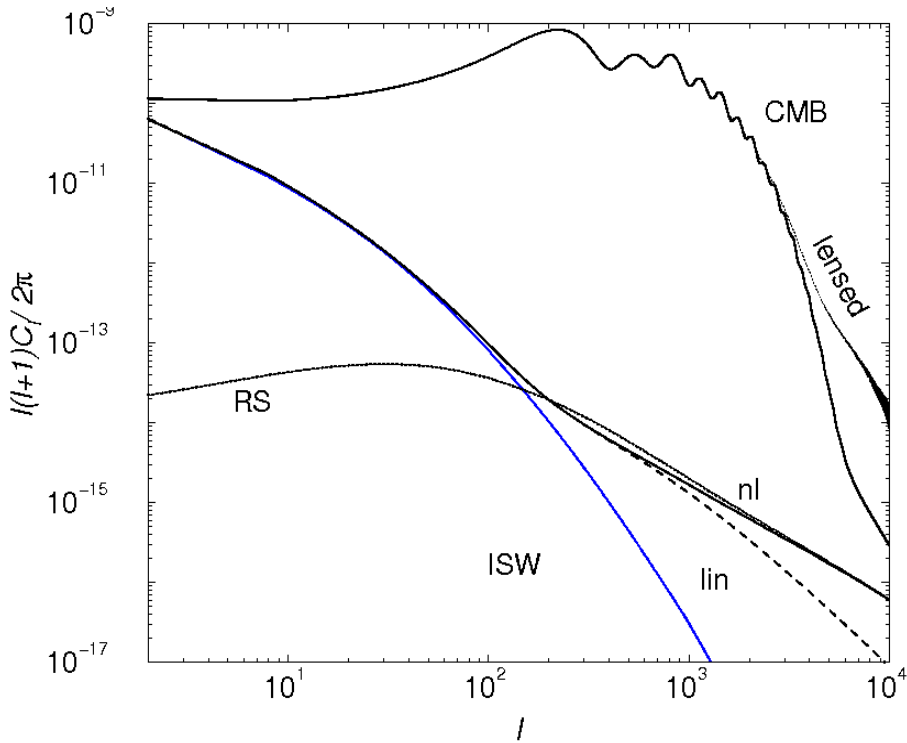


Figure 6. From Cooray (2002a): The power spectrum of the ISW effect, including non-linear contribution. The Rees-Sciama effect shows the non-linear extension. The curve labeled “nl” is the non-linear contribution while the curve labeled “lin” is the contribution from the momentum field under the second order perturbation theory. The primary anisotropy power spectrum accounting for the lensing effect is shown for comparison.

structure. This idea was first proposed by Crittenden & Turok (1996) and has been widely discussed in the literature (Kamionkowski 1996, Kinkhabwala & Kamionkowski 1999, Cooray 2002b, Afshordi 2004, Hu & Scranton 2004). The ISW detection was attempted using the COBE data and radio sources or the X-ray background (Boughn, Crittenden & Turok 1998, Boughn & Crittenden 2002) without much success. The recent WMAP data (Spergel et al. 2003, 2007) provide for the first time all-sky high quality CMB measurements at large scales. Those data were used recently in combination with many large scale structure tracers to detect the ISW signal. The correlations are presently performed mainly using galaxy surveys (2MASS, SDSS, NVSS, SDSS, APM, HEAO), see Figure 7 for a recent result. However, despite numerous attempts both in real space (Diego, Hansen & Silk 2003, Boughn & Crittenden 2004, Fosalba & Gaztanaga 2004, Hernandez-Monteagudo & Rubiono-Martin 2004, Nolta et al. 2004, Afshordi, Lin & Sanderson 2005, Padmanabhan et al. 2005, Gaztanaga, Maneram & Multamaki 2006, Rassat et al. 2006) or in the wavelet domain (e.g. Vielva, Martinez-Gonzalez & Tucci 2006), there is very weak (or null) detection of the ISW effect through correlations. The ISW effect provides and offers a promising new way of inferring cosmological constraints (e.g. Corasaniti, Gianantonio & Melchiorri 2005, Pogosian

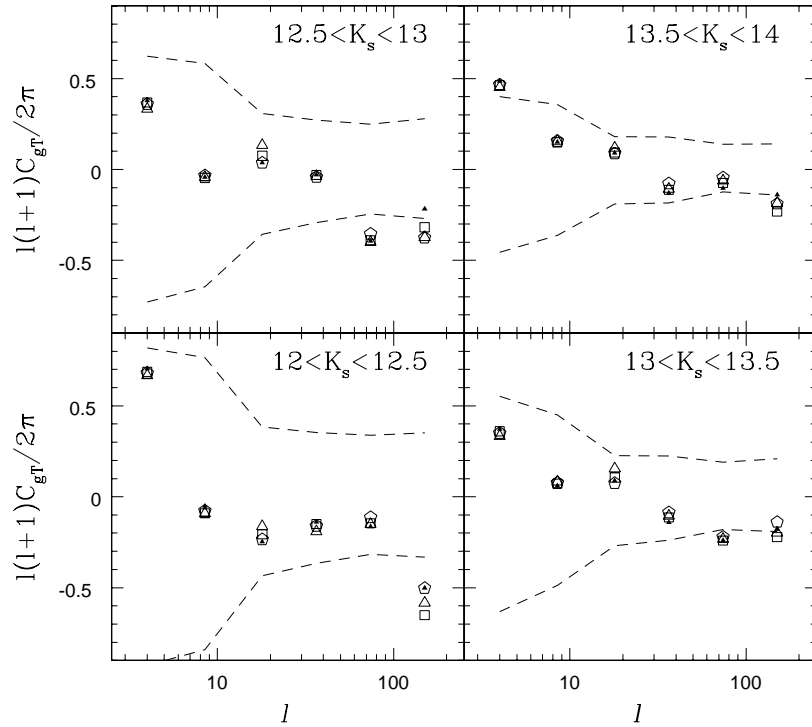


Figure 7. From Rassat et al.(2006): Results of the cross-correlation $C_{gT}(\mu K)$ for the Internal Linear Combination (small triangle), Q (open triangle), V (open square), and W (open pentagon) WMAP maps with different magnitude bins of the 2MASS galaxy survey. The dashed lines are 1σ error bars about the null hypothesis. An ISW effect is expected to be achromatic, which is observed, but the null hypothesis is not ruled out.

2006).

3.2. The Rees-Sciama and the moving halo effects

As mentioned in the previous section, the ISW is linear in first order perturbation theory. Cancellations of the ISW on small spatial scales leave second order and non-linear effects. In hierarchical structure formation, the collapse of a structure can present a changing gravitational potential to passing photons. If the photon crossing time is a non-negligible fraction of the evolution time-scale, the net effect of the blue and redshift is different from zero and the path through the structures leaves a signature on the CMB. This was first pointed out by Reese & Sciama (1968) for evolving density profiles of any individual large scale structures (see also Dyer 1976). This goes by the name of the Rees-Sciama (RS) effect. Subsequently, there have been many studies of the RS effect from isolated structures using the ‘Swiss-Cheese’ model (Kaiser 1982, Thompson & Vishniac 1987, Martinez-Gonzalez, Sanz & Silk 1990, Chodorowski 1992,1994), Tolman-Bondi

solutions (Panek 1992, Lasenby et al.1999) and from clustering (Fang & Wu 1993). Calculations have also been done for non-linear regimes, both analytically (e.g. Cooray 2002a) and using numerical simulation (e.g. Seljak 1996a, Dabrowski et al.1999). Much of this work was concerned with the possible contamination of primary anisotropies by the RS effect, since both are present at similar angular scales and cannot be distinguished using multi-frequency observations. As we shall see below, the RS effect is negligibly small at all angular scales (Figure 6). The non-linear evolution of primordial scalar fields generates some vector and tensor modes, inducing, in turn, B mode polarisation anisotropies (Mollerach, Harary & Matarrese 2004). This secondary signal although smaller than the one associated with gravitational lensing effects (see Section 4) might constitute a limiting background for future CMB polarisation experiments.

For an isolated collapsed structure, there can be a change in the gravitational potential along the line of sight due to its bulk motion across the line of sight. For clusters of galaxies, this was first shown by Birkinshaw & Gull (1983); (see also Birkinshaw (1989) for a correction to the original results) as a way to measure their transverse velocities and is known as the “moving-halo” effect. At the same time, these authors pointed out to the fact that CMB anisotropies should be gravitationally lensed by such moving halos. A similar proposal for temperature anisotropies due to the presence of cosmic string wakes was proposed by Kaisser & Stebbins (1984) (see also Stebbins 1988). The CMB photons entering ahead of a moving structure (galaxy cluster or super cluster) traversing the line of sight will be redshifted, while those entering the structure wake are blueshifted. The transverse motion induces a bipolar imprint in CMB whose amplitude is proportional to the velocity v_t and to the depth of the potential well M_{tot} and aligned with the direction of motion. The effect of moving local mass concentrations like the Great Attractor or the Shapley concentration was recently investigated Cooray & Seto (2005) (see also Tomita 2005, 2006) to explain the quadrupole and octopole alignment in the WMAP first year data. This effect was found to be much smaller than that required for explaining the low multipole anomalies (but see Vale (2005)). In general, the bulk motion of dark matter halos of all masses would contribute to this effect and is found to be negligible for all angular scales (Aghanim et al.1998, Molnar & Birkinshaw 2000). Lensing by moving massive clusters only induce a few μK temperature distortion (Dodelson 2004, Holder & Kosowsky 2004).

We can try to combine the temperature anisotropy due to the RS and moving-halo effects to make a simple estimate ‘non-linear ISW’ effect. For an isolated structure, the anisotropy can be written as

$$\frac{\Delta T}{T} \sim \frac{\phi}{t_c} \delta t + \frac{v_t}{d} \delta t, \quad (19)$$

where t_c is the characteristic dynamical time namely the free-fall time, δt is the photon crossing time, $d \sim c \delta t$ is the physical size. The potential ϕ can be determined from $\phi \sim M_{\text{tot}}/d$. The matter crossing time d/v_t is taken as the evolution time t_c . From energy balance arguments, we get $\phi \sim v_t^2$. Thus, we have $t_c \sim d/\phi^{1/2}$. Putting all these

together in equation (19), we can write

$$\frac{\Delta T}{T} \sim \phi^{3/2} + v_t \phi. \quad (20)$$

The first term is the RS term and the second is the moving-halo term. Finally, from linear perturbation theory, we have $v_t \sim \phi(1+z)^{-3/2}(dH_0)^{-1}$ and $\delta \sim \phi(1+z)^{-3}(dH_0)^{-2}$, so we can rewrite equation (20) as

$$\frac{\Delta T}{T} \sim 10^{-7} (\delta^{3/2} + \delta^2) \left(\frac{d}{14h^{-1}\text{Mpc}} \right)^3 (1+z)^{9/2}. \quad (21)$$

The above estimate is rather crude since we have used linear perturbation theory to describe non-linear regions. Moreover, it only applies to an isolated structure (for which the RS effect is independently treated from the velocity effect) and a proper justification can be only done using simulations where the phase dependence of the growth factor is naturally taken into account. The non-linear ISW effect can also be calculated using the halo model which allows us to describe both the density and velocity fields of the large scale structure in a coherent way (for details see Cooray & Sheth 2002). In such an approach, the basic idea is to take the time derivative of the Poisson equation (i.e. equation (18)) and using the continuity equation in k -space given by

$$\dot{\delta} + i\vec{k} \cdot \vec{p} = 0, \quad (22)$$

where the momentum density field $\vec{p}(\vec{r}) = (1+\delta)\vec{v}(\vec{r})$; one then obtains the following expression:

$$\dot{\phi} = \frac{3}{2} \frac{\Omega_m}{a} \left(\frac{H_0}{k} \right)^2 \left(\frac{\dot{a}}{a} \delta + i\vec{k} \cdot \vec{v} \right), . \quad (23)$$

This relation connects the potential time derivative to the density and the momentum density. One can now obtain the power spectrum of $\dot{\phi}$ by averaging over all the k -modes. It is easy to see from equation 23 that the power spectrum will involve correlation between density fields and time derivatives of density fields, as well as cross-correlation between density and momentum fields. Thus the general result has information about both the classical RS effect as well as the moving-halo effect. Numerical simulations capture an important point that is often missed in analytical perturbation theory calculations which is that in the strongly non-linear regime the power spectrum of $\dot{\phi}$ is dominated by the momentum density.

The angular power spectrum including the non linear ISW effect is shown in figure 6. For all cases, the temperature anisotropy $\frac{\Delta T}{T}$ is between 10^{-6} and 10^{-7} . The amplitude of the power spectrum goes as the normalisation parameter σ_8^4 . Moreover for a given σ_8 , change in $\Omega_m h$ significantly affects the power spectrum at the low ℓ -values. Depending upon the background cosmology, the power spectrum peaks at ℓ between 100 and 300 and is always 2–3 orders of magnitude less than primary CMB power spectrum. The non linear ISW effect becomes equal to the primary anisotropy at $\ell \sim 5000$. However, well before this equality is reached, it is overtaken by other sources of secondary anisotropies such as the thermal SZ effect.

4. Lensing of the CMB

4.1. Lensing by large scale structure

As the CMB photons propagate from the last scattering surface, the intervening large scale structure can not only generate new secondary anisotropies (as shown in the last section, Sect. 3) but can also gravitationally lens the primary anisotropies (Blanchard & Schneider 1987, Kashlinsky 1988, Linder 1988, Cayon, Martinez-Gonzalez & Sanz 1993, Seljak 1996b, Metcalf & Silk 1997, Hu 2000). For a detailed description of the process we refer the reader to a recent and thorough review by Lewis & Challinor (2006). Formally, lensing does not generate any new temperature anisotropies. There are indeed no new anisotropies generated if the gravitational potential is not evolving (see previous section for this case), whereas lensing occurs whenever there is a gravitational potential. Since lensing conserves surface brightness, the effect of gravitational lensing of the primary CMB can only be observed if the latter has anisotropies. In this case lensing magnifies certain patches in the sky and demagnifies others (Figure 9). If the primary CMB were completely isotropic, one would not be able to differentiate between the different (de)magnifications.

For gravitational lensing, the absolute value of the light deflection does not matter. What matters is the relative deflection of close-by light rays. If all the adjacent CMB photons are isotropically deflected, there would only be a coherent shift relative to the actual pattern. However, if they are not isotropically deflected, then the net dispersion of the deflection angles would change the intrinsic anisotropies at the relevant angular scales. The net result of gravitational lensing is to transfer power from larger scales (thus smoothing the initial peaks in the CMB power spectrum) to smaller scales. In the following, we detail the lensing effects on both the temperature anisotropies as well as on the polarised signal.

In order to understand the effects of gravitational lensing on the CMB power spectrum we have to write its effect on a single temperature and polarisation anisotropy. Gravitational lensing modifies the CMB anisotropies, which are then measured as an angular displacement in the following way

$$T_{\text{obs}}(\theta) = T(\theta + \xi(\theta)), \quad (24)$$

where θ is the original undistorted angle. However, it is inaccurate to approximate the observed temperature by a truncated expansion in the deflection angle. This is only a good approximation on scales where the CMB is very over the relevant lensing deflection, i.e. on large scales, or very small (see Challinor & Lewis 2005). In the weak lensing limit, the regime of interest for CMB studies, we can use the perturbative approach and write the lensed CMB anisotropies as:

$$T_{\text{obs}}(\theta) \sim T(\theta) + \xi^i(\theta) \cdot T_{,i} + \frac{1}{2} \xi^i(\theta) \xi^j(\theta) \cdot T_{,ij} \quad (25)$$

with ξ given by:

$$\xi_i(\theta) = \frac{-3}{2} \Omega_0 \int \frac{dz'}{H(z')} \frac{1}{a} \frac{D_0(z') D_0(z, z')}{D_0(z)} \varphi_{,i}^{(1)}(\theta, z), \quad (26)$$

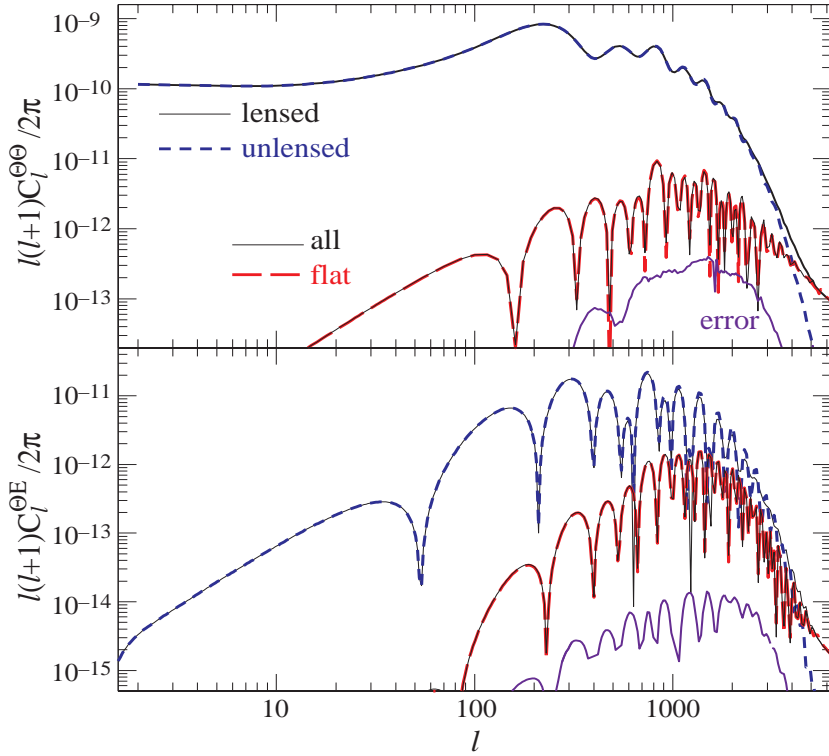


Figure 8. From Hu (2000): The lensed and unlensed power spectra. The error due to the flat sky approximation with respect to the all sky computation is also shown. The corrections of the all sky computations can be even larger (see Challinor & Lewis 2005)

$D_0(z, z')$ is the angular diameter distance between redshifts z and z' and $\varphi_{,i}^{(1)}(\theta, z)$ is the perpendicular gradient of the Newtonian potential in the direction θ . In the same way, the modified polarisation anisotropy is written as $P_{\text{obs}}(\theta) = P(\theta_{\text{obs}}) = P(\theta + \xi)$ which similarly gives second order:

$$P_{\text{obs}}(\theta) \sim P(\theta) + \xi^i(\theta) \cdot P_{,i} + \frac{1}{2} \xi^i(\theta) \xi^j(\theta) \cdot P_{,ij} \quad (27)$$

4.1.1. Lensed CMB power spectrum In order to have an idea of the effect of gravitational lensing on the CMB power spectrum, we can consider its counterpart the two point correlation function. In the small angle approximation, we can use the perturbative approach to second order and obtain:

$$\begin{aligned} \langle T_{\text{obs}}(0)T_{\text{obs}}(\theta) \rangle &= \langle T(0 + \xi(0))T(\theta + \xi(\theta)) \rangle \\ &= \langle T(0)T(\theta) \rangle + \langle \xi^i(0)\xi^j(\theta) \rangle \langle T_{,i}(0)T_{,j}(\theta) \rangle \\ &\quad + \frac{1}{2} \langle \xi^i(0)\xi^j(0) \rangle \langle T_{,ij}(0)T(\theta) \rangle + \frac{1}{2} \langle \xi^i(\theta)\xi^j(\theta) \rangle \langle T(0)T_{,ij}(\theta) \rangle \end{aligned}$$

The lensed power spectrum C_{ℓ}^{lens} as a function of the unaltered power spectrum C_{ℓ} is obtained after Fourier transformation, which is directly associated with multipole

decomposition. It is given by

$$C_\ell^{\text{obs}} = C_\ell \left[1 - \int \frac{d^2 k}{(2\pi)^2} \frac{(\ell \cdot \mathbf{k})^2}{k^4} \bar{P}(k) \right] + \int \frac{d^2 k}{(2\pi)^2} \frac{(\ell \cdot \mathbf{k})^2 - k^4}{k^4} \bar{P}(k) C_{|\ell-\mathbf{k}|}, \quad (28)$$

where \bar{P} is the projected power spectrum of the lensing convergence. A generalisation of the computation (Hu 2000) shows that the errors introduced by the flat sky approximation are negligible as shown in figure 8.

The expression of C_ℓ^{obs} clearly shows the effect of the gravitational lensing on the CMB:

- The first term is a renormalisation due to the second order effect introduced by the lenses in the perturbative formulae.
- The second term is a mode coupling due to the convolution of the unperturbed spectrum by the projected power spectrum \bar{P} . Both cause the smoothing of the acoustic peaks at small scales.

Weak lensing does not introduce any characteristic scale in the CMB. Its effects are mostly noticeable at small scales where they modify the CMB damping tail through power transfer from large to small scales. This increase in power at large ℓ s is significantly smaller than the modifications due to scattering effects (e.g. SZ effect). To identify the effects of gravitational lensing on the CMB it is necessary to explore not only the power spectrum but also higher order moments that possibly reveal the induced non-Gaussian signatures left by the non-linear coupling (Bernardeau 1997, 1998, Zaldarriaga 2000, Cooray 2002c, Kesden, Cooray & Kamionkowski 2003). The projected mass distribution from $z \sim 1000$ to present and hence the lensing effect can be reconstructed in principle via maximum likelihood estimators or quadratic statistics in the temperature and polarisation (e.g. Goldberg & Spergel 1999, Hu 2001, Okamoto & Hu 2003, Cooray & Kesden 2003, Hirata & Seljak 2003). However, as shown for example in Amblard, Vale & White (2004), lensing reconstruction is affected by other secondary effects indistinguishable from lensing such as the KSZ effect or residual foreground contaminations. In addition to providing the projected mass density, the weak lensing effect on the CMB is a potentially powerful tool to probe the neutrino mass and dark energy equation of state (e.g. Kaplinghat, Knox & Song 2003, Lesgourges et al. 2006).

4.1.2. Effects of lensing on CMB Polarisation A curl-free vector field does not remain scalar if it is distorted. Consequently in the case of CMB polarisation vector field, we expect that gravitational lensing will mix the E and B components of the polarisation. Computing equation 27 for E and B components implies second derivatives of a distorted field (e.g. Benabed, Berbardeau & van Waerbeke 2001) and gives:

$$\Delta E_{\text{obs}} = (1 - 2\kappa)\Delta E + \xi \cdot \nabla(\Delta E) - 2\delta^{ij}(\gamma_i \Delta P_j + \nabla \gamma_i \cdot \nabla P_j) \quad (29)$$

and

$$\Delta B_{\text{obs}} = (1 - 2\kappa)\Delta B + \xi \cdot \nabla(\Delta B) - 2\epsilon^{ij}(\gamma_i \Delta P_j + \nabla \gamma_i \cdot \nabla P_j), \quad (30)$$

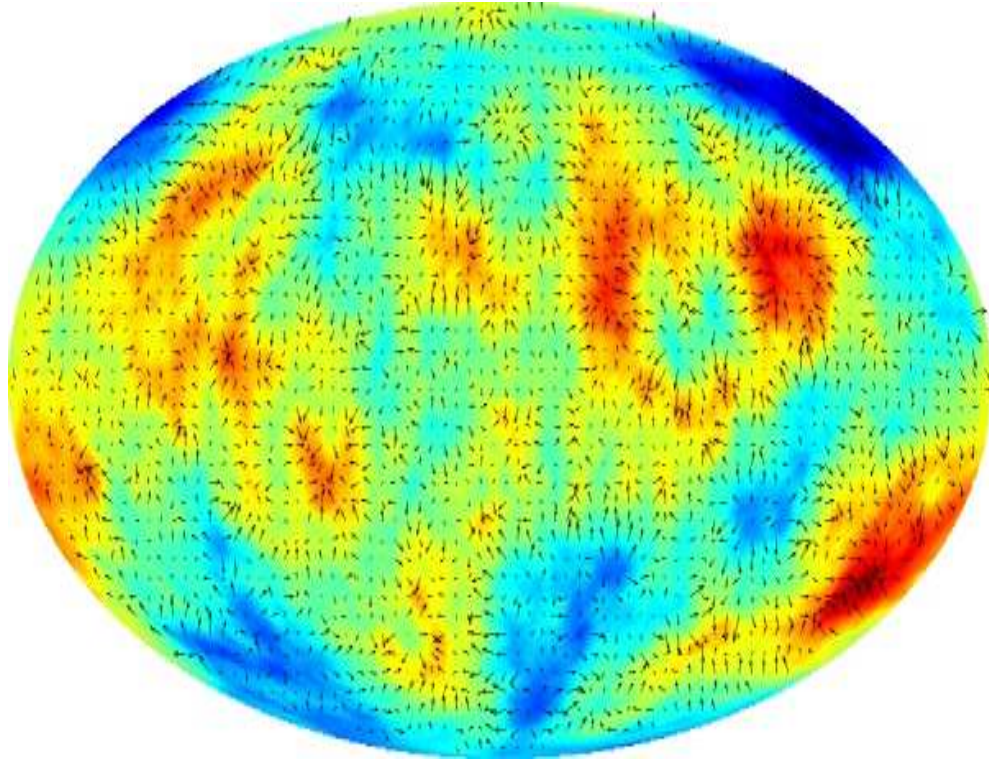


Figure 9. From <http://cosmologist.info/lenspix/>: All-sky maps of the lensed CMB temperature and polarisation anisotropies performed using the formalism developed in Lewis (2005).

where Δ denotes the Laplacian, κ and γ are the convergence and shear of the gravitational field, and δ and ϵ the identity and the anti-symmetric tensors.

These two expressions already show the three major effects of gravitational lensing on polarisation:

- A displacement shown by the term $(1 + \xi \cdot \nabla(\Delta E/B))$.
- An amplification expressed by $-2\kappa(\Delta E/B)$ and controlled by the convergence of the lensing.
- A mixing term representing the coupling between the shear of the gravitational lensing and its gradient, with the polarisation vector \mathbf{P} .

From the previous set of equations we immediately note that if gravitational waves are negligible as it is the case for scalar density perturbations the equation for the B modes is written as:

$$\Delta B = -2\epsilon^{ij}(\gamma_i \Delta P_j + \nabla \gamma_i \cdot \nabla P_j).$$

This means that the convolution of the primary polarisation, of initially scalar type (from Thomson scattering) with the shear of the gravitational lensing generates a B mode polarisation.

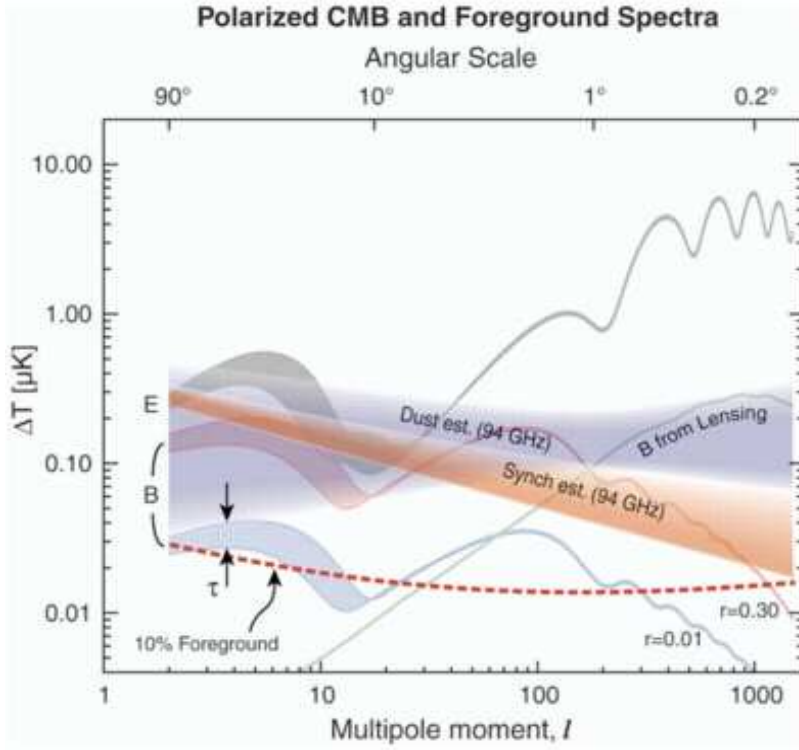


Figure 10. From Bock et al.(2006): CMB polarisation power spectra of the primary E -modes (grey line), the primary B -modes for two values of the scalar to tensor ratio r (light red and light blue lines) and the lensing-induced B -modes (light green curve). Overplotted are the current estimates of the polarised galactic foregrounds and their uncertainty. The red dashed line is an estimate of the residual foreground contamination using multi-frequency observations.

The observed or lensed power spectrum of the CMB polarisation can be computed in the flat sky approximation (e.g. Zaldarriaga & Seljak 1997, 1998). It gives:

$$(C_\ell^E)_{\text{obs}} = C_\ell^E[1 - l^2\sigma] + \int \frac{d^2k}{(2\pi)^2} \frac{(\ell \cdot \mathbf{k})^2 - k^4}{2k^4} \bar{P}(k) \times [(C_{|\ell-\mathbf{k}|}^E + C_{|\ell-\mathbf{k}|}^B) + \cos(4\phi_{\ell-\mathbf{k}}) (C_{|\ell-\mathbf{k}|}^E - C_{|\ell-\mathbf{k}|}^B)]$$

and

$$(C_\ell^B)_{\text{obs}} = C_\ell^B[1 - l^2\sigma] + \int \frac{d^2k}{(2\pi)^2} \frac{(\ell \cdot \mathbf{k})^2 - k^4}{2k^4} \bar{P}(k) \times [(C_{|\ell-\mathbf{k}|}^E + C_{|\ell-\mathbf{k}|}^B) - \cos(4\phi_{\ell-\mathbf{k}}) (C_{|\ell-\mathbf{k}|}^E - C_{|\ell-\mathbf{k}|}^B)],$$

where $\sigma = \int \frac{d^2k}{(2\pi)^2} \frac{(\ell \cdot \mathbf{k})^2}{k^4} \bar{P}(k)$. In the case of no or negligible primary B mode polarisation the first term in the $(C_\ell^B)_{\text{obs}}$ is neglected and we are left with the coupling term. A comparison of the full sky approach (Hu 2000) and a flat sky computation shows that the error introduced by the simplification are negligible.

Weak lensing induced- B mode polarisation, in addition to galactic emission, is one of the major contamination for the future post-Planck polarisation-devoted CMB

experiments (see Figure 10), whose main scientific goal will be to detect inflation-generated gravitational waves. If the inflaton potential is such that $V \leq 4. \times 10^{15}$ GeV, cleaning for lensing-induced polarisation is a requirement. However for larger potentials, deep integrations of moderately large patches of the sky at low resolution should suffice to account for the noise induced by lensing (this is the case for, e.g., Planck, QUAD, BICEP, B-POL). However, if the inflaton potential is much smaller lensing-induced polarisation will be the dominant foreground in the range $\ell \sim 50$ to 100, once the galactic contamination is removed (Figure 10). The lensing signal can be separated from gravitational wave- B modes using high order statistics as is the case for the temperature anisotropies (e.g. Hu & Okamoto 2002, Kesden, Cooray & Kamionkowski 2003, Kaplinghat, Knox & Song 2003). The separation between primordial B modes and lensing-induced B polarisation depends on the reconstruction of the lensing signal. For the secondary polarisation signal to be reduced by a factor 10 in power spectrum amplitude, a full sky measure of temperature and polarisation with a resolution of a few arc minutes and a noise of $1\mu\text{K}\text{-arc min}$ is needed.

5. The Sunyaev-Zel'dovich effect

The best known and most studied secondary contribution due to cosmic structure is definitively the Sunyaev-Zel'dovich (SZ) effect (Zel'dovich & Sunyaev 1972, 1980; see also Rephaeli 1995, Birkinshaw 1999, Carlstrom, Holder & Reese 2002). It is caused by the inverse Compton interaction between the CMB photons and the free electrons of a hot ionised gas along the line of sight. The SZ effect can be broadly subdivided into: the thermal SZ (TSZ) effect where the photons are scattered by the random motion of the thermal electrons and the kinetic SZ (KSZ) effect which is due to the bulk motion of the electrons. In the former case, the resultant CMB photons have a unique spectral dependence, whereas the final spectrum remains Planckian in the case of KSZ effect since it only Doppler shifts the incident spectrum.

5.1. The thermal SZ effect

The TSZ effect describes comptonization, the process by which electron scattering brings a photon gas to equilibrium. The term Comptonization is used if the electrons are in thermal equilibrium at some temperature T_e , and if both $k_B T_e \ll m_e c^2$ and $h_{\text{pl}} \nu \ll m_e c^2$, where ν is the frequency of the photon. This defines the non-relativistic nature of the problem. Comptonization becomes important when the temperature of a low density electron gas becomes higher than the temperature of a Planck function with the same energy density, and the absorption optical depth is low enough that the photon spectrum falls below a Planck function at the same electron temperature. This is typically the situation in ionized regions (like the ICM, accretion flows around compact objects, ionized bubbles around high redshift quasars, etc). This makes the absorption process, proportional to the square of the density, negligible compared to Compton

scattering. Since low energy photons are available, there can be energy transfer from the electrons to the photons. This is what is seen in the SZ effect observed for clusters of galaxies and predicted for other astrophysical sources of hot plasma.

In the non-relativistic limit, a differential Fokker-Planck equation, the Kompaneets equation, can be written down to describe the time evolution of the photon occupation number $n(\nu)$, which is assumed to be isotropic. Due to scattering, there is net energy transfer from the electrons to the photons (or vice versa). However, the total photon number is conserved. In the fully relativistic case, discussed in the next section, a Fokker-Planck type equation cannot be given because the change in the photon frequency $\Delta\nu$ due to scattering is not negligible compared to its incident frequency ν .

To derive the Kompaneets equation, one has to start the scattering process between an electron and a photon (see Sect. 2.1). This is given by the Boltzmann equation (see Eq. (6)), describing the evolution of the photon occupation number. The electrons are assumed to have a Maxwellian distribution with temperature T_e . Keeping in mind that Compton scattering conserves the total number of photons, one ends up with the Kompaneets equation given by

$$\partial n \partial y = 1 \partial x^2 \partial \phi \partial x [x^4 (\partial n \partial x + n + n^2)]. \quad (31)$$

where $x = \frac{h_{\text{pl}}\nu}{k_B T_e}$ and one defines a dimensionless scaled variable y (called the “Comptonization parameter” or “Compton y-parameter”) given by

$$y \equiv t c k_B T_e \partial m_e c^2 n_e \sigma_T \quad (32)$$

Note, that equation (32) can also be written as the integral of the gas pressure, p_e , along the line of sight through the extent of the plasma, i.e.

$$y = \frac{\sigma_T}{m_e c^2} \int p_e dl. \quad (33)$$

The stationary solution of the Kompaneets equation is given by the Bose-Einstein equilibrium distribution. Under the assumption that $h_{\text{pl}}\nu \ll k_B T_e$, we have $x \ll 1$, one can neglect the n and n^2 terms.

The resulting form of the Kompaneets equation has a solution of the form

$$n(x, y) = \exp [y \partial x^2 \partial \phi \partial x x^4 \partial \phi \partial x] n(x, 0), \quad (34)$$

where $n(x, 0) = (e^x - 1)^{-1}$, since in the absence of distortions (*i.e.*, $y = 0$), the photon spectrum is a black body. If $x^2 y < 1$, then one can expand the exponential in equation (34) around $n(x, 0)$ for small y .

The final distortion can then be written as

$$\Delta n \partial n = n(x, y) - n(x, 0) \partial n(x, 0) = y x e^x \phi (e^x - 1) [x \coth(x/2) - 4]. \quad (35)$$

Since the change in radiation spectrum $\Delta I(x)$ at frequency x is given by $\Delta I(x) = x^3 \Delta n(x) I_0$, where $I_0 = \frac{2 h_{\text{pl}}}{c^2} \left(\frac{k_B T_{\text{CMB}}}{h_{\text{pl}}} \right)^3$, we obtain the distinct spectral signature of the TSZ effect:

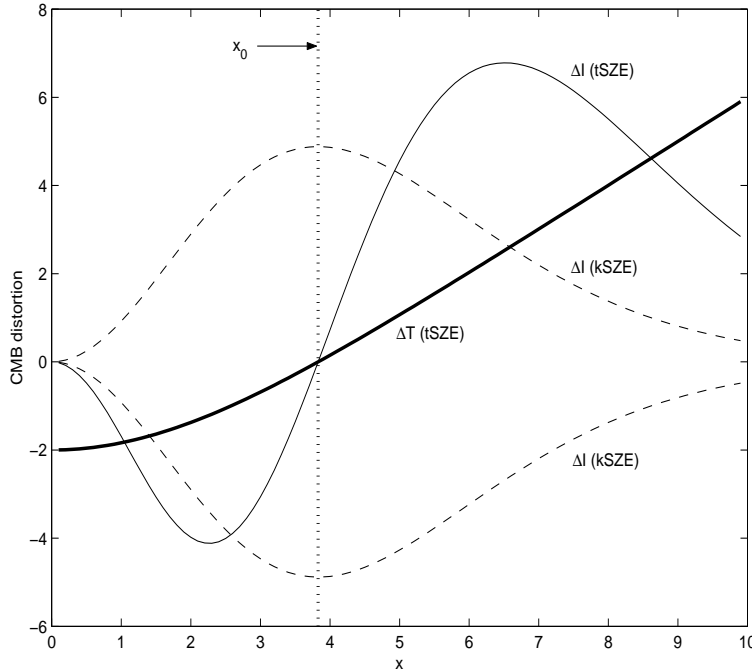


Figure 11. Frequency dependence of TSZ and KSZ effects. The thick line shows the frequency dependence of $\Delta T/T_{\text{cmb}}$ from TSZ effect, whereas the thin solid line shows the same for the change in spectral intensity $\Delta I(x)$. The thin dashed lines show the change in spectral intensity for KSZ effect, the upper one for an approaching source and the lower one for a receding source. The vertical dotted line shows the scaled frequency at which TSZ is zero and KSZ effect is maximum. In here, y , I_0 and T_{cmb} are all scaled to unity.

$$\Delta I(x) = I_0 y x^4 e^x \phi(e^x - 1)^2 [x \coth(x/2) - 4] . \quad (36)$$

This signature assumes an incident Planckian spectrum and is valid in the single-scattering approximation. The temperature anisotropy due to inverse Compton scattering of CMB photons is given by:

$$\frac{\Delta T}{T} = \frac{\Delta I(x)}{I(x)} \frac{d \ln I(x)}{d \ln T} \frac{d \ln T}{d \ln I(x)} = y [x \coth(x/2) - 4] . \quad (37)$$

In the non-relativistic limit, the frequency dependence of the distortion, shown in figure (11), is characterized by three distinct frequencies : $x_0 = 3.83$, where TSZ effect vanishes; $x_{\min} = 2.26$ which gives the minimum decrement of the CMB intensity and $x_{\max} = 6.51$ which gives the maximum distortion. In the Rayleigh-Jeans (R-J) limit (*i.e.*, when $x \rightarrow 0$) and in the Wien region we have $\frac{\Delta T_{\text{cmb}}}{T_{\text{cmb}}} = -2y$ and $x^2 y$ respectively. Thus at low frequencies we would see an apparent *decrease* in the sky brightness of the CMB sky sometimes referred to as “holes in the sky” (Birkinshaw & Gull 1978).

5.2. The kinetic SZ effect

The KSZ effect occurs, along with TSZ effect, if the scattering plasma has a bulk motion relative to the CMB. In that case, the CMB photons appear anisotropic in the reference frame of the scatterer and KSZ effect tends to isotropise the radiation. This, however, makes the radiation anisotropic in the reference frame of the observer, and there is a distortion towards the scatterer with amplitude proportional to the radial peculiar velocity v_r of the scattering gas (Sunyaev & Zel'dovich 1972, Rephaeli 1991). To derive the expression for the CMB temperature distortion due to KSZ effect, one can either start with the Boltzmann equation (for example, see Nozawa, Itoh & Kohyama 1998) or use the radiative transfer equation (see Birkinshaw 1999). In the limit of non-relativistic plasma moving with $v_r \ll c$, the change in the flux and temperature of the CMB in the direction of an object giving rise to KSZ effect is given by

$$\begin{aligned} \frac{\Delta I(x)}{I(x)} &= -\tau_{\text{clus}} \frac{v_r}{c} \frac{x e^x}{e^x - 1} \\ \frac{\Delta T}{T} &= -\frac{v_r}{c} \tau_{\text{clus}}, \end{aligned} \quad (38)$$

where τ_{clus} is the optical depth of the intra-cluster medium. Unlike TSZ effect, the spectral distribution of the kinetic SZE, figure (11), is Planckian making it impossible to disentangle from CMB at overlapping angular scales. The ratio of the change in brightness temperatures caused by TSZ effect and KSZ is, at a typical frequency for large galaxy cluster is

$$\begin{aligned} \frac{\Delta T_{\text{kinetic}}}{\Delta T_{\text{thermal}}} &= \frac{1}{2} \frac{v_r}{c} \left(\frac{k_B T_e}{m_e c^2} \right)^{-1} \\ &\approx 0.09 (v_r / 1000 \text{ km s}^{-1}) (k_B T_e / 10 \text{ keV})^{-1}. \end{aligned} \quad (39)$$

Since typical peculiar velocities are around a few hundred kilometers per second and typical temperatures a few keV, the kinetic effect comes out to be at least an order of magnitude less than the thermal effect. However, there can be cases when the kinetic distortion is larger than the corresponding thermal distortion. This is so when the plasma is either too tenuous or relatively cool or both and the peculiar velocity is large. We discuss such scenarios in section 8. For clusters of galaxies, which are the main source of SZ distortion, it is very difficult to measure the KSZ effect in the presence of TSZ effect. In CDM universes, $v_r = 300 - 400 \text{ km s}^{-1}$, and hence the signal due to the presence of KSZ effect is generally less than 5 %. However, the two effects differ in their spectral shape and so can be, in principle, separated. In fact, for non-relativistic cases, the kinetic effect attains the maximum distortion at the frequency where the thermal effect is zero (Figure 11). However, to be precise, one has to take the exact value of the cross-over frequency which depends on both the plasma temperature, the optical depth and the nature of the scattering medium which could include non-thermal population (e.g. Aghanim et al. (2003)).

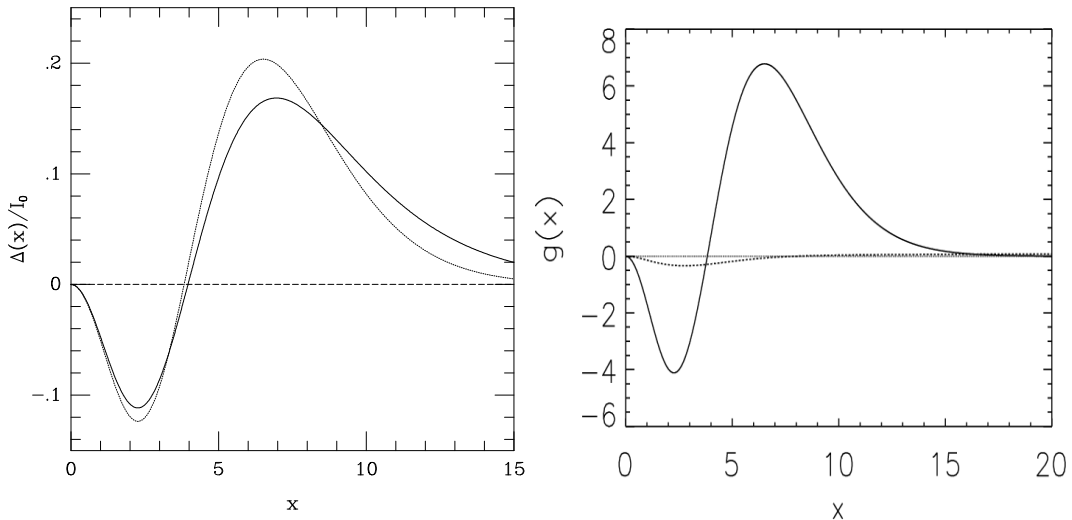


Figure 12. Left Panel: From Birkinshaw (1999), $\Delta I/I_0$ is plotted against $x = h_{\text{pl}}\nu/k_B T$ for the relativistic correction to SZ effect, from direct numerical integration shown in solid line, and obtained from the corresponding Kompaneets kernel in dotted line. The results are computed for a temperature $k_B T_e = 15 \text{ keV}$. Right Panel: From Colafrancesco, Marchegiani & Palladino (2003): Comparison of frequency dependence $g(x)$ in the thermal distribution (solid line) versus frequency dependence $g'(x)$ for a single power law non-thermal population of electrons (dotted line).

5.3. Corrections to the SZ effect

When one deals with hotter and denser scattering media there are corrections to the simple expressions of TSZ effect (equation (37)) and KSZ effect (equation(39)) derived in the previous sections, which become important. These issues have been addressed in detail in many studies (Itoh, Kohyama & Nozawa 1998, Itoh et al. 2001, Nozawa, Itoh & Kohyama 1998, Nozawa et al. 2000, Challinor & Lasenby 1998, 1999, Molnar & Birkinshaw 1999, Colafrancesco, Marchegiani & Palladino 2003, Shimon & Rephaeli 2004). The first step in most procedures, to calculate such corrections, is to expand the Kompaneets equation in a power series in $\theta_e = k_B T_e/m_e c^2$. This can be done for many choices of parameters such as $p/m, v \equiv E/p$ etc. The convergence of such expansions which are, in general, asymptotic expansions in nature and converge slowly, is then an important issue. For scattering media having high temperatures, corrections up to 3-5 orders in θ_e are sufficient and match fully relativistic numerical calculations well. The relativistic corrections modify the frequency dependence of the SZE (see Figure 12 left panel). There is an associated correction to the cross-over frequency (Itoh, Kohyama & Nozawa 1998) well approximated by a linear function in θ_e for $k_B T_e < 20 \text{ keV}$, and a quadratic function in θ_e up to 50 keV. The numerical fit is given by:

$$x_0 = 3.830 (1 + 1.1674\theta_e - 0.8533\theta_e^2) . \quad (40)$$

The relativistic corrections to the KSZ effect can be obtained by starting again from a generalized Kompaneets equation and applying a Lorentz boost to the direction of the

peculiar velocity. The electron distribution functions are connected between the cluster frame and the CMB frame by Lorentz transformations. One expands the Kompaneets solution in powers of θ_e including cross terms like $\beta\theta_e$, $\beta\theta_e^2$ etc. The $\beta\theta_e$ term can give rise to a correction of the order of 10 % for a typical electron temperature of 10 keV (Figure 12). The other higher order terms lead to negligible corrections for temperatures of interest. The relativistic correction in the R-J limit is written:

$$\frac{\Delta n(X)}{n_0(X)} \rightarrow -2y\theta_e \left[1 - \frac{17}{10}\theta_e + \frac{123}{40}\theta_e^2 \right] + y\beta \left[1 - \frac{2}{5}\theta_e + \frac{13}{5}\theta_e^2 \right] .., \quad (41)$$

where we considered cluster moving along the the line of sight such that $\beta = v_r/c$, and neglected all β^2 and higher order terms. Similarly, there is a correction to the cross-over frequency which is very small.

Finally, one can relax the assumption of low optical depth and look at multiple scatterings of the incident photon spectrum. In general, the multiple scattering contribution is found out to be rather small compared to single scatterings. As an example, for a 15 keV cluster, the multiple scattering affects the final result by -0.3 % in the Wien region and -0.03 % in the R-J region. One can think of other effects that will add further corrections to the SZ distortion. The presence of magnetic fields would give rise to magnetic pressure which will add to the gas pressure in determining the hydrostatic equilibrium of the gas. Simple calculations that incorporates this effect show a net decrease in the SZ effect distortion (Koch, Jetzer & Puy 2003, Zhang 2004). It has been proposed that the presence of magnetic fields would lead to an anisotropic velocity distribution such that one ends up with a two-temperature relativistic Maxwellian distribution of the thermal electrons. This can lead to a net enhancement of the SZ effect. Finally, it has been shown that the presence of a temperature gradient in the cluster temperature would lead to corrections to the electron momentum distribution thereby leading to corrections of the TSZ spectrum (Hattori & Okabe 2004). Unfortunately, the expected amplitude of the corrections is almost two orders of magnitude smaller than that of TSZ effect. Presence of a significant amount of non-thermal population of electrons can also lead to deviations from the thermal SZ spectrum. A self consistent treatment of several corrections to the thermal SZ effect in the presence of both thermal and non-thermal populations of electrons is given in Colafrancesco, Marchegiani & Palladino (2003) (see Figure 12 right panel).

5.4. SZ observations

The first observations of SZ effect were targetted in nature and looked at specific X-ray selected clusters. The SZ flux from these observations were used along with X-ray modeling of the clusters to estimate, in particular, the value of the Hubble Constant (Sect. 5.5). The major instruments responsible for such measurements were OVRO 5 meter telescope at 32 GHz, IRAM 30 meter telescope at 140 GHz, the Nobeyama 45 metre telescope at 21 GHZ, 43 GHz and, 150 GHz, the SuZIE array at 140 GHz and the BOLOCAM 151 element array. Additionally, interferometers like the BIMA array at 30

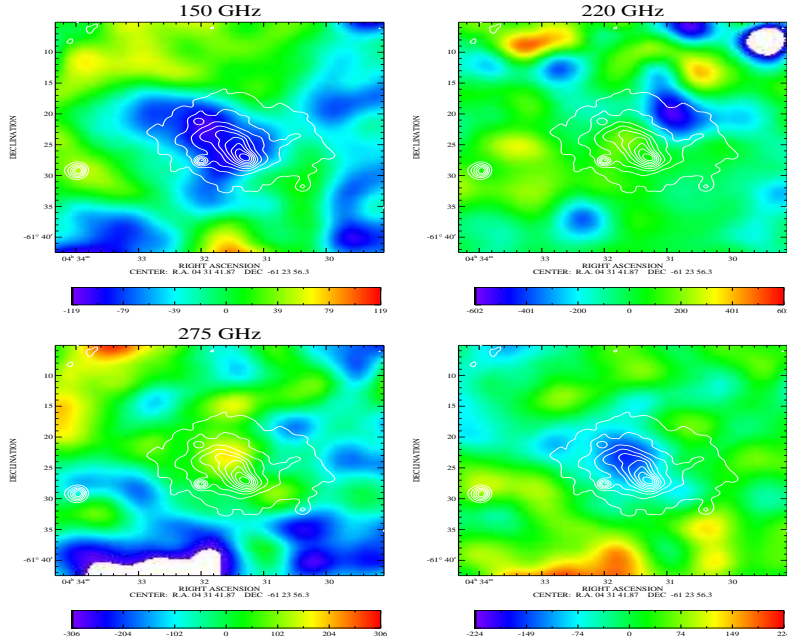


Figure 13. From Gomez et al. (2003): Mosaic of the 150 GHz, 220 GHz, 275 GHz, and CMB spectrally subtracted colorscale images of Abell 3266 (convolved with a Gaussian with FWHM ~ 4.5 arc minutes) overlaid onto the ROSAT contours. The rms noise level of $\sim 25\mu\text{K}/\text{beam}$. Most of the CMB present in the 150 GHz, 220 GHz, and 275 GHz channels has been minimized in the CMB subtracted map. As expected, the SZ signal at 220 GHz is minimum.

GHz, the Ryle Telescope at 15 GHz, CBI working between 25–36 GHz, ACBAR and AMI at 15 GHz have also been used (see Carlstrom, Holder & Reese (2002), Birkinshaw & Lancaster (2004) for a recent review). In figure 13, the SZ image of the cluster A3266 taken by ACBAR, with a beam of ~ 4.5 arc minutes, is shown for three frequencies 150 GHz, 220 and 275 GHz including the crossover frequency of 217 GHz. Note that for 150 GHz, the cluster SZ effect appears as a decrement while for 275 GHz it is an increment. Note also that the combination of the three frequencies permits to subtract the CMB contamination which remains important at the beam scale.

5.5. Hubble Constant from SZ effect

After the first TSZ observations of clusters started in the seventies, it was pointed out by Silk & White (1978) that the distance to a cluster can be estimated from the SZ and X-ray cluster observations. If we put in plausible values for the matter and energy budget of the universe, then one can estimate the value of H_0 from this distance. This has been attempted or performed using SZ effect observations: Single dish at

radio wavelengths (Birkinshaw & Hughes 1994, Hughes & Birkinshaw 1998) millimeter wavelengths (Holzapfel et al 1997, Pointecouteau et al.1999), submillimeter wavelengths (Komatsu et al.1999) and also using interferometers (Jones at al.1993, Grego et al 2001, Reese et al. 2002, Bonamente et al. 2006).

The gist of the method can be understood simply: the SZ temperature decrement $\Delta T/T$ and the X-Ray surface brightness $S_X(r)$ depend on the cluster gas structure differently; $\Delta T/T \propto n_e T_e L_{\text{cluster}}$ and $S_X(r) \propto n_e^2 T_e^{1/2} L_{\text{cluster}}$, where n_e , T_e and L_{cluster} are the characteristic density, temperature and extent of the cluster gas. Eliminating the gas density, one can obtain the cluster size in terms of the SZ and X-ray observables and the gas temperature. Once the angular size of the cluster θ_{cluster} is measured, we are able to obtain the cosmologically sensitive angular diameter distance $d_A = L_{\text{cluster}}/\theta_{\text{cluster}}$. For nearby ($z \ll 1$) clusters, d_A can be approximated in terms of the deceleration parameter $q_0 = \Omega_0/2 - \Omega_\Lambda$ as

$$d_A = \frac{c}{H_0(1+z)} [z - 1 + q_0 \phi 2 z^2]. \quad (42)$$

The derived value of the Hubble constant depends on the other cosmological parameters, Ω_0 and Ω_Λ . As long as the redshift is less than 0.2, d_A does not change significantly with small variation in the presently acceptable values of the the cosmological parameters. For example, changing q_0 from 0 to 0.5 for clusters A665 or A2218 (having $z \sim 0.17 - 0.18$) leads to a change in H_0 by $\sim 3\%$. For a high redshift cluster, the changes in H_0 due to different cosmology can be higher by $\sim 5 - 10\%$ (Kobayashi, Sasaki & Suto 1996, Reese et al 2002). More generally, the combination of SZ effect and X-ray observations can be used to probe dark energy. This is done especially when searching for violations of the duality relation between the angular diameter distance and the luminosity distance. The test of the reciprocity relation (between the source angular distance and the observer area distance) and the distance duality relation that derives from it was proposed as an additional test of dark energy (Bassett & Kunz 2004). While the reciprocity relation holds when photons follow null geodesic and that the geodesics deviation equation is valid, the distance duality relation will hold if the reciprocity relation is valid and the number of photons is conserved. Violations can thus occur if the number of photons is not conserved (e.g. in the case of absorption by dust) or if gravity is not described by a metric theory, i.e. photons do not follow null geodesic. Uzan, Aghanim & Mellier (2004) tested for the duality relation. Using a data set of SZ effect and X-ray clusters, they found no significant departure from the reciprocity.

The procedure described here both for H_0 determinations or for distance duality tests, in general, interprets the SZ effect and X-ray observations with simple modeling of the cluster gas as spherical, unclumped and isothermal distribution such as the β -model (Cavaliere & Fusco-Femiano 1978). All clusters, however, show departures from these simplistic assumptions (Evrard 1990, Navarro, Frenk & White 1997 ,Makino & Sasaki 1998, Mohr et al.1995, Mohr, Mathiesen & Evrard 1999, Mathiesen, Evrard & Mohr 1999). As a result, sources of error in the determination of H_0 as well as limitations to the distance duality test are observational in nature and come from the uncertainty in the

cluster parameters such as its core radius and temperature; the intracluster parameters such as the central electron density $n_{e,0}$ and the central values of the SZ effect and X-ray measurement. Errors can also be due to contamination of SZ effect from point sources or a poor knowledge of their spectra (e.g. Holder 2002, Aghanim, Hansen & Lagache 2005). There can also be systematic errors due to overall flux and brightness temperature calibration uncertainties and from improper subtraction of a zero level offset to the SZ data.

Without proper accounting for the many systematics present in the observations, the estimates made from this method are biased (Birkinshaw, Hughes & Arnaud 1991, Inagaki, Sugino & Suto 1995, Majumdar & Nath 2000, Puy et al. 2002, Reese et al. 2002). They seem, in particular, to favour a low value of H_0 compared to other methods. However, with a more careful treatment of the systematics the discrepancies appear to be much less (Reese et al 2002, Ameglio et al. 2006). Combining recent Chandra X-ray data with BIMA/OVRO SZ effect data on a large sample of clusters at $0.14 < z < 0.89$ yields $H_0 = 75 \pm 10$ km/s/Mpc for the standard LCDM model (Bonamente et al. 2006). This result holds whether or not virial equilibrium is assumed, and is consistent with the HST determination of H_0 .

6. SZ cluster counts

Counts of galaxy clusters, detected through their SZ effect, can be used as major probe of cosmological as well as cluster properties. The frequency dependence of the SZ effect can be used to extract the clusters from a radio survey of the sky, making SZ cluster catalogs possible. Once the clusters are detected, follow-up redshift measurements can be carried out to get the cluster redshift counts. The abundance of the clusters N_{tot} , their redshift distribution dN/dz , as well as their clustering $\xi(r)$, are governed by the geometry of the Universe and the power spectrum of the initial density perturbations. Gas physics related to cluster structure and evolution also enters through mapping of the cluster SZ flux relative to the true mass of the cluster.

6.1. Cluster mass and cluster mass–function

The fundamental quantity that goes into calculating the observed cluster counts is the cluster mass function, dn/dM , which predicts the multiplicity function of clusters having mass in the range $[M, M + \Delta M]$ at a given redshift for a choice of cosmology. One starts by calculating the variance of the linear density field, extrapolated to the redshift z at which halos (i.e. clusters) are identified, after smoothing the mean density field with a spherical top-hat filter so as to enclose the mass M . This variance can be expressed in terms of the power spectrum $P(k)$ of the linear density field extrapolated to redshift zero as:

$$\sigma^2(M, z) = \frac{D^2(z)}{2\pi^2} \int_0^\infty k^2 P(k) W^2(k, M) dk, \quad (43)$$

where $D(z)$ is the growth factor of linear perturbations normalised to unity at $z = 0$, and $W(k, M)$ is the Fourier transform of a real-space top-hat filter

$$W(k) = \frac{3}{(kR_h)^3} [\sin(kR_h) - (kR_h) \cos(kR_h)]. \quad (44)$$

In equation 44, the mass M is enclosed within a comoving radius R_h . An important cosmological parameter, related to the amplitude of fluctuations, is the mass variance at $R_h = 8h^{-1}\text{Mpc}$ denoted by σ_8 .

One can define the mass function for a particular cosmological model in terms of the quantity $\ln \sigma^{-1}(M, z)$ instead of M as given by Jenkins et al.(2001) :

$$f(\sigma, z) \equiv \frac{M}{\bar{\rho}} \frac{dn(M, z)}{d \ln \sigma^{-1}}, \quad (45)$$

where $n(M, z)$ is the abundance of halos with mass less than M at redshift z , and $\bar{\rho}(z)$ is the mean density of the universe at that time. This implies that the mass function depends only on $\sigma(M, z)$ which in turn depends on the background cosmology. Further, the mass function is normalized to have $\int_{-\infty}^{\infty} f(\sigma) d \ln \sigma^{-1} = 1$. In the following paragraphs we list the four most commonly used mass functions.

The first mass function was based on theoretical considerations (Press & Schechter 1974). The number density of clusters is derived by applying the statistics of peaks in a Gaussian random field (Bond et al 1991, Lacey & Cole 1993, Sheth, Mo & Tormen 2001) to the initial density perturbations. It assumed that the fraction of matter residing in objects of a mass M can be traced to a portion of the initial density lying at an overdensity over a critical threshold value, δ_c . This mass function is given by

$$f(\sigma)_{\text{PS}} = \sqrt{\frac{2}{\pi}} \frac{\delta_c}{\sigma} \exp \left[-\frac{\delta_c^2}{2\sigma^2} \right], \quad (46)$$

where δ_c is the extrapolated linear overdensity of a spherical perturbation at the time of collapses and is a weak function of Ω_m and Ω_Λ (Eke, Cole & Frenk 1996). Notice, that the abundance of objects is exponentially sensitive to their masses at a particular redshift. Recently, other mass functions, mainly from fits to dark matter simulations have been proposed in the literature. For example, the mass function of Sheth and Tormen (1999) can be written as

$$f(\sigma)_{\text{ST}} = A \sqrt{\frac{2a}{\pi}} \left[1 + \left(\frac{\sigma^2}{a\delta_c^2} \right)^p \right] \frac{\delta_c}{\sigma} \exp \left[-\frac{a\delta_c^2}{2\sigma^2} \right], \quad (47)$$

with $A=0.3222$, $a = 0.707$ and $p = 0.3$ and the masses were estimated with a spherical overdensity algorithm, by computing the mass within the radius encompassing a mean overdensity equal to the virial one. Jenkins et al. (2001), using a much larger simulation and a friend-of-friend algorithm for cluster finding, proposed

$$f(\sigma)_{\text{Jenkins}} = 0.315 \exp(-|\ln \sigma^{-1} + 0.61|^{3.8}). \quad (48)$$

This fit, which is widely used, has a fractional accuracy better than 20% for $-1.2 \leq \ln \sigma^{-1} \leq 1$. Recently, Warren et al.(2006) have come up with an improved fit given by

$$f(\sigma)_{\text{Warren}} = A(\sigma^{-a} + b) \exp(-c/\sigma^2) \quad (49)$$

with $A = 0.7234$, $a = 1.625$, $b = 0.2538$ and $c = 1.1982$.

In spite of the progress in obtaining the mass function from dark matter simulations, there have been considerable differences between different simulation fits, especially at high redshifts. Precision cosmology with clusters may, ultimately, be limited by our understanding of these differences. The first step in this direction has already been taken recently by Lukic et al.(2007).

6.2. Cluster abundance and redshift distribution

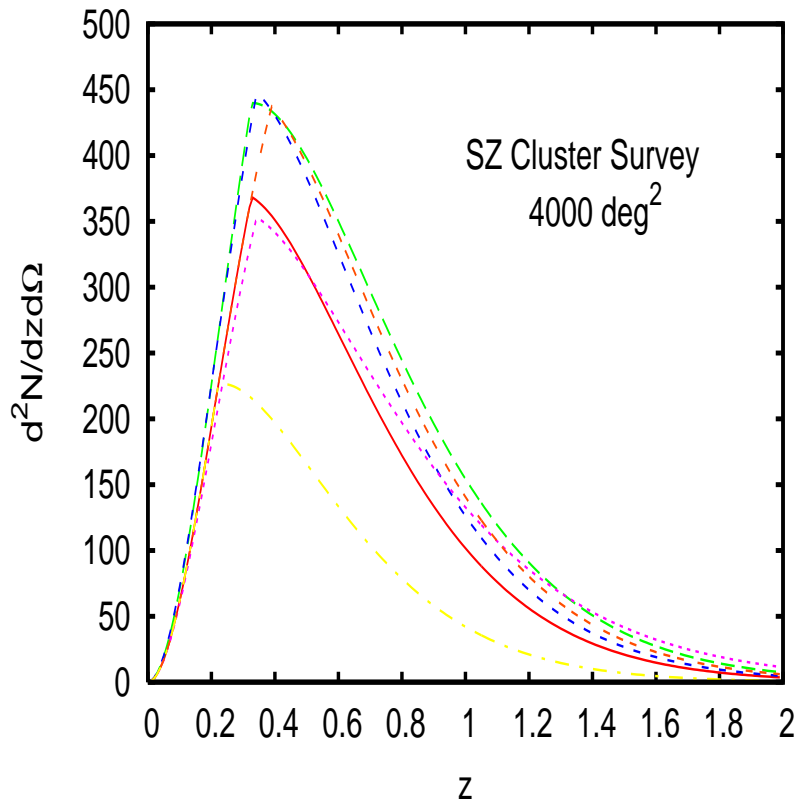


Figure 14. Cluster redshift counts for a 4000 deg^2 SZ survey having a flux limit of 5 mJy. The solid red line is for fiducial ΛCDM model with WMAP-3yrs cosmological parameters. The green long-dashed line is for 10% increase in the value of σ_8 and blue short-dashed line is for similar increase in the value of Ω_m . The purple dotted line is for a dark energy model with the equation state given by $w(a) = -0.8 + 0.3a$. The brown triple-dashed line shows the effect due 20% change in the normalisation SZ flux to cluster mass. Finally, the yellow dot-dashed line shows the expected number counts for a flux limit of 8 mJy.

Once the halo mass function and its evolution are quantified, the cluster redshift distribution, $d^2N/dzd\Omega$ (i.e the number of clusters per unit redshift per unit solid angle), can be estimated by multiplying the number density or abundance of clusters $n(z)$ with the volume $d^2V/dzd\Omega$ surveyed. This volume depends on the angular diameter distance $d_A(z)$ and the Hubble parameter $H(z)$ at that redshift. The abundance can then be

easily computed by integrating the mass function of over the limiting mass of a survey which depends on the selection function $f_{\text{survey}}(M, z)$ of the survey,

$$\frac{d^2N}{dz d\Omega} = \frac{c}{H(z)} d_A^2(z) (1+z)^2 \int_0^\infty f_{\text{survey}}(M, z) \frac{dn}{dM}(M, z) dM, \quad (50)$$

where $\frac{dn}{dM}$ is calculated using equation 45. The cosmological information contained in the observed cluster counts comes through its dependence on the expansion history of the Universe and on the growth rate of structures (Haiman, Mohr & Holder 2001).

Once the mass function is written in the universal form (Eq. 45), its evolution is completely governed by the growth factor $D(z)$. The difference in the cluster counts with varying energy density of different components are explained as follows: small-amplitude density perturbations grow as $D(z) = (1+z)^{-1}$ when $\Omega_m(z) \approx 1$, but perturbation growth stalls at around $z \sim \frac{1}{\Omega_m} - 1$ when $\Omega_m(z) \ll 1$. For a fixed Ω_m at $z = 0$, its behaviour at a higher redshift depends on the Hubble expansion factor $H(z)$ which inturn depends on the different energy densities including parameters for the amount of dark energy, Ω_Λ , and its equation of state w . Dark energy starts to dominate the universe at a later time for large Ω_Λ and a more negative value of w . The different growth histories are manifest most strongly in high-mass clusters where the exponential dependence of the mass functon on $\sigma(M, z) = D(z)\sigma(M, 0)$ has a dramatic effect on the abundance of clusters. These cosmological sensitivities of cluster redshift distribution (see Figure 14) has led clusters to be considered as probes of precision cosmology.

6.3. Precision cosmology with cluster counts

Galaxy cluster surveys of the nearby universe (Abell (1958)) have been done for many decades. However, with the beginning of SZ surveys, ambitious plans to do detect clusters at faraway universe has started to take place. In recent past, a 12 deg^2 interferometric SZ survey of the high redshift universe (Holder et al. 2000) has been carried out. Future surveys covering many hundreds to thousands of degrees capable of detecting tens of thousands of clusters are already being attempted. The goal of all these surveys is to use the sensitivity of the cluster redshift distribution to the cosmological parameter as cosmological tools. Especially, it has been demonstrated by many that a suitably large cluster survey can be used as a strong discriminator of dark energy models (Haiman, Mohr & Holder 2001, Weller, Battye & Kneissl 2002, Levine, Schulz & White 2002, Majumdar & Mohr 2003, 2004). All of these authors forecast few percent level constraints on cosmological parameters, including those of dark energy.

At this point, let us stress the fact that the exponential sensitivity of the cluster mass function to the cluster mass (equations 46, 47, 48, 49) is both the boon and bane for cosmological studies with clusters. Any systematic error in the estimation of cluster mass, including conversion between one definition of mass to the other, are exponentially magnified by the steep slope of the mass function. Numerous techniques have been proposed in the last few years to tackle this complication, as described below.

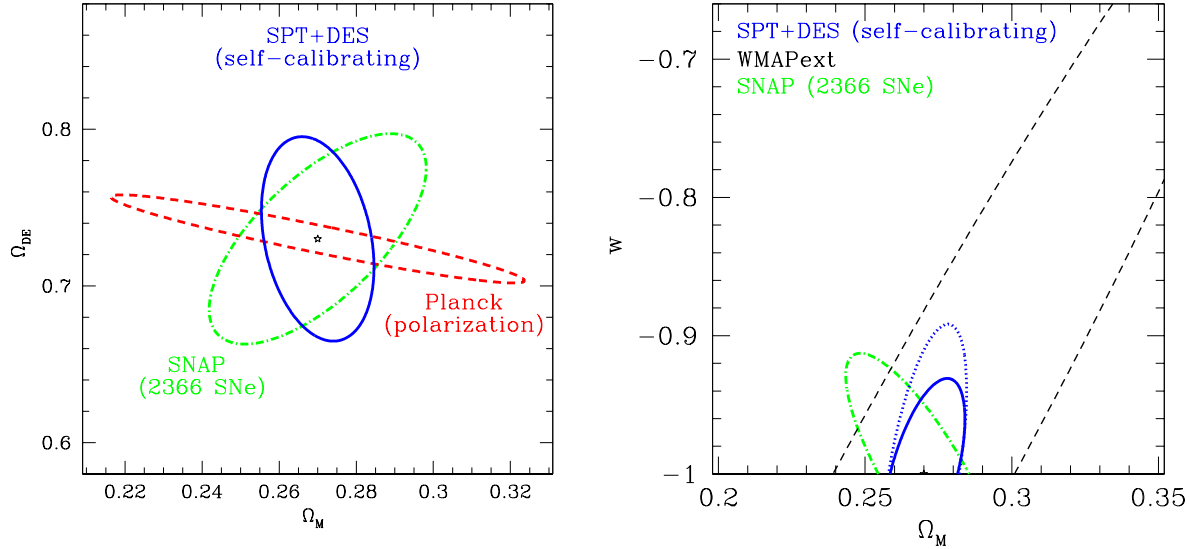


Figure 15. Left Panel: Forecasts for $\Omega_m - \Omega_\Lambda$ constraints from the SPT galaxy cluster survey, the SNAP SNe Ia mission, and the *Planck* CMB anisotropy mission. Right Panel: Same, but for joint $\Omega_m - w$ constraints from the WMAP CMB anisotropy mission, SNAP and SPT. Figure courtesy J. Mohr.

In spite of the cosmological usefulness of cluster number counts, there are several theoretical and observational requirements needed to achieve precise cosmological constraints. These include advances in understanding the formation and evolution of cluster size halos (in practice, a tighter fitting for the mass function), a well understood/controlled cluster selection function as well as a robust observational proxy for the cluster mass. Additionally, one would need a follow-up program to estimate the redshifts of these clusters[§]. Finally, one needs to calibrate and control any instrumental systematics. For a SZ survey detecting 10,000-20,000 Poisson distributed clusters in roughly 10 redshift bins with equal weights, the statistical uncertainty is $\sim 10\% - 7\%$. This gives a ballpark number at which systematic uncertainties need to be controlled.

The first requirement depends on our ability to perform large simulations. This becomes more feasible with the increase in computational power. The second requirement translates into understanding cluster selection function (the limiting mass and the completeness level of the survey) from, as realistic as possible, mock cluster catalogs. For telescope beam larger than the cluster, a survey is limited by SZ flux. Moreover, since for SZ fluxes, the redshift dependence enters through the angular diameter distance rather than the luminosity distance, the mass selection function is more uniform than that of X-Ray surveys, except at nearby redshifts ($z < 0.2$) where the clusters will be partially resolved. The mass-selection function is directly linked with the cluster SZ-flux measurements through cluster scaling relations (Kaiser 1982, Borgani 2006). Finally, it has been pointed out (da Silva et al. 2001, Motl et al. 2005,

[§] Only photometric redshifts are plausible for a sample of tens of thousands of clusters

Pfrommer et al. 2006) that the SZ-flux of a galaxy cluster is a good proxy for its virial mass with a tight scatter in the scaling relation. The relation between the virial mass M and the SZ-flux f_{SZ} can be written as

$$f_{\text{SZ}}(z, \nu) d_A^2 = f(\nu) f_{\text{gas}} A_{\text{SZ}} M_{\text{vir}}^{\beta_{\text{SZ}}} E(z)^{2/3} \mathcal{F}(\gamma, z), \quad (51)$$

where $H(z) = H_0 E(z)^2$, $f(\nu)$ is the SZ frequency dependence, f_{gas} is the gas fraction of the cluster out to the virial radius, A_{SZ} and β_{SZ} are the amplitude and slope of the scaling relation and $\mathcal{F}(\gamma, z)$ denotes any deviation from the standard evolution. For simplicity, we usually set $\mathcal{F}(\gamma, z) = (1+z)^\gamma$. The complexity of cluster structure is then encoded in the three parameters of the SZ flux–mass relation $A_{\text{SZ}}, \beta_{\text{SZ}}$ and γ . Uncertainties in the mass–observable relation can in principle be reduced by the use of “self-calibration” techniques (Majumdar & Mohr 2004)|| where one uses additional observables such as the power spectrum of galaxy clusters (Majumdar & Mohr 2004, Lima & Hu 2004). Moreover, the distribution of clusters in observed flux at each redshift provides additional mass information (Hu 2003). Finally, direct mass measurements—through X-ray observations, optical spectroscopy or weak lensing—provide important additional leverage on cluster masses and hence on cosmology (Majumdar & Mohr 2003, 2004). Once parameter degeneracies are broken through use of multiple cluster information, it is possible to achieve strong cosmological constraints from upcoming cluster surveys. As an example, in figure 15, we show forecasts for Ω_m, Ω_Λ and w constraint from South Pole Telescope (SPT) survey¶. It also shows that SZ clusters as probes are highly complementary to other experiments since each experiment constrains a different combination of cosmological parameters and is subject to different systematics.

However, due to the very nature of the entanglement between gas physics and cosmology in using clusters as cosmological probes, there must be cosmology-cluster physics degeneracies (Majumdar & Mohr 2003, Majumdar & Cox 2007). These degeneracies can be broken by adding constraints from complementary information within cluster surveys (such as $dN/dz + P_{\text{cluster}}(k)$) or external information (e.g. mass follow-up).

7. The SZ power spectrum

The SZ effect from galaxy clusters is one of the major sources of secondary temperature anisotropies. A convenient way of describing its effect on the CMB is by computing its angular power spectrum. The fluctuations in the temperature background due to SZ effect from clusters of galaxies can be expressed in terms of correlations between the fluctuations along two lines of sight separated by an angle. The rms distortion can be quantified by the spherical harmonic coefficients $a_{\ell m}$, which is defined as $\Delta T(\mathbf{n}) = T_0^{-1} \sum_{\ell m} a_{\ell m} Y_{\ell m}(\mathbf{n})$. The angular power spectrum of the SZ effect is then given by $C_\ell = \langle |a_{\ell m}|^2 \rangle$, the brackets denoting an ensemble average.

|| For application to actual data, see Gladders et al.(2007).

¶ The Dark Energy Survey (DES) would be used to follow-up SPT clusters to get their redshifts

7.1. Modeling the SZ power spectrum

The SZ power spectrum can be derived from numerical simulation of structure formation and evolution or from analytical computations. In the first approach, hydrodynamical numerical simulations are the most appropriate way to describe both the dark matter of which the gravitational potential wells are made of, and the baryonic gas which is responsible of the SZ effect. Various groups (Scaramella, Cen & Ostriker 1993, da Silva et al. 2000, Refregier et al. 2000, Refregier & Teyssier 2002, Seljak, Burwell & Pen 2001, Zhang, Pen & Wang 2002) have performed such kind of simulations and computed the associated power spectra. A compilation of the predictions from the different groups can be found in Springel, White & Herquist (2001). The SZ power spectra computed from numerical simulations globally agree within a factor of two. However, the results are quite sensitive to the resolution of the simulations which acts as an artificial damping effect at small angular scales, and to the size of simulation which if not large enough underestimates the number of massive clusters and thus the power at large angular scales.

In the second approach, the SZ power spectrum can be computed analytically (Cole & Kaiser 1988, Makino & Suto 1993, Atrio-Barandela & Mucket 1999, Molnar & Birkinshaw 2000, Komatsu & Kitayama 1999, Cooray 2000, 2001, Majumdar 2001, Komatsu & Seljak 2002) The computation is based on two quantities:

- The cluster number counts or mass function dn/dM which provides us with the number of clusters of a given mass M present at a redshift z (see Section 6).
- The cluster model or mass-SZ flux relation, i.e. its temperature and density profiles which give the spatial form factor of the associated SZ effect.

To begin with, let us assume that the cluster cross-correlation function can be known (for details see Peebles 1980, Cole & Kaiser 1988). The pattern of temperature anisotropy on the sky, induced by a population of clusters, is found by the convolution of the temperature anisotropy due a single “template” cluster of mass M at redshift z with the angular distribution of the clusters, and then integrating over their mass and redshift distributions. If one takes an ensemble average and further assumes that $n(M, z)$ is constant over the range of comoving separations for which the cross-correlation function $\xi(M_1, M_2, z, \delta r)$ is non zero, then the angular temperature power spectrum C_ℓ can be written as the sum of two terms, the “1-halo” or the Poisson term and “2-halo” or the clustering term, i.e

$$C_\ell^{\text{total}} = C_\ell^{\text{Poisson}} + C_\ell^{\text{clustering}} . \quad (52)$$

The power spectrum for the Poisson distribution of objects can then be written as (Cole & Kaiser 1988)

$$C_\ell^{\text{Poisson}} = \int_0^{z_{\max}} dz \frac{dV(z)}{dz} \int_{M_{\min}}^{M_{\max}} dM \frac{dn(M, z)}{dM} |y_\ell(M, z)|^2, \quad (53)$$

where $dV(z)/dz$ is the differential comoving volume and dn/dM is the number density of objects and y_ℓ is the 2D Fourier transform of the projected Compton y -parameter. The mass range is chosen so as to cover from group scale to the largest cluster scales. Since these fluctuations occur at small angular scales, we can use the small angle approximation of the Legendre transformation and write y_ℓ as the angular Fourier transform of $y(\theta)$ as $y_\ell = 2\pi \int y(\theta) J_0[(\ell+1/2)\theta] \theta d\theta$ (Peebles 1980, Molnar & Birkinshaw 2000), where J_0 is the Bessel function of the first kind and zero order.

The clustering power spectra depends on lines of sight passing though an ensemble of correlated clusters. It can be estimated (Komatsu & Kitayama 1999) as

$$C_\ell^{\text{clustering}} = \int_0^{z_{\max}} dz \frac{dV(z)}{dz} P(k) \times \left[\int_{M_{\min}}^{M_{\max}} dM \frac{dn(M, z)}{dM} b(M, z) y_\ell(M, z) \right]^2, \quad (54)$$

where $b(M, z)$ is the time dependent linear bias factor. The matter power spectrum, $P(k, z)$, is related to the power spectrum of cluster correlation function $P_{\text{cluster}}(k, M_1, M_2, z)$ through the bias, *i.e.*, $P_{\text{cluster}}(k, M_1, M_2, z) = b(M_1, z)b(M_2, z)D^2(z)P(k, z=0)$. Convenient expressions for the bias at cluster scales are given by Sheth & Tormen (1999) and Jing (1999).

When one calculates the variance in beams of fixed size, the Poissonian model is a good approximation if the probability that a cluster has a neighbour is small inside the beam. This probability is the product of the number density and the volume integral of the cross-correlation function over the region probed by the beam. It can be shown that for beams comparable to the size of rich clusters ($R \sim 1.5h^{-1}$ Mpc), the Poissonian approach is a valid approximation. Only for very large beams, the variance will increase due to positive correlation of the clusters. It can be shown that the Poisson power spectrum dominates at all ℓ values greater than 100. However, by subtracting, X-ray selected clusters of galaxies over a certain flux ($S_X > 10^{-13}$ erg cm $^{-2}$ s $^{-1}$), from both power spectra, one can make the clustering part of the spectrum dominates around $\ell \sim 700$ (Komatsu & Kitayama 1999, Majumdar 2001b).

To calculate the 2D profile of each cluster in the cluster ensemble, one needs a cluster gas density and temperature model. This can be either the empirical truncated β -profile (e.g. in Molnar & Birkinshaw 2000), or it can be derived by solving the hydrostatic equilibrium equation of a gas within a NFW dark matter potential (e.g. in Komatsu & Seljak 2001), or it can simply be obtained from fits to simulated cluster profiles as in Diego & Majumdar (2004).

7.2. Cosmological studies with SZ power spectrum

Both the volume element and the abundance of clusters depend on the cosmological model. As a consequence the power spectrum will also vary with varying cosmological parameters (Komatsu & Seljak 2002, see also Figure 16 left panel). For example, SZ power spectrum is sensitive to the density parameter Ω_m which mainly affects the number of low and moderate redshift clusters, and the equation of state of the dark

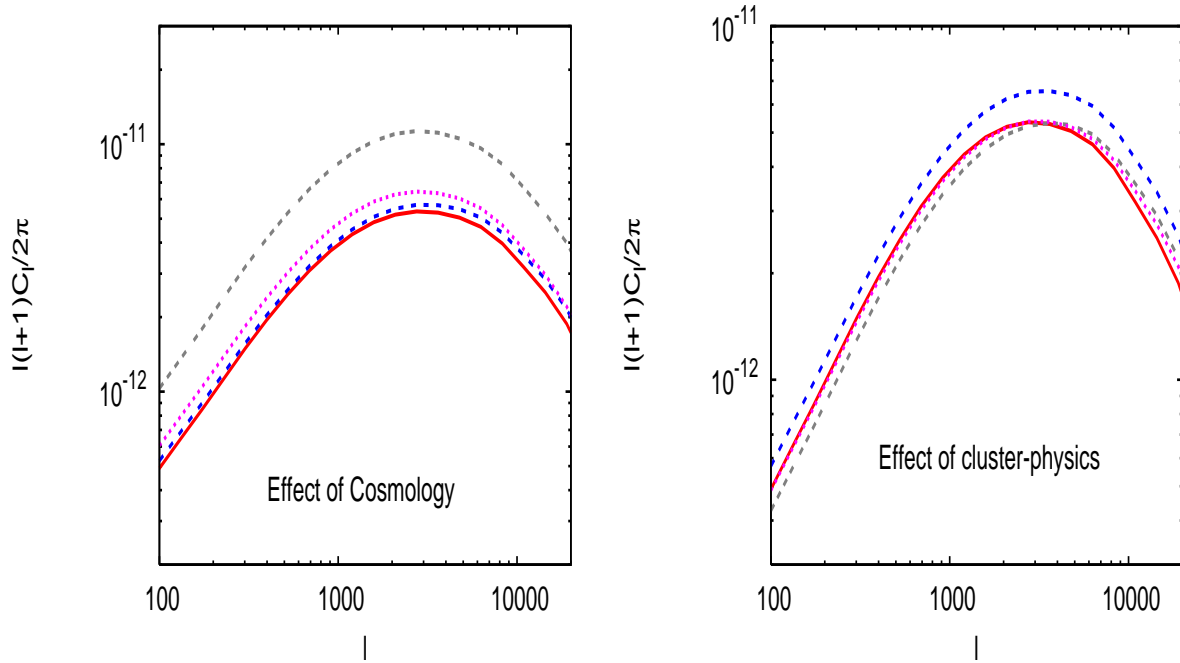


Figure 16. Left Panel: The variation of the SZ power spectrum with the cosmological parameters. The solid red line is for the fiducial model for WMAP-3yrs cosmological parameters and cluster model from Komatsu & Seljak (2001). The triple dashed grey line shows the effect of 10% increase in σ_8 , the purple dotted line for 10% increase in Ω_b and blue dashed line for 10% increase in Ω_m . The sensitivity of SZ C_ℓ to σ_8 is maximum. Right Panel: The same as in the left panel but with changes in the parameters relating to cluster physics while fixing the cosmology. The blue dashed and the grey triple-dashed lines are for cluster $M_{500} - T$ relation normalised to two different observational results (Arnaud, Pointecouteau & Pratt 2005) for an ensemble of clusters. In these cases the normalisation and the slope of the $M_{500} - T$ are both different than that obtained in the Komatsu & Seljak (2001) cluster model. The purple dotted line is for a 10% difference on the cluster halo central concentration. The red solid line is for the fiducial model. The calculations are done for R-J band.

energy $w = P/\rho_{\text{DE}}$ which mainly affects the number of high redshift clusters. However in the range of allowed values for Ω_m and w the effects are rather small. As for the other parameters the effects are quite negligible, except that of σ_8 . The SZ power spectrum is strongly sensitive to the normalisation of mass fluctuations at cluster scales, i.e. σ_8 . Numerical simulations of SZ clusters show $C_\ell \propto \sigma_8^7$. Using simple scaling analysis, one can show that $C_\ell \propto \sigma_8^{14/(3+n)}$ where n is the effective spectral index of mass fluctuations at cluster scales. If the highest mass halos contribute to the power spectrum then $n \sim -1$ and we recover back the simulation results. Note that when smaller mass halos contribute significantly to the rms⁺, then the effective n is greater than -1 and C_ℓ can have a stronger dependence on σ_8 . The cluster power spectrum depends, just like the mass function, on the cluster physics more specifically the mass–observable relation

⁺ For example, observed smaller mass clusters show increased entropy over simple self-similar predictions.

affects the power spectrum (Figure 16, right panel).

Recently, the estimated power spectrum from the CBI-ACBAR-BIMA data interpreted as an SZ signal has been used to constrain the value of σ_8 . The resulting value $\sigma_8 = 0.9$ was found higher than other estimates of σ_8 which are now converging to the range [0.7–0.8]. By forcing the clusters in the simulations or in the analytic calculations of $SZ-C_\ell$ to have scaling properties compatible with observed clusters, one can fit the CBI excess with a σ_8 closer to WMAP 3 years value. Note, however, that the excess σ_8 only appears if we believe that the resulting excess CMB fluctuations at the CBI scales is due to SZ effect from galaxy clusters. It has indeed been pointed out (Toffolatti et al. 2005, Douspis, Aghanim & Langer 2006) that SZ from clusters are only mildly needed if there are unremoved point sources below the detection limit. On a more speculative note, non-Gaussianity in the primordial power spectrum can boost the SZ power spectrum at cluster scales up to CBI excess (Mathis, Diego & Silk 2004, Sadeh, Rephaeli & Silk 2006).

7.3. Extraction of SZ effect from CMB data

The SZ contribution to the CMB power spectrum is dominant as compared with other sources of secondary anisotropies. It was shown in Douspis, Aghanim & Langer (2006) that the SZ contribution, if coherently taken into account, affects the determination of cosmological parameters such as the normalisation σ_8 , the optical depth τ and the initial power spectrum index n . However, the TSZ contribution should in principle be removed down to a given cluster mass from the measured power spectrum provided multi-frequency observations are conducted. To this aim many methods have been proposed and developed especially in the context of Planck experiment (Sanz, Herranz & Martinez-Gonzalez 2001, Vielva et al. 2001, Diego et al. 2002, Schaefer et al. 2006a, 2006b, Pierpaoli et al. 2006, Pires et al. 2006). All of them take benefit from the specific spectral signature of TSZ signal discussed in Sect.5. These methods also use additional spatial constraint based on adapted or matched filters, wavelets, etc. They are mainly aimed at providing us with SZ cluster catalogues that will be further used as cosmological probes. Consequently they help in cleaning out the primary CMB signal. In practice the sensitivity limits of the experiments, their frequency coverages as well as their finite beams prevent us from a complete cleaning of the TSZ effect. The TSZ effect is not the only source of power at small scales. One can also probe KSZ by its effect on the power spectrum at high ℓ . From amplitude arguments, it is easy to find that the amplitude of the KSZ power spectrum is much smaller than that of the TSZ. However, patchy reionisation has interesting implications for the KSZ effect power spectrum (Iliev et al. 2007b). At fixed optical depth, patchy reionisation approximately doubles the total KSZ power above $\ell = 3000$ by up to an order of magnitude compared to a uniform reionisation scenario. The KSZ effect has the same dependence as the CMB anisotropies and the multi-frequency observations do not serve in removing this contribution. Optimised methods to extract a map of the KSZ temperature fluctuations

from the CMB anisotropies can be developed (Forni & Aghanim 2004). Assuming that a map of Compton parameters for the TSZ effect can be obtained by multi-frequency separation, one can take benefit from the spatial correlation between KSZ and TSZ effects which are due to the same galaxy clusters. This correlation allows us to use the TSZ map as a spatial template in order to mask, in the temperature anisotropy map encompassing both CMB and KSZ signal, the regions where clusters must have imprinted an SZ fluctuation. By further using the statistical properties of KSZ, which is a non-Gaussian, one can perform achieve good separation of the KSZ signal out of the primary CMB.

8. The SZ effect from other astrophysical sources

The SZ effect, as proposed originally by Sunyaev & Zel'dovich, represents the shift experienced by the CMB photons when they undergo inverse Compton interactions with the free electrons of the hot ionised intra-cluster gas. The SZ effect is thus historically associated with the galaxy clusters. However and more generally, inverse Compton scattering can take place in all astrophysical environments where both conditions of ionisation and high temperature are fulfilled. As a result, the SZ effect was studied in a variety of redshift domains and astrophysical sources from early proto-galaxies and galaxies, to local galaxies like M31, as suggested by Taylor, Moodley & Diego (2003).

In the standard scenario of structure formation, baryonic matter is believed to lay in the potential wells formed by the DM. The baryonic matter in dynamical equilibrium with the DM can thus reach high temperatures at virialisation. The baryonic gas can be heated by additional means (photoionisation, mechanical heating, ...). Therefore, induced SZ anisotropies are expected to span a large range amplitudes and angular scales.

At intermediate and large angular scales, a warm-hot gas ($T_e = 10^5 - 10^7$ keV) is likely to exist in the large structures of the cosmic web. This gas might account for a fraction of the missing baryons (e.g. Fukugita, Hogan & Peebles 1998). Due to its relatively large temperature, this warm medium is expected to exhibit an SZ signal but also an X-ray emission. Observing the SZ signal from this warm medium, which would contribute to the CMB signal at large scales, is certainly important from the CMB point of view for disentangling between primary and secondary anisotropies. Observing the warm medium may be also a unique way to seek for, and find, the missing baryons in the universe. Several studies have aimed at studying and describing this contribution. Since it is associated with non-linear structures the ideal tool is numerical simulations (e.g. Springel, White & Hernquist 2001, da Silva et al. 2001, Zhang, Pen & Wang 2002). The expected SZ signal was found to have quite low amplitudes ,thus, making it difficult to detect directly. One way around the problem might to target the correlations between SZ signal and X-ray emission. Future experiments will tell us to what extent this will be possible.

At smaller angular scale scales, when structures collapse to form galaxies the

temperature of the baryonic gas increases to larger values due to shock heating. Moreover, the thermal content of the collapsed structures increases due to feed-back processes (star formation, AGN activity, ...). In both cases, an SZ signal is expected at the galaxy scale. Its detailed amplitude depends on the efficiency of the heating mechanisms and of the galactic environment (mainly the gas density). The predicted SZ signal has been computed in both cases for shock heating and feed-back. In the first case, Valageas, Balbi & Silk (2001) found that the contribution from collapsed objects dominates only at very small scales $\ell > 10^4$. The SZ signal from galaxies can be even larger if they host central supermassive black-holes (BH). In that case the galactic outflows powered by the mechanical energy of accreting matter onto the BH induce an important SZ signal as large as the COBE limit (e.g. Natarajan & Sigurdsson 1999, Aghanim, Balland & Silk 2000, Lapi, Cavaliere & De Zotti 2003). SZ effect from quasar feedback (Chatterjee & Kosowsky 2007) has been predicted at $1\mu\text{K}$ level which is potentially detectable by ALMA. The feed-back from stars and its associated SZ effect was also studied. Rosa-Gonzalez et al.(2004) calculated the signal expected from star-formation activity during the formation of the most luminous bulges of normal galaxies. They found that the temperatures and densities were high enough to produce y parameters comparable to those of galaxy clusters. The supernova driven galactic winds during the early stages of evolution of normal galaxies can also cause the distortion of the CMB radiation as proposed by (Majumdar & Nath 2001). Finally, SZ effect can not only arise from forming or early formed objects but it can also be associated with relic objects such as hot regions, “cocoons”, around radio galaxies as proposed by Yamada, Sugiyama & Silk (1999). In that case, the Compton parameter associated with the ensemble of cocoons was found to be of the same order as the COBE constraint. Radio galaxies in galaxy clusters can eject large quantities of energy which is either thermalised or remains as relativistic radio plasma (radio ghost) in the galaxy clusters. Ensslin & Kaiser (2000) estimated the Compton parameter from these two phases and found it too small to be detected. However a statistical estimate of the relativistic population in clusters can be envisaged by stacking the SZ signal from all the cluster detected by future Planck satellite (Ensslin & Hansen 2004).

In some cases the ionised regions have too low temperatures or densities, or both, to exhibit significant Compton distortions. In these cases, the kinetic SZ effect (if the gas moves with respect to the CMB) becomes the dominant source of secondary anisotropies. This is, particularly, the case for the patchy reionisation (Aghanim et al.1996). Here, the temperature of the ionised bubbles generated by emitting and ionising sources is low (typically $\sim 10^4\text{K}$) implying a negligible y distortion, but the proper motion of the ionised bubbles causes significant KSZ fluctuations. The secondary anisotropies due to Doppler effect have been the subject of quite a large number of studies, in the context of the reionisation problem, especially in view of the first year WMAP constraints on optical depth (see Sect. 2 and references therein for details). A large TSZ signal from the sources responsible for the reionisation is however not excluded yet. It might on the contrary contribute to the excess power measured by CBI and BIMA. An example

for this is the case in which early massive stars have played an important role in the reionisation history of the universe (Oh, Cooray & Kamionkowski 2003).

9. Polarisation from galaxy clusters

As shown by Sunyaev & Zel'dovich (1980) not only CMB intensity is altered by the presence of clusters, through the TSZ and KSZ effects, the CMB polarisation is affected by the presence of galaxy clusters along the photon lines of sight. Polarisation anisotropies are generated when the photons scatter off free electrons in the intracluster medium. The cluster-induced polarisation can be of a different origin: due to the CMB quadrupole itself, to the cluster transverse motion or rotation (Chluba & Mannheim 2002), to its finite optical depth or to the presence of cluster magnetic fields. In the following we briefly review each of these processes

(i) Transverse motion-induced polarisation:

The proper motion of the galaxy cluster relative to the CMB produces a polarisation (Sunyaev & Zel'dovich 1980, Itoh, Kohyama & Nozawa 1998, Audit & Simmons 1999, Sazonov & Sunyaev 1999, Shimon et al. 2006). Keeping only the first and second order terms in velocity, the polarisation towards a cluster moving with a transverse velocity v_t is given by:

$$P_\nu = 0.1 \frac{x^2 e^x (e^x + 1)}{2(e^x - 1)^2} \left(\frac{v_t}{c}\right)^2 \tau$$

The amplitude depends on the observed frequency. It is higher in the Wien part of the spectrum. The frequency-integrated polarisation is simply proportional to $\left(\frac{v_t}{c}\right)^2 \tau$. The polarisation vector is perpendicular to the plane formed by the velocity vector and the observing direction.

(ii) Double scattering-induced polarisation:

This process is also called the finite optical depth effect. When the CMB photons scatter off free electrons in the intra-cluster gas they acquire anisotropies due to TSZ ($\propto \tau \left(\frac{k_B T_e}{m_e c^2}\right)$) and KSZ ($\propto \tau \left(\frac{v_r}{c}\right)$) effects. A second scattering within the cluster induces polarisation of the order of $\left(\frac{k_B T_e}{m_e c^2}\right) \tau^2$ and $\left(\frac{v}{c}\right) \tau^2$ without modifying the frequency dependences. This effect can be generalised to any other source of local anisotropy such as gravitational effects (moving gravitational lens effects were computed by Gibilisco (1997), bulk motions of moving gas clouds in the inner part of clusters (Diego, Mazzotta & Silk 2003), collapse or expansion effects). The amplitude of the polarisation depends on the gas distribution $\rho(r)$. For a homogeneous spherical cloud with gas density ρ_0 , (Sazonov & Sunyaev 1999) found that the maximal polarisation degrees are $0.025 \left(\frac{v_t}{c}\right) \tau_0^2 g(x)$ and $0.014 \left(\frac{k_B T_e}{m_e c^2}\right) \tau_0^2 f(x)$, with $\tau_0 = 2\sigma_T \rho_0$ and $f(x)$ and $g(x)$ the spectral dependences of the TSZ and KSZ respectively. This results in a unique spectral signature displayed in Figure 17).

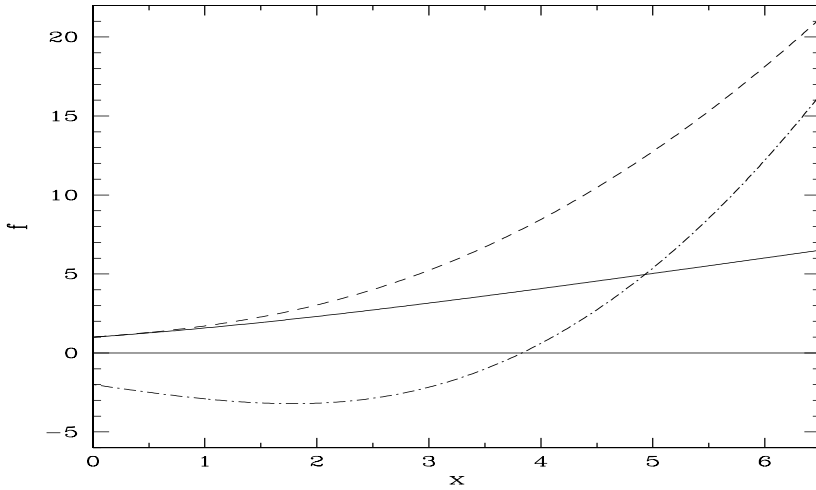


Figure 17. From Sazonov & Sunyaev (1999): The frequency dependencies of the cluster-induced polarisation effects: CMB quadrupole-induced and the $(\frac{v_t}{c})^2 \tau$ effects (solid line), $(\frac{v_t}{c}) \tau^2$ effect (dashed line), and the $(\frac{k_B T_e}{m_e c^2}) \tau^2$ effect (dash-dotted line). The last effect changes its sign at $x = 3.83$.

(iii) Faraday rotation in magnetised intra-cluster medium:

A radiation of frequency ν propagating through a plasma in presence of a magnetic field \mathbf{B} along direction \mathbf{n} sees its linear polarisation vector rotated by an angle $\Delta\varphi$. This effect is the Faraday rotation (FR). Clusters show evidence for magnetic fields (e.g. Murgia et al. (2004), and references there in). The CMB polarised radiation passing through magnetised galaxy clusters undergoes FR. This mixes the Stokes parameters Q and U and thus generates B modes out of E polarisation. The B -mode power spectrum depends on the details of the electron density distribution per individual cluster, on the mass function of clusters, as well as on the magnetic field distribution and evolution. Such a contribution was computed by Takada, Ohno & Sugiyama (2001) and recently revisited by Tashiro, Aghanim & Langer (2007). It is proportional to the product $B_0^2 \nu_{\text{obs}}^{-4}$. At the frequencies typically used for CMB observations, the amplitude of the FR-induced B polarisation is small. However, the polarisation observed at the cluster scale could be a powerful tool for probing the gas distribution (Ohno et al. 2003).

(iv) CMB Quadrupole-induced polarisation:

The presence of a quadrupole component produces a polarisation signal proportional to the cluster optical depth τ . It has a maximum amplitude of $P_{\max} \sim 2 \cdot 10^{-6} g(x) \tau$ which changes with frequency ($x = h_{\text{pl}} \nu / k_B T$) following $g(x) = x e^x / (e^x - 1)$. This effect should be the dominant source of polarisation

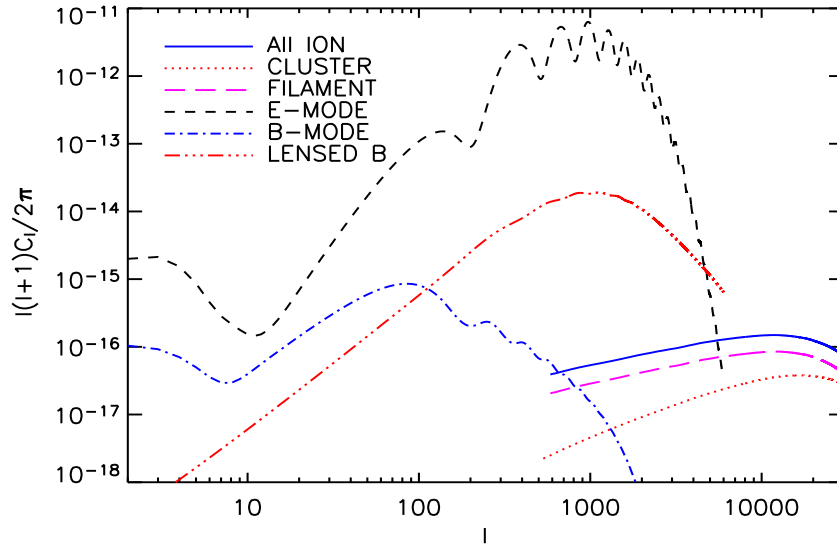


Figure 18. From Liu, da Silva & Aghanim (2005): The power spectra of the polarised E and B modes from primary and secondary anisotropies due to quadrupole-induced interactions.

related to clusters. The primary quadrupole-induced polarisation due to galaxy clusters and to warm gas in filamentary structures has been investigated using hydrodynamical simulations (Liu, da Silva & Aghanim 2005). As shown in Figure 18, this effect dominates at very small angular scales. On the larger scales the signal is dominated by the contributions from the filamentary structures. At the smallest scales it is the galaxy cluster contribution which dominates.

Galaxy clusters produce both E and B polarisation but at a level that is much smaller than the primary signal. However, despite the relatively low signal amplitudes, the study of cluster induced-polarisation has gained a new interest since it appears to be a potentially interesting cosmological probe (see e.g. Cooray & Baumann 2003). Cluster polarisation measurement were proposed to probe the large scale velocity fields through measuring the cluster transverse motions, as well as the galaxy cluster dynamics. However, the most promising application of cluster polarisation measurement is associated with the dominant effect, the quadrupole induced polarisation. The polarised signal from numerous galaxy clusters has been suggested by Kamionkowski & Loeb (1997) as a method to probe CMB quadrupole by reducing the cosmic variance uncertainty (see also Portsmouth 2004). This in turn provides a new way to obtain accurate ISW measurements and probe the dark energy content of the universe (e.g. Cooray, Huterer & Baumann 2004, Bunn 2006).

10. High-order statistics of secondary anisotropies

Most, and indeed the simplest, inflationary scenarios (e.g. Guth 1981, Sato 1981) predict that the temperature anisotropy field obeys Gaussian statistics to first order. In this case, the statistical distribution of the CMB anisotropies is fully described by its second moment, the power spectrum, given by:

$$C_\ell = \sum_{m=\ell}^{\ell} |a_{\ell m}|^2,$$

where the $a_{\ell m}$ are the multipole coefficients in the spherical harmonic expansion $\Delta T(\theta)/T = \sum_{\ell,m} a_{\ell m} Y_\ell^m(\theta)$. Nevertheless, other cosmological scenarios such as topological defects (e.g. Vilenkin & Shellard 1994, Landriau & Shellard 2003 and references therein) and multi-field inflation (Gangui et al. 1994, Bernardeau & Uzan 2002) suggest departures from the Gaussian hypothesis. One example of a Non-Gaussian model that lends itself to specific predictions is the so-called χ_m^2 model for the multi-field inflaton potential (Koyama, Soda & Taruya 1999) implemented for $m = 2$ (2 fields) by Sadeh, Rephaeli & Silk (2006) to study SZ observables. The issue of testing, through higher order statistics, assumptions about the early universe is quite important and is becoming feasible in the context of present and future CMB experiments. Therefore, a battery of non-Gaussian (NG) estimators have been recently developed and tested. Among the most commonly used, there are the three and four-point functions and their harmonic analogues the bi- (T_3) and trispectrum (T_4) (e.g. Hu 2001, Komatsu & Spergel 2001, Kunz et al. 2001) respectively given by:

$$\langle T(\ell_1)T(\ell_2)T(\ell_3) \rangle_c = (2\pi)^2 \delta(\ell_{123}) T_3(\ell_1, \ell_2, \ell_3) \quad (55)$$

and

$$\langle T(\ell_1)T(\ell_2)T(\ell_3)T(\ell_4) \rangle_c = (2\pi)^2 \delta(\ell_{1234}) T_4(\ell_1, \ell_2, \ell_3, \ell_4), \quad (56)$$

where $\ell_{123} = \ell_1 + \ell_2 + \ell_3$ and $\ell_{1234} = \ell_1 + \ell_2 + \ell_3 + \ell_4$. Also widely used are the higher order moments of the wavelet coefficients (skewness and excess kurtosis) (e.g. Pando, Valls-Gabaud & Fanf 1998, Forni & Aghanim 1999, Hobson, Jones & Lasenby 1999, Barreiro & Hobson 2001). The wavelet analysis, in the dyadic wavelet transform scheme, decomposes a signal s in a series of the form :

$$s(l) = \sum_k c_{J,k} (\phi_A)_{J,l}(k) + \sum_k \sum_{j=1}^J (\psi_A)_{j,l}(k) w_{j,k} \quad (57)$$

where J is the number of decomposition levels, $w_{j,k}$ the wavelet (or detail) coefficients at position k and scale j (the indexing is such that $j = 1$ corresponds to the finest scale, i.e. highest frequencies), and c_J is a coarse or smooth version of the original signal s . Other tests of non-Gaussianity are the global Minkowski functionals like the total area of excursion regions enclosed by isotherm contours or total contour length and genus (e.g. Gott et al. 1990, Schmalzing & Gorski 1998, Novikov, Schmalzing & Mukhanov

2000, Shandarin 2002), the harmonic space analysis (Hansen, Pastor & Semikoz 2002), the peak statistics (e.g. Bond & Efstathiou 1987, Vittorio & Juszkiewicz 1987).

Not only departures from the simplest inflation model can generate non-Gaussian signatures. Systematic effects, point source and foreground-induced non-Gaussianities will inevitably arise at small scales from the secondary anisotropies, either through the non-linear growth of fluctuations or through the interactions of CMB photons with the potential wells or ionised matter along their lines of sight. Besides, the study of secondary non-Gaussianities is very interesting on its own, since it is related to the cosmic structures, their evolution and spatial distribution; it is also of great importance in order to go beyond the information provided by the power spectrum of the CMB primary anisotropies. In this context, the higher order statistics of the secondary anisotropies are used to predict the NG signatures of non-primordial origin in the CMB, and to better detect and understand the structures themselves.

The NG signatures are of particular importance in the case of gravitational lensing since they allow us in theory to reconstruct the mass distribution of the lenses. As a matter of fact, the deflection angles are small compared to the scale of structures and the lensing effect is hardly seen directly in a CMB map. The effects on the power spectrum are generally small and sub-dominant, and the two point-statistics is thus not sufficient to allow for the reconstruction of the mass distribution of lenses. To better identify the effects of gravitational lensing on the CMB, one has therefore to consider the induced NG signatures, naturally arising from the second order effects in the anisotropies (correlations between large scale gradients and small scale generated power), through higher-order statistics. The weak lensing of primary anisotropies produces a four-point signature (e.g. Bernardeau 1997, Zaldarriaga 2000, Kesden, Cooray & Kamionkowski 2003). Quadratic statistics (such as the power spectrum of the squared temperature maps) permit us to recover the information in the four-point function about the mass distribution of the lens field (e.g. Zaldarriaga & Seljak 1999, Hu 2001, Takada 2001, Hu & Okamoto 2002, Cooray & Kesden 2003). These methods use lensed anisotropy maps only, or combine them with the polarisation field (especially the B field) which is less contaminated by the primary signal. In all cases, mapping the lens, and thus dark matter, distribution requires high resolution, high signal-to-noise maps of the CMB temperature fluctuations and polarisation fields.

The interactions of CMB photons with the free electrons along their lines of sight, through Compton or Doppler effects, also produce secondary NG signatures. These sources of secondary anisotropies are expected to be important; it was therefore necessary to forecast their NG signal and study its detectability. This was done mainly for the SZ effect and the inhomogeneous reionisation through the trispectrum (Cooray 2001) and through the high-order moments of the wavelet coefficients (Aghanim & Forni 1999). For the SZ thermal effect, Cooray (2001) gave the expression for the trispectrum of the TSZ effect in the flat sky approximation

$$\langle y(\ell_1)y(\ell_2)y(\ell_3)y(\ell_4) \rangle_c = (2\pi)^2 \delta(\ell_{1234}) T^{\text{TSZ}}(\ell_1, \ell_2, \ell_3, \ell_4), \quad (58)$$

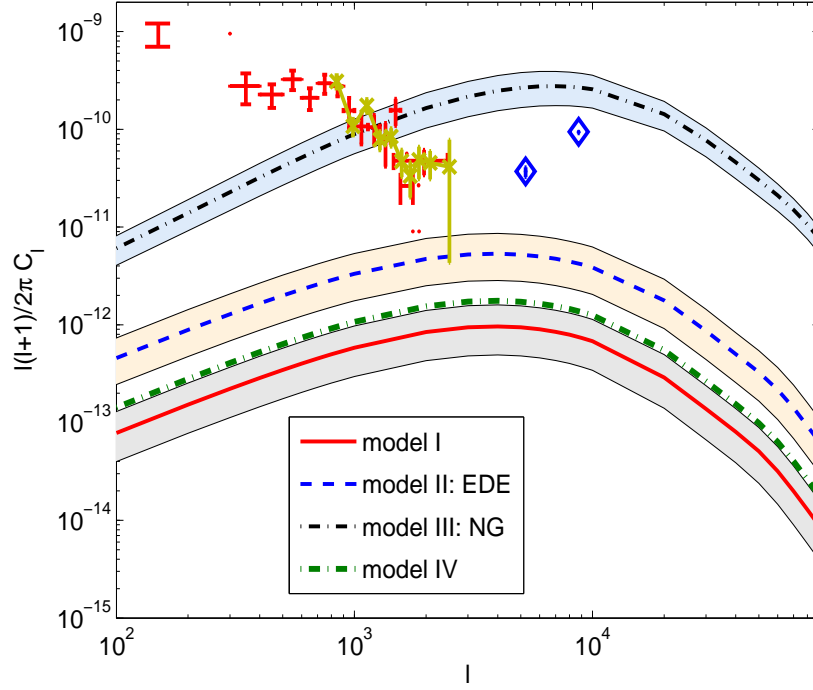


Figure 19. From Sadeh, Rephaeli & Silk (2007): SZ power spectrum obtained for a Λ CDM model with $\sigma_8 = 0.74$ (solid line) and 0.8 (thick dash-dotted line), an early dark energy model (dashed line) and a non-Gaussian χ_m^2 model (dash-dotted line). Shaded area correspond to WMAP 1σ error on σ_8 . The data points are those of BIMA (diamonds), ACBAR (x symbols) and CBI (crosses).

where $_c$ designate the connected part and T^{TSZ} is given by

$$T^{\text{TSZ}} = \int dr \frac{W^{\text{TSZ}}(r)^4}{d_A^6} T_{\Pi} \left(\frac{\ell_1}{d_A}, \frac{\ell_2}{d_A}, \frac{\ell_3}{d_A}, \frac{\ell_4}{d_A}; r \right). \quad (59)$$

where T_{Π} is the pressure trispectrum. The weight function $W^{\text{TSZ}}(r) = -2 \frac{k_B \sigma_T \bar{n}_e}{a(r)^2 m_e c^2}$ is given in the Rayleigh-Jeans regime. In all cases, the signal from SZ effect dominates at small angular scales. For all vector-like fields such as the Ostriker-Vishniac effect, but also the mildly non-linear regime probed by the KSZ effect for large scale structures, even moments were shown to dominate over odd moments, making the trispectrum a more sensitive estimator of non-Gaussianity than the bispectrum (Castro 2004). As a result while the bispectrum is most likely undetectable by future CMB experiments, the trispectrum of the OV effect could be measured by Planck or by arc-minute scale interferometric experiments.

The NG signatures associated with the secondary effects can be used to probe and trace the matter distribution, they can also be used as additional constraints to separate the secondary effects from the primary CMB signal (e.g. Forni & Aghanim 2004). However in all these cases, this signal at small angular scales is the sum of the CMB anisotropies and all the secondary contributions. This makes it harder to disentangle

them and requires the use of the polarisation field or cross-correlations and couplings between components.

Figure 19 shows an example of SZ angular power spectra for the galaxy cluster contribution, demonstrating that the non-Gaussian χ_m^2 model can have a substantial impact for $10^3 < \ell < 10^4$, especially in the case of WMAP-3 yrs normalisation ($\sigma_8 = 0.74$). Also shown are examples of Gaussian models with different normalisations ($\sigma_8 = 0.74, 0.8$) and an early dark energy model (Bartelmann, Doran & Wetterich 2006).

11. Discussion and conclusion

Secondary effects induce temperature and polarisation anisotropies. These additional anisotropies contribute to the CMB signal and modify (at certain scales) both its amplitude and its statistical character. Such contribution was not actually important within the context of first generation of CMB experiments (e.g. COBE). Already now with WMAP, and even more so with future Planck satellite, the aim of measuring the CMB signal with fundamental instrumental noise limits forces us to investigate with extreme care the effects of the secondary anisotropies. They might constitute in some cases important limiting factor on the scientific objectives of future CMB studies such that constraining the energy scale of inflation through the *B*-mode polarisation induced by the stochastic gravitational wave background, or constraining the inflationary field through the statistical nature of the temperature anisotropies. Present day CMB experiments are now reaching sensitivities and angular resolutions such that secondary effects can be no longer neglected. This is the case for lensing by large scale structures which convert the *E*-mode primary polarisation into a *B*-mode secondary contribution and is by far the largest contaminant. This is also the case for the example of the SZ effect from galaxy clusters which could explain the excess of power at high multipoles measured by ACBAR, BIMA and CBI.

The SZ effect is more than a nuisance factor to cosmological parameter extraction. It is a potentially powerful tool for cosmology. SZ cluster counts can be used to probe the cosmological model and put constraints on the nature of dark energy. In combination with other observations, especially at X-ray energies, it allows us to measure cosmological parameters such as the Hubble constant and the cluster gas mass fraction (e.g. Grego et al. 2001). The SZ effect can also be used to characterise the clusters themselves as it potentially can measure their radial peculiar velocities (Lamarre et al. 1998, Benson et al. 2003). The non-relativistic corrections to the SZ effect can also be used to measure the gas temperature directly for massive clusters. This might be an important issue for future SZ surveys for which X-ray counterparts will not be available. The spectral signature of the SZ effect can in principle probe the electron gas distribution and constrain any non-thermal electron population in the intracluster medium. Moreover multi-frequency SZ measurements might provide a novel way of constraining the CMB temperature and its evolution with redshift (Battistelli et al. 2003, Horellou et al. 2005).

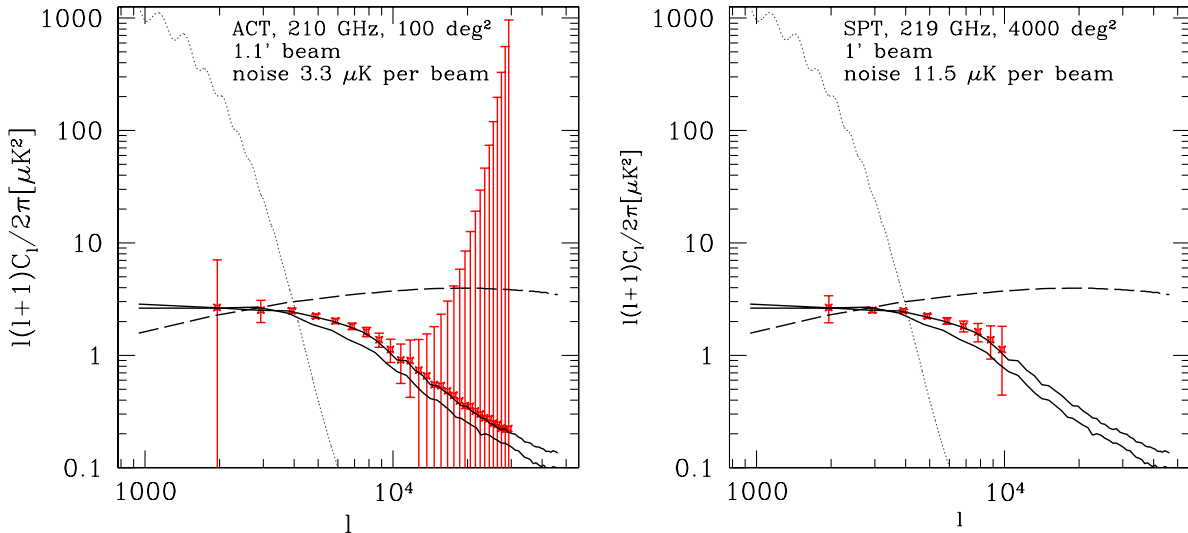


Figure 20. From Iliev et al. (2007b): Observability of the Doppler induced temperature anisotropies: the sky power spectrum of the reionization signal (black, solid; from two simulations) with the forecast error bars for ACT (left) and SPT (right). The primary CMB anisotropy (dotted) and the post-reionization KSZ signal (dashed) are also shown and are added to the noise error bars for the reionization signal. The TSZ component is assumed to be completely separated.

To achieve these goals, high precision measurements of the SZ effect will be needed over large areas of the sky. This requires a new generation of SZ telescopes that are already being built or designed. Following OVRO and BIMA, the Sunyaev-Zel'dovich Array (SZA) which consists of eight 3.5 metre telescopes is operating at 26–36 GHz and 85–115 GHz. The SZA along with BIMA/OVRO forms the Combined ARray for Millimeter Astronomy (CARMA) telescope which aims at providing high resolution, detailed imaging of SZ clusters. Several other telescopes are being commissioned (e.g. AMI), in 2007, with the aim of surveying large areas of the SZ sky for blind detection of clusters. These deep SZ cluster surveys will be performed by the AMIBA interferometer, the South Pole Telescope (SPT), the Atacama Cosmology Telescope (ACT) and the Atacama Pathfinder Experiment (APEX). Moreover, the Planck satellite scheduled to be launched in 2008 will detect thousands of SZ clusters over the whole sky.

Although both ACT and SPT are primarily designed for SZ cluster detection, the predicted KSZ signal, at a few arc minute scales, induced by the reionisation might be sufficiently strong to be detected by these upcoming experiments (Figure 20). These high ℓ measurements of the reionisation-induced temperature anisotropies will however not suffice to unravel the ionisation history. Polarisation measurements at low ℓ are the optimal CMB tool to achieve this. In the near future, Planck will provide all sky E -mode polarisation maps and will be sensitive to partial or double reionisation models at the percent level. In principle this could help discriminate between different models

with identical optical depths (Kaplinghat et al. 2003), subject to our being able to understand, model and remove the relevant galactic foregrounds. In combination with low frequency radio interferometer such as LOFAR and eventually SKA it should be possible to probe the onset of the reionisation and the end of the dark ages by anti-correlating 21 cm emission and CMB temperature fluctuations (Alvarez et al. 2006).

The next generation of polarisation-optimised satellites, such as B-POL or EPIC, is being designed to measure the primary B -modes from inflation. These experiments will inevitably have high enough sensitivity to actually reconstruct the ionisation history of the universe. A new generation of moderate resolution ground-based and balloon-born CMB polarisation (CLOVER, at 97, 150, and 220 GHz, QUIET at 40 and 90 GHz, QUA-D, EBEX, BICEP, SPIDER, BRAIN) are under operation, construction or design. The principal aim is to measure primordial B -modes. They will also measure weak lensing-induced B -modes with resolution over multipoles $20 < \ell < 1000$ and down to $\sim 0.1\mu\text{K}$ precision. This is an essential prerequisite to searching, at these scales, for the gravity-wave induced B -mode background from inflation. For $20 < \ell < 100$, current constraints on the scalar to tensor ration should allow the primordial signal to dominate lensing.

Secondary effects are not simply a “foreground” that adds noise and limits our knowledge. They are by nature the best tools to probe structure formation and evolution providing a complementary picture of the late time universe to that obtained from traditional tools like galaxy surveys.

Acknowledgments

The authors would like to thank an anonymous referee and Matthias Bartlemann for careful reading and commenting of the article. NA and SM wish to thank Oxford University for hospitality. SM would like to thank CITA where a large part of the work was done as well as IAS-Orsay for hospitality during the final stages of the review.

References

- Abell, G.O. 1958, *Astrophys. J. Supp.*, **3**, 211
- Abel T., Bryan G. L. & Norman M. L. 2000, *Astrophys. J.*, **540**, 39
- Abel T., Bryan G. L. & Norman M. L. 2002, *Science*, **295**, 93
- Abroe, M. E., et al. 2004, *Astrophys. J.*, **605**, 607
- Afshordi, N. 2004, *Physical. Rev. D*, **70**, 083536
- Afshordi, N. Lin, Y.-T., & Sanderson, A. J. R. 2005, *Astrophys. J.*, **629**, 1
- Aghanim, N., De Luca, A., Bouchet, F. R., Gispert, R. & Puget, J. L. 1997, *Astron. Astrop.*, **325**, 9
- Aghanim, N., Prunet, S., Forni, O. & Bouchet, F. R. 1998, *Astron. Astrop.*, **334**, 409
- Aghanim, N. & Forni, O. 1999, *Astron. Astrop.*, **347**, 409
- Aghanim, N., Balland, C. & Silk J. 2000, *Astron. Astrop.*, **357**, 1
- Aghanim, N., Hansen, S. H., Pastor, S., & Semikoz, D. V. 2003, *JCAP*, **5**, 7.
- Aghanim, N., Hansen, S.H., Lagache, G. 2005, *Astron. Astrop.*, **439**, 901
- Alvarez, M.A., Shapiro, P.R., Ahn, K., Iliev, I.T. 2006, *Astrophys. J.*, **644**, L101
- Alvarez, M. A., Komatsu, E., Doré, O. & Shapiro, P. R. 2006, *Astrophys. J.*, **647**, 840

- Amblard, A., Vale, C., White, M. 2004, *astr-ph/0403075*
- Ameglio, S., Borgani, S., Diaferio, A., Dolag, K. 2006, *Mon. Not. Roy. Ast. Soc.*, **369**, 1459
- Arnaud, M.; Pointecouteau, E. & Pratt, G. W., 2005, *Astron. Astrop.*, **441**, 893
- Atrio-Barandela, F. & Mucket, J., 1999, *Astrophys. J.*, **515**, 465
- Audit, E. & Simmons, J. F. L., 1999, *Mon. Not. Roy. Ast. Soc.*, **305**, L27
- Barreiro, R. B. & Hobson, M. P. 2001, *Mon. Not. Roy. Ast. Soc.*, **327**, 813
- Bartelmann, M., Doran, M., Wetterich, C. 2006, *Astron. Astrop.*, **454**, 27
- Bassett, B.A. & Kunz, M. 2004, *Astrophys. J.*, **607**, 661
- Battistelli, E. S. et al. 2003, *Astrophys. J.*, **598**, L75
- Bean, R., Melchiorri, A., Silk, J. 2007, *Physical. Rev. D*, **75**, 063505
- Benabed, K., Bernardeau, F. & van Waerbeke, L. 2001, *Physical. Rev. D*, **63**, 3501
- Benson, B. A., Church, S. E., Ade, P. A. R., et al. 2003, *Astrophys. J.*, **592**, 674
- Bernardeau, F. 1997, *Astron. Astrop.*, **324**, 15
- Bernardeau, F., 1998, *Astron. Astrop.*, **338**, 767
- Bernardeau, F. & Uzan, J.-P. 2002, *Physical. Rev. D*, **66**, 103506
- Birkinshaw, M. & Gull, S. F. 1978, *Nature*, **274**, 111
- Birkinshaw, M. & Gull, S. F. 1983, *Nature*, **302**, 315
- Birkinshaw, M. 1989, in Moving Gravitational lenses, p. 59, eds. J. Moran, J. Hewitt & K.Y. Lo; Springer-Verlag, Berlin
- Birkinshaw, M., Hughes, J.P., & Arnaud, K. A. 1991, *Astrophys. J.*, **379**, 466
- Birkinshaw, M. & Hughes, J.P. 1994, *Astrophys. J.*, **420**, 33
- Birkinshaw, M., 1999, *Phys. Rept.*, **310**, 97
- Birkinshaw, M. & Lancaster, K., 2004, Background Microwave Radiation and Intracluster Cosmology, Proceedings of the International School of Physics "Enrico Fermi", *astro-ph/0410336*
- Blanchard, A. & Schneider, J., 1987, *Astron. Astrop.*, **184**, 1
- Bock, J., et al. 2006, *astro-ph/0604101*
- Bonamente, M., Joy, M., La Roque, S., Carlstrom, J., Reese, E., Dawson, K., 2006, *Astrophys. J.*, **647**, 25
- Bond, J. R. & Efstathiou, G., 1984, *Astrophys. J.*, **285**, 45
- Bond, J. R.; Efstathiou, G., 1987, *Mon. Not. Roy. Ast. Soc.*, **226**, 655
- Bond, J., Kaiser, N., Cole, S. & Efstathiou, G., 1991, *Astrophys. J.*, **379**, 440
- Borgani, 2006, Lectures for 2005 Guillermo Haro Summer School on Clusters, to appear in "Lecture notes in Physics", *astro-ph/0605575*
- Boughn, S. P.; Crittenden, R. G.; Turok, N. G., 1998, *New Astron.*, **3**, 275
- Boughn, S.P. & Crittenden, R.G. 2002, *Physical. Rev. Lett.*, **88**, 021302
- Boughn, S.P. & Crittenden, R.G. 2004, *Nature*, **427**, 45
- Bromm, V., Kudritzki, R. P. & Loeb, A., 2001, *Astrophys. J.*, **552**, 464
- Bromm, V., Coppi, P. S. & Larson, R. B., 2002, *Astrophys. J.*, **564**, 23
- Bunn, E. F., 2006, *Physical. Rev. D*, **73**, 3517
- Carlstrom, J. E., Holder, G. P. & Reese, E. D. 2002, *Ann. Rev. of Astron. Astrop.*, **40**, 643
- Carroll, S. M., Press, W. H. & Turner, E. L., 1992, *Ann. Rev. of Astron. Astrop.*, **30**, 499
- Castro, P. G., 2004, *Physical. Rev. D*, **67**, 044039
- Cavaliere, A. & Fusco-Femiano, R., 1978, *Astron. Astrop.*, **70**, 677
- Cayon, L., Martinez-Gonzalez, E., Sanz, J., 1993, *Astrophys. J.*, **413**, 10
- Cen, R., 2003, *Astrophys. J.*, **591**, 5
- Challinor, A. D. & Lasenby, A. N., 1998, *Astrophys. J.*, **499**, 1
- Challinor, A. D. & Lasenby, A. N., 1999, *Astrophys. J.*, **510**, 930
- Challinor, A. D. & Lewis, A. , 2005, *Physical. Rev. D*, **71**, 103010
- Chatterjee, S. & Kosowsky, A., 2007, *astrop-ph/0701759*
- Chluba, J. & Mannheim, K., 2002, *Astron. Astrop.*, **396**, 419
- Chodorowski, M., 1992, *Mon. Not. Roy. Ast. Soc.*, **259**, 218

- Chodorowski, M., 1994, *Mon. Not. Roy. Ast. Soc.*, **266**, 897
- Ciardi, B. & Madau, P., 2003, *Astrophys. J.*, **596**, 1
- Ciardi, B., Ferrara, A. & White, S. D. M., 2003, *Mon. Not. Roy. Ast. Soc.*, **344**, L7
- Colafrancesco, S., Marchegiani, P. & Palladino, E., 2003, *Astron. Astrop.*, **397**, 27
- Cole, S. & Kaiser, N., 1988, *Mon. Not. Roy. Ast. Soc.*, **233**, 637
- Cooray A. 2001, *Physical. Rev. D*, **64**, 0635
- Cooray, A. 2002a, *Physical. Rev. D*, **65**, 083518
- Cooray, A. 2002b, *Physical. Rev. D*, **65**, 3510
- Cooray, A. 2002c, *Physical. Rev. D*, **65**, 3512
- Cooray, A. & Sheth, R., 2002, *Phys. Rep.*, **372**, 1
- Cooray, A. & Baumann, D., 2003, *Physical. Rev. D*, **67**, 063505
- Cooray, A. & Kesden, M. 2003, *New Astron.*, **8**, 231
- Cooray, A., Huterer, D., Baumann, D., 2004, *Physical. Rev. D*, **69**, 027301
- Cooray, A. & Seto, N., 2005, *Journal of Cosm. & Astropart.*, **12**, 004
- Corasaniti, P.-S., Gianantonio, T., Melchiorri, A., 2005, *Physical. Rev. D*, **71**, 123521
- Crittenden, R.G. & Turok, N., 1996, *Physical. Rev. Lett.*, **76**, 575
- Dabrowski, Y., Hobson, M.P., Lasenby, A.N., Doran, C.J.L. 1999, *Mon. Not. Roy. Ast. Soc.*, **302**, 757
- Daigne F., Olive K. A., Vangioni-Flam E., Silk J., Audouze, J. 2004, *Astrophys. J.*, **617**, 693
- Dickinson, C., et al., 2004, *Mon. Not. Roy. Ast. Soc.*, **353**, 732
- Diego, J. M., Vielva, P., Martínez-González, E., Silk, J. & Sanz, J. L., 2002, *Mon. Not. Roy. Ast. Soc.*, **336**, 1351
- Diego, J. M., Hansen, S. H. & Silk, J., 2003, *Mon. Not. Roy. Ast. Soc.*, **338**, 796
- Diego, J. M.; Mazzotta, P.; Silk, J., 2003, *Astrophys. J.*, **597**, 1
- Diego, J. M. R., & Majumdar, S., 2004, *Mon. Not. Roy. Ast. Soc.*, **352**, 993
- Dijkstra, M., Haiman, Z. & Loeb, A., 2004, *Astrophys. J.*, **613**, 646
- Dijkstra, M., Haiman, Z., Loeb, A., 2004, *Astrophys. J.*, **613**, 646
- Dodelson, S. & Jubas, J. M. 1995, *Astrophys. J.*, **439**, 503
- Dodelson, S. 2004, *Physical. Rev. D*, **70**, 3009
- Doré, O., Holder, G., Alvarez, M., Iliev, I.T., Mellema, G., Pen, U.-L., Shapiro, P.R., 2007, *astro-ph/0701784*.
- Douspis, M., Aghanim, N. & Langer, M., 2006, *Astron. Astrop.*, **456**, 819
- Dyer, C. C. 1976, *Mon. Not. Roy. Ast. Soc.*, **175**, 429
- Eke, V. R., Cole, S. & Frenk, C. S., 1996, *Mon. Not. Roy. Ast. Soc.*, **282** 263
- Ensslin, T. A. & Kaiser, C. R., 2000, *Astron. Astrop.*, **360**, 417
- Ensslin, T. A. & Hansen, S. H., 2004, preprint, *astro-ph/0401337*
- Evraud, A. E. 1990, *ApJ*, **363**, 349.
- Fan, et al., 2003, *Astron. J.*, **125**, 1649
- Fang, L.-Z. & Wu, X.-P., 1993, *Astrophys. J.*, **408**, 25
- Ferrarese, L. & Merritt, D., 2000, *Astrophys. J.*, **539**, 9
- Forni, O. & Aghanim, N., 1999, *Astron. Astrop. Suppl.*, **137**, 553
- Forni, O. & Aghanim, N. 2004, *Astron. Astrop.*, **420**, 49
- Fosalba, P. & Gaztanaga, E., 2005, *Mon. Not. Roy. Ast. Soc.*, **350**, 37
- Fukugita, M., Hogan, C. J., & Peebles, P. J. E., 1998, *Astrophys. J.*, **503**, 518
- Gangui, A., Lucchin, F., Matarrese, S. & Mollerach, S., 1994, *Astrophys. J.*, **430**, 447
- Gaztanaga, E., Manera, M., Multamaki, T. 2006, *Mon. Not. Roy. Ast. Soc.*, **365**, 171
- Gebhardt et al, 2000, *Astrophys. J.*, **543**, L5
- Gibilisco, M., 1997, *Astrop. & Space Suppl.*, **249**, 189
- Gladders, M. D., Yee, H. K. C., Majumdar, S., Barrientos, L. F., Hoekstra, H., Hall, P. B. & Infante, L., 2007, *Astrophys. J.*, **655**, 128
- Gnedin, N. Y., 2000, *Astrophys. J.*, **535**, 530
- Gnedin, N. Y. & Jaffe, A. H., 2001, *Astrophys. J.*, **551**, 3

- Gnedin, N. Y. & Prada, F., 2004, *Astrophys. J.*, **608**, 77
- Goldberg, D.M. & Spergel, D.N., 1999, *Physical. Rev. D*, **59**, 3002
- Gomez, P.L. et al., 2003, Contribution to "Matter and Energy in Clusters of Galaxies", Taipei April 2002, astro-ph/0301024.
- Gott, J. R.; Park, C.; Juszkiewicz, R.; Bies, W. E.; Bennett, D. P.; Bouchet, F. R.; Stebbins, A., 1990, *Astrophys. J.*, **352**, 1
- Grego, L., Carlstrom, J. E., Reese, E. D., Holder, G. P., Holzapfel, W. L., Joy, M. K., Mohr, J. J. & Patel, S., 2001, *Astrophys. J.*, **552**, 2
- Gruzinov, A. & Hu, W., 1998, *Astrophys. J.*, **508**, 435
- Guth, A., 1981, *Physical. Rev. D*, **23**, 347
- Haiman, Z., Abel, T. & Madau, P., 2001, *Astrophys. J.*, **551**, 599
- Haiman, Z., Mohr, J. J. & Holder, G. P., 2001, *Astrophys. J.*, **553**, 545
- Haiman, Z., Holder, G. P., 2003, *Astrophys. J.*, **595**, 1
- Hansen, S. H., Pastor, S. & Semikoz, D. V., 2002, *Astrophys. J.*, **573**, L69
- Hansen, S. & Haiman, Z., 2004, *Astrophys. J.*, **600**, 26
- Hattori, M. & Okabe, N., 2004, JKAS, **37**, 543.
- Hernández-Monteagudo, C. & Rubino-Martin, J. A., 2004, *Mon. Not. Roy. Ast. Soc.*, **347**, 403.
- Hirata, C.M. & Seljak, U., 2003, *Physical. Rev. D*, **67**, 043001
- Hobson M. P., Jones A. W., Lasenby A. N., Bouchet F. R., 1998, *Mon. Not. Roy. Ast. Soc.*, **300**, 1
- Holder, G. P., Mohr, J. J., Carlstrom, J. E., Evrard, A. E. & Leitch, E. M., 2000, *Astrophys. J.*, **544**, 629
- Holder, G. P., 2002, *Astrophys. J.*, **580**, 36
- Holder G.P. et al. 2003, *Astrophys. J.*, **595**, 13
- Holder, G. & Kosowsky, A. 2004, *Astrophys. J.*, **616**, 8
- Holzapfel, W. L., Ade, P. A. R., Church, S. E., et al. Mauskopf, P. D., Rephaeli, Y., Wilbanks, T. M. & Lange, A. E., 1997, *Astrophys. J.*, **481**, 35
- Horellou, C.; Nord, M.; Johansson, D.; Lévy, A., 2005, *Astron. Astrop.*, **441**, 435
- Hu, W. & White, M., 1996, *Astrophys. J.*, **471**, 30
- Hu, W. & White, M., 1997, *Physical. Rev. D*, **56**, 596
- Hu, W., 2000, *Astrophys. J.*, **529**, 12
- Hu, W., 2001, *Physical. Rev. D*, **64**, 083005
- Hu, W. & Dodelson, S., 2002, *Ann. Rev. of Astron. Astrop.*, **40**, 171
- Hu, W. & Okamoto, T., 2002, *Astrophys. J.*, **574**, 566
- Hu, W., 2003, *Physical. Rev. D*, **67**, 081304
- Hu, W. & Okamoto , T., 2004, *Physical. Rev. D*, **69**, 043004
- Hu, W., Scott, D. & Silk, J., 1994, *Physical. Rev. D*, **49**, 648
- Hughes, J.P. & Birkinshaw, M., 1998, *Astrophys. J.*, **501**, 1
- Iliev, I.T., Pen, U.-L., Bond, J.R., Mellema, G., Shapiro, P.R., 2007a, *Astrophys. J.*, **660**, 933
- Iliev, I.T., Mellema, G., Pen, U.-L., Bond, J.R., Shapiro, P.R. 2007b, preprint, astro-ph/0702099
- Inagaki, Y., Sugino, T., Suto, Y., 1995, *Proc. of the Astrop. Soc. of Japan*, **47**, 411
- Islam, R. R., Taylor, J. E. & Silk J., 2003, *Mon. Not. Roy. Ast. Soc.*, **340**, 647
- Itoh, N., Kohyama, Y. & Nozawa, S., 1998, *Astrophys. J.*, **502**, 7
- Itoh, N., Kawana, Y., Nozawa, S., & Kohyama Y., 2001, *Mon. Not. Roy. Ast. Soc.*, **327**, 567
- Jaffe, A. H. & Kamionkowski, 1998, *Physical. Rev. D*, **58**, 043001
- Jenkins, A. et al., 2001, *Mon. Not. Roy. Ast. Soc.*, **321**, 372
- Jing, Y. P., 1999, *Astrophys. J.*, **515**, L45
- Jones, M. et al. 1993, *Nature*, **365**, 320
- Kaiser, N. 1982, *Mon. Not. Roy. Ast. Soc.*, **198**, 1033
- Kaiser, N., & Stebbins, A., 1984, *Nature*, **310**, 391
- Kamionkowski, M. & Spergel, D. N., 1994, *Astrophys. J.*, **432**, 7
- Kamionkowski, M. 1996, *Physical. Rev. D*, **54**, 4169

- Kamionkowski, M. & Loeb, A., 1997, *Physical. Rev. D*, **56**, 4511
 Kaplinghat, M., Knox, L., Song, Y.-S., 2003, *Physical. Rev. Lett.*, **89**, 011303
 Kaplinghat, M. et al., 2003, *Astrophys. J.*, **583**, 24
 Kashlinsky, 1988, *Astrophys. J.*, **331**, 1
 Kesden, M., Cooray, A., Kamionkowski, M. 2003, *Physical. Rev. D*, **67**, 123507
 Kinkhabwala, A. & Kamionkowski, M. 1999, *Physical. Rev. Lett.*, **83**, 4172
 Knox, L., Scoccimarro, R. & Dodelson, S., 1998, *Physical. Rev. Lett.*, **81**, 2004
 Kobayashi, S., Sasaki, S. & Suto, Y., 1996, *Proc. of the Astrop. Soc. of Japan*, **48**, 107
 Koch, P. M., Jetzer, P. & Puy, D., 2003, *New Astron.*, **8**, 1
 kofman85 Kofman, L. A. & Starobinskii, A. A. 1985, Sov. Astr. Let., 11, 271.
 Kogut, A. et al., 2003, *Astrophys. J. Supp.*, **148**, 161
 Komatsu, E. et al, 1999, *Astrophys. J.*, **516**, L1
 Komatsu, E. & Kitayama, T., 1999, *Astrophys. J.*, **526**, L1
 Komatsu, E. & Seljak, U., 2001 *Mon. Not. Roy. Ast. Soc.*, **327**, 1353
 Komatsu, E. & Seljak, U., 2002, *Mon. Not. Roy. Ast. Soc.*, **336**, 1256
 Komatsu, E. & Spergel, D. N., 2001, *Physical. Rev. D*, **63**, 3002.
 Koyama, K., Soda, J., Taruya, A. 1999, *Mon. Not. Roy. Ast. Soc.*, **310**, 1111
 Kunz, M., Banday, A. J., Castro, P. G., Ferreira, P. G., Górski, K. M. , 2001, *Astrophys. J.*, **563**, L99
 Kuo, C. L., et al. 2004, *Astrophys. J.*, **600**, 32
 Lacey, C. & Cole, S., 1993, *Mon. Not. Roy. Ast. Soc.*, **262**, 627
 Lamarre, J. M., Giard, M., Pointecouteau, E., et al. Bernard, J. P., Serra, G., Pajot, F., Désert, F. X., Ristorcelli, I., Torre, J. P., Church, S., Coron, N., Puget, J. L. & Bock, J. J., 1998, *Astrophys. J.*, **507**, L5.
 Landriau, M.; Shellard, E. P., 2003, *Physical. Rev. D*, **67**, 3512
 Lapi, A.; Cavaliere, A.; De Zotti, G., 2003, *Astrophys. J.*, **597**, 93
 Lasenby, A.N., Doran, C.J.L., Hobson, M.P., Dabrowski, Y., Challinor, A.D., 1999, *Mon. Not. Roy. Ast. Soc.*, **302**, 748
 Lesgourgues, J., Perotto, L., Pastor, S., Piat, M., 2006, *Physical. Rev. D*, **73**, 5021
 Levine, E. S., Schulz, A. E. & White, M., 2002, *Astrophys. J.*, **577**, 569
 Lewis, A. 2005, *Physical. Rev. D*, **71**, 083008
 Lewis, A. & Challinor, A. 2006, *Phys. Rept.*, **429**, 1
 Lima, M. & Hu, W. 2004, *Physical. Rev. D*, **70**, 043504
 Linder, E., 1988, *Astron. Astrop.*, **206**, 199
 Liu, G., et al., 2001, *Astrophys. J.*, **561**, 504
 Liu, G., da Silva, A. & Aghanim, N. 2005, *Astrophys. J.*, **561**, 504
 Lukic, Z., Heitmann, K., Habib, S., Bashinsky, S. & Ricker, P. M., 2007, preprint, *astro-ph/0702360*
 Ma, C.-P. & Bertschinger, E., 1995, *Astrophys. J.*, **455**, 7
 Ma, C.P. & Fry, J.N., 2000, *Astrophys. J.*, **543**, 503
 Ma, C.P. & Fry, J.N., 2002, *Physical. Rev. D*, **88**, 211301
 Madau, P., Meiksin, A. & Rees, M.J., 1997, *Astrophys. J.*, **475**, 429
 Madau, P., Rees, M. J., Volonteri, M., Haardt, F. & Oh, S. P. 2004, *Astrophys. J.*, **604**, 484
 Majumdar, S. & Nath, B. B., 2000, *Astrophys. J.*, **542**, 597
 Majumdar, S. & Nath, B. B., 2001, *Mon. Not. Roy. Ast. Soc.*, **324**, 537
 Majumdar, S., 2001, *Astrophys. J.*, **555**, L7
 Majumdar, S. , 2001b, PhD Thesis, Indian Institute of Science, Bangalore
 Majumdar, S. & Mohr, J. J., 2003, *Astrophys. J.*, **585**, 603
 Majumdar, S. & Mohr, J. J., 2004, *Astrophys. J.*, **613**, 41
 Majumdar, S. & Cox, G., 2007, preprint in preparation
 Makino, N. & Suto, Y., 1993, *Astrophys. J.*, **405**, 1
 Makino, N., Sasaki, S. Suto, Y., 1998, *Astrophys. J.*, **497**, 555
 Martinez-González, E., Sanz, J.-L., & Silk, J., 1990, *Astrophys. J.*, **355**, L5

- Mathiesen, B., Evrard, A. E., & Mohr, J. J., 1999, *Astrophys. J.*, **520**, 21
 Mathis, H., Diego, C. & Silk, J., 2004, *Mon. Not. Roy. Ast. Soc.*, **353**, 681
 Metcalf, R.B. & Silk, J., 1997, *Astrophys. J.*, **489**, 1
 Mohr, J. J., Evrard, A. E., Fabricant, D. G., & Geller, M. J., 1995, *Astrophys. J.*, **447**, 8
 Mohr, J. J., Mathiesen, B., & Evrard, A. E. 1999, *Astrophys. J.*, **517**, 627
 Mollerach, S., Harary, D., & Matarrese, S., 2004, *Physical. Rev. D*, **69**, 3002
 Molnar, S. M. & Birkinshaw, M., 1999, *Astrophys. J.*, **523**, 78.
 Molnar, S. & Birkinshaw, M., 2000, *Astrophys. J.*, **537**, 542
 Mortonson, M.J. & Hu, W., 2007, *Astrophys. J.*, **657**, 1
 Motl, P. M., Hallman, E. J., Burns, J. O. & Norman, M. L., 2005 *Astrophys. J.*, **623**, L63
 Mukhanov, V. F., Feldman, H. A. & Brandenberger, R. H. ,1992, *Physical. Rev. D*, **215**, 203
 Murgia, M., Govoni, F., Ferretti, L., Dallacasa, D., Giovaninni, G., Fanti, R., Taylor, G.B., Dolag, K., 2004, *Astron. Astrop.*, **424**, 429
 Natarajan, P. & Sigurdsson, S. 1999, *Mon. Not. Roy. Ast. Soc.*, **302**, 288
 Navarro, J. F., Frenk, C. S. & White, S. D. M., 1997, *Astrophys. J.*, **490**, 493
 Ng, K. L. & Ng, K.-W., 1996, *Astrophys. J.*, **456**, 413
 Nolta, M.R. et al. , 2004, *Astrophys. J.*, **608**, 10
 Novikov, D., Schmalzing, J. & Mukhanov, V. F., 2000, *Astron. Astrop.*, **364**, 17
 Nozawa, S., Itoh, N. & Kohyama, Y., 1998, *Astrophys. J.*, **508**, 17
 Nozawa, S., Itoh, N., Kawana, Y. & Kohyama, Y., 2000, *Astrophys. J.*, **536**, 31
 Oh, S. P., 2001, *Astrophys. J.*, **553**, 499
 Oh, S. P., Cooray, A., & Kamionkowski, M., 2003, *Mon. Not. Roy. Ast. Soc.*, **342**, 20
 Ohno, H., Takada, M., Dolag, K., Bartelmann, M. & Sugiyama, N., 2003, *Astrophys. J.*, **584**, 599
 Okamoto, T. & Hu, W., 2003, *Physical. Rev. D*, **67**, 3002
 Ostriker, J. P. & Vishniac, E. T., 1986, *Astrophys. J.*, **306**, L51
 Padmanabhan, N. & Finkbeiner, D. 2005, *Physical. Rev. D*, **72**, 023508.
 Padmanabhan, N. et al. 2005, *Physical. Rev. D*, **72**, 043525
 Pando, J., Valls-Gabaud, D. & Fang, L. Z. 1998, *Physical. Rev. Lett.*, **81**, 4568
 Panek, M. 1992, *Astrophys. J.*, **388**, 225
 Peebles, P. J. E. & Yu, J. T. 1970, *Astrophys. J.*, **162**, 815
 Peebles P. J. E., 1980, Large Scale Structure of the Universe., Princeton University Press, Princeton
 Pfrommer, C., Ensslin, T. A., Springel, V., Jubelgas, M. & Dolag, K., 2006, preprint, *astro-ph/0611037*
 Pierpaoli, E., Anthoine, S., Huffenberger, K. & Daubechies, I., 2006, *Mon. Not. Roy. Ast. Soc.*, **359**, 261
 Pires, S., Juin, J. B., Yvon, D., Moudden, Y., Anthoine, S. & Pierpaoli, E. 2006, *Astron. Astrop.*, **455**, 741
 Pogosian, L. 2006, *New Astr. Rev.*, **50**, 932
 Portsmouth, J. 2004, *Physical. Rev. D*, **70**, 063504
 Pointecouteau, E. 1999, *Astrophys. J.*, **519**, 115.
 Press, W. H. & Schechter, P., 1974, *Astrophys. J.*, **187**, 425
 Puy, D., Grenacher, L., Jetzer, Ph., Signore, M. 2000, *Astron. Astrop.*, **363**, 415
 Rassat, A., Land, K., Lahav, O., Abdalla, F.B. 2006, *astro-ph/0610911*
 Readhead, A. C. S., et al. 2004, *Astrophys. J.*, **609**, 498
 Rees, M. J. & Sciama, D. W. 1968, *Nature*, **511**, 611
 Reese, E. D., Carlstrom, J. E., Joy, M., Mohr, J. J., Grego, L. & Holzapfel, W. L. 2002, *Astrophys. J.*, **581**, 53
 Refregier, A., Komatsu, E., Spergel, D. N. & Pen, U., 2000, *Physical. Rev. D*, **61**, 123001
 Refregier, A. & Teyssier, R., 2002, *Physical. Rev. D*, **66**, 043002
 Rephaeli, Y. 1995, *Ann. Rev. of Astron. Astrop.*, **33**, 541
 Ricotti, M. & Ostriker, J. 2004, *Mon. Not. Roy. Ast. Soc.*, **352**, 547
 Ricotti, M., Ostriker, J. & Gnedin, N. 2005, *Mon. Not. Roy. Ast. Soc.*, **357**, 207

- Rosa-Gonzalez, D.; Terlevich, R.; Terlevich, E.; Friaca, A.; Gaztanaga, E. 2004, *Mon. Not. Roy. Ast. Soc.*, **348**, 669
- Ruhl, J. E., et al. 2003, *Astrophys. J.*, **599**, 786
- Sachs, R.K., Wolfe, A.M. 1967, *Astrophys. J.*, **147**, 73
- Sadeh, S., Rephaeli, Y., Silk, J. 2006, *Mon. Not. Roy. Ast. Soc.*, **368**, 1583
- Sadeh, S., Rephaeli, Y., Silk, J. 2007, astro-ph/0706.1340
- Sanz J. L., Herranz D. & Martinez-Gonzalez E., 2001, *Astrophys. J.*, **552**, 484
- Santos, M. B., Cooray, A., Haiman, Z., Knox, L., Ma, C.-P. 2003, *Astrophys. J.*, **598**, 756
- Sato, K. 1981, *Mon. Not. Roy. Ast. Soc.*, **195**, 467
- Sazonov, S. Y.; Sunyaev, R. A. 1999, *Mon. Not. Roy. Ast. Soc.*, **310**, 765.
- Scannapieco, E. 2000, *Astrophys. J.*, **540**, 20
- Scaramella, R., Cen, R., & Ostriker, J., 1993, *Astrophys. J.*, **416**, 399
- Schaerer, D. 2002, *Astron. Astrop.*, **24**, 337
- Schäfer, B. M., Pfrommer, C., Bartelmann, M., Springel, V. & Hernquist, L. 2006a, *Mon. Not. Roy. Ast. Soc.*, **370**, 1309
- Schäfer, B. M., Pfrommer, C., Hell, R. M. & Bartelmann, M. 2006b, *Mon. Not. Roy. Ast. Soc.*, **370**, 1713
- Schmalzing, J.; Gorski, K. M. 1998, *Mon. Not. Roy. Ast. Soc.*, **297**, 355
- Seljak, U. 1996a, *Astrophys. J.*, **460**, 549
- Seljak, U. 1996b, *Astrophys. J.*, **463**, 1
- Seljak, U., Burwell, J. & Pen, U., 2001, *Physical. Rev. D*, **63**, 063001.
- Seshadri, T. R. & Subramanian, K. 1998, *Physical. Rev. D*, **58**, 3002.
- Shandarin, S. F. 2002, *Mon. Not. Roy. Ast. Soc.*, **331**, 865
- Sheth, R. K. & Tormen, G. 1999, *Mon. Not. Roy. Ast. Soc.*, **308**, 119.
- Sheth, R. K., Mo, H. J. & Tormen, G., 2001, *Mon. Not. Roy. Ast. Soc.*, **323**, 1
- Shimon, M. & Rephaeli, Y. 2004, *New Astron.*, **9**, 69.
- Shimon, M., Rephaeli, Y., O'Shea, B.W., Norman, M.L. 2006, *Mon. Not. Roy. Ast. Soc.*, **368**, 511
- Silk, J. 1967, *Nature*, **215**, 1155
- Silk, J. & White, S. D. M. 1978, *Astrophys. J.*, **226**, 103
- da Silva, A. C., Barbosa, D., Liddle, A. R. & Thomas, P. A. 2000, *Mon. Not. Roy. Ast. Soc.*, **317**, 37.
- da Silva, A. C.; Kay, S. T.; Liddle, A. R.; Thomas, P. A.; Pearce, F. R.; Barbosa, D 2001, *Astrophys. J.*, **561**, 15
- Sokasian, A., Abel, T., Hernquist, L., & Springel, V. 2003, *Mon. Not. Roy. Ast. Soc.*, **344**, 607
- Sokasian, A. et al. 2004, *Mon. Not. Roy. Ast. Soc.*, **350**, 47
- Somerville, R. & Livio, M. 2003, *Astrophys. J.*, **593**, 611
- Spergel, et al. 2003, *Astrophys. J. Supp.*, **148**, 175
- Spergel, et al. 2007, *Astrophys. J. Supp.*, **170**, 377.
- Springel, V., White, M. & Hernquist, L., 2001, *Astrophys. J.*, **549**, 681
- Stebbins, A. 1988, *Astrophys. J.*, **327**, 584.
- Sugiyama, N., Zaroubi, S. & Silk, J. 2004, *Mon. Not. Roy. Ast. Soc.*, **354**, 543
- Sunyaev, R. A. & Zel'dovich, Ya. B., 1970, *Astroph. & Space Sc.*, **7**, 20
- Sunyaev, R. A. & Zel'dovich, Ya. B. 1972, *Comments Astrop. Space Phys.*, **4**, 173
- Sunyaev, R. A. & Zel'dovich, Ya. B. 1980, *Ann. Rev. of Astron. Astrop.*, **18**, 537
- Takada, M. 2001, *Astrophys. J.*, **558**, 29
- Takada M., Ohno H.,& Sugiyama N. *Preprint astro-ph/0112412*
- Tashiro H., Aghanim N., & Langer M. 2007, astro-ph/0705.2861
- Taylor, J. E.; Moodley, K.; Diego, J. M. 2003, *Mon. Not. Roy. Ast. Soc.*, **345**, 1127
- Theuns et al. 2002, *Astrophys. J.*, **574**, 111
- Thompson, K.L. & Vishniac, E.T. 1987, *Astrophys. J.*, **313**, 517
- Toffolatti, L., Negrello, M., González-Nuevo, J., De Zotti, G., Silva, L., Granato, G. L. & Argueso, F., 2005, *Astron. Astrop.*, **438**, 475

- Tomita, K. 2005, *Physical. Rev. D*, **72**, 3526
Tomita, K. 2006, *Physical. Rev. D*, **73**, 9901
Tului, R., Laguna, P., Anninos, P. 1996, *Astrophys. J.*, **463**, 15
Uzan, J.-P., Aghanim, N., Mellier, Y. 2004, *Physical. Rev. D*, **70**, 083533.
Valageas, P.; Balbi, A.; Silk, J. 2001, *Astron. Astrop.*, **367**, 1
Valdés, M., Ciardi, B., Ferrara, A., Johnston-Hollitt, M., Rottgering, H. 2006, *Mon. Not. Roy. Ast. Soc.*, **369**, 66.
Vale, C. 2005, astro-ph/0509039.
Vielva, P., Barreiro, R. B., Hobson, M. P., Martinez-González, E., Lasenby, A. N., Sanz, J. L. & Toffolatti, L. 2001, *Mon. Not. Roy. Ast. Soc.*, **328**, 1.
Vielva, P., Martinez-Gonzalez, E., Tucci, M. 2006, *Mon. Not. Roy. Ast. Soc.*, **365**, 891.
Vilenkin, A.; Shellard, E. P. S. 1995, *Science*, **267**, 1845
Vishniac, E. T. 1987, *Astrophys. J.*, **322**, 597.
Vittorio, N.; Juszkiewicz, R. 1987, *Astrophys. J.*, **314**, 29
Volonteri, M., Haardt, F. & Madau P. 2003, *Astrophys. J.*, **582**, 559
Walter, et al. 2004, *Astrophys. J.*, **615**, L17
Warren, M. S., Abazajian, K., Holz, D. E., & Teodoro, L. 2006, *Astrophys. J.*, **646**, L881
Weller, J., Battye, R. A. & Kneissl, R., 2002, *Physical. Rev. D*, **88**, 231301
Wyithe, & Loeb, A. 2003, *Astrophys. J.*, **588**, 69
Yamada, M.; Sugiyama, N.; Silk, J. 1999, *Astrophys. J.*, **522**, 66
Zhang, P.J, Pen, U.-L. & Wang, B., 2002, *Astrophys. J.*, **577**, 555
Zhang, P.J. 2004, *Mon. Not. Roy. Ast. Soc.*, **348**, 1348
Zhang, P.J., Pen,U.-L, Trac, H. 2004, *Mon. Not. Roy. Ast. Soc.*, **347**, 1224
Zaldarriaga, M. & Seljak, U. 1997, *Physical. Rev. D*, **55**, 1830
Zaldarriaga, M. & Seljak, U. 1998, *Physical. Rev. D*, **58**, 3003
Zaldarriaga, M. & Seljak, U. 1999, *Physical. Rev. D*, **59**, 3507
Zaldarriaga, M. 2000, *Physical. Rev. D*, **62**, 063510
Zaroubi, S. & Silk, J. 2005, *Mon. Not. Roy. Ast. Soc.*, **360**, 64

